Non-coding RNAs Function on Olfactory Sensory Neuron Development

Thesis

Non-coding RNAs function on olfactory sensory neuron development

Wenjing Xu, B.Sc.

A thesis submitted in fulfillment of the requirements of the Open University

for the Degree of Doctor of Philosophy

The Stowers Institute for Medical Research

Kansas City, Missouri USA

an Affiliated Research Center of the Open University, UK

December 2020

Abstract

Neuronal plasticity in the brain is greatly enhanced early in life, during a time window referred to as the critical period. Mechanisms underlying heightened plasticity in this early developmental period remain largely unknown.

Employing the murine olfactory sensory neuron (OSN) as a model, I identify the long non-coding RNA H19 as one important regulator of the developmental critical period. H19 is one of the most abundant transcripts in the early embryonic and neonatal olfactory epithelium. Although H19 knockout does not affect olfactory axon projection pattern, it affects plasticity during the critical period. H19 knockout mice are deficient in the ability to recover convergent axon projection following odorant exposure during the critical period. Transgenic expression of H19 in the OSNs disrupts the singular projection pattern of OSN axons. This effect is associated with the ability of H19 to influence the maturation of OSNs, and its ability to extend the lifespan of navigator OSNs, which exhibit dynamic axon growth during the critical period. In contrast, transgenic expression of H19 transcript without the embedded miR-675 does not affect the plasticity of OSN axon projection. These results suggest H19 regulates the olfactory neuron developmental plasticity through regulating miR-675 expression.

I also investigated the role of ADAR, an enzyme that is involved in RNA editing and circular RNAs biogenesis, in the developmental of olfactory system. Adar-deficient OSNs display impaired axon targeting for certain olfactory receptor (OR) types. Transgenic expression of Adar1La, but not the isoform Adar1p150, widely downregulates circular RNAs. However, only ectopic expression of Adar1p150 disrupts olfactory axon projection. It is associated with an increase in neuronal activity. These results indicate that Adar influences axon projection during development, but this influence is unlikely to depend on circular RNA.

Acknowledgements

First and foremost, I would like to thank my research supervisor Dr. C. Ron Yu for his strong support, patient guidance, and excellent practical advice throughout my research years as a PhD student. It was an honor for me to share his exceptional scientific knowledge and his extraordinary ability to tell complex stories in a simple great way, which were indispensable for me to accomplish the work presented in this thesis.

I also would like to thank my committee members Dr. Joan Conaway, Dr. Tatjana Piotrowski, Dr. Ariel Bazzini, and Dr. Peter Baumann for their constructive suggestions and crucial input in scientific discussions, which were helpful and valuable for shaping up my ideas and presentations during my entire period of my PhD research.

I wish to show my gratitude to Dr. Leanne Wiedemann and Ms. Lisa Hodges for all the help on my PhD program. I would not have been able to complete my PhD training without their efforts on the program admission, report submission, and committee meeting organization.

I sincerely thank Yu lab colleagues for their kind help, for their companionship, and for providing such an enjoyable working atmosphere. Dr. Limei Ma was always willing to help me with my experiments, and she provided many significant suggestions for my presentation. I appreciate the collaboration of Dr. Yunming Wu in the development of this research work. It would be tough and slow without his help in progressing and troubleshooting experiments. I would like to thank Mr. Max Hills, as a bioinformatician, for his contribution to RNA sequencing data analysis. I thank Mr. Kyle Duyck for his valuable help. During my doctoral research, I learned a great deal from Kyle about the implementation of bioinformatic tools for data analysis. I would like to thank Mr. Rishabh Raj, who as a good friend and colleague was always willing to help me with my presentation and writing.

During this work, I have collaborated with many core facilities people, and I wish to extend my warmest thanks to all the people who helped me with my work at the Stowers Institute for Medical Research.

The funding support from the Stowers Institute for Medical Research is gratefully acknowledged.

My parents, my cousins, and my friends Dr. Yunming Wu and Ms. Xingyu Liu deserve special mention for their inseparable support and unconditional caring. Encouragement from my family and friends always inspired me to move forward during my predoctoral years.

Table of Contents

Table of Figures

Chapter 1

Chapter 3

Chapter 4

Table of Abbreviations

7-AAD	7-Aminoactinomycin D
AAV	adeno-associated virus
Adar	RNA-specific adenosine deaminase 1
Adcy3	adenylyl cyclase 3
AdV	adenovirus
Ano2	anoctamin 2
ANOVA	analysis of variance
AOB	accessory olfactory bulb
A-P	anterior-posterior
ASCI	acute spinal cord injury
Ascl	achaete-Scute Family BHLH Transcription Factor
Atf5	activating transcription factor 5
BDNF	brain-derived neurotrophic factor
BMPs	bone morphogenetic proteins
cAMP	cyclic adenosine monophosphate
Cdc6	cell division control protein 6 homolog
CDR1as/CIRS7	cerebellar degeneration related protein 1 antisense transcript
circRNA	circular RNA
CNG	cyclic nucleotide gated channel
CNS	central nervous system
CTCF	CCCTC-binding factor
DAPI	4',6-diamidino-2-phenylindole, a nuclear staining dye
Dbpht2	DNA binding protein with his-thr domain
DIG	digoxigenin
Dlx1as	distal-less homeobox 1, antisense
Dlx3	distal-less homeobox 3
Dlx5	distal-less homeobox 5
DMR	differentially methylated region
DNA	deoxyribonucleic acid
DOX	doxycycline
DTA	diphtheria toxin A
D-V	dorsal-ventral
EDTA	Ethylenediaminetetraacetic acid
Eif2a	eukaryotic translation initiation factor 2A
Emx2	empty spiracles homeobox 2
EphA5	Eph receptor A5
EPL	external plexiform layer

ER	endoplasmic reticulum
Evf2	Dlx6as; distal-less homeobox 6, antisense
FACS	fluorescence activated cell sorting
FDR	false discovery rate
Fez	FES proto-pncogene, tyrosine kinase
FGF	fibroblast growth factors
Fgf4	fibroblast growth factor 4
Fgf8	fibroblast growth factor 8
Fgfr1	fibroblast growth factor receptor 1
FISH	fluorescence in situ hybridization
FoxG1	forkhead box G1
FoxO3	forkhead box O3
GABA	gamma aminobutyric acid
Gad1	glutamate decarboxylase 1
GAP43	growthcorn associated protein 43
GBC	globose basal cell
GC-D	Guanylyl cyclase-D
GFP	green fluorescent protein
GG	Gruenenberg ganglion
Gli3	GLI family zinc finger 3
Glo	glomeruli
Gnal/Golf	G protein subunit alpha L
Gnas/Gs	guanine nucleotide binding protein, alpha stimulating
GO	gene ontology
GPCR	G protein coupled receptor
H19	H19, imprinted maternally expressed transcript
HBC	horizontal basal cell
Hes1	Hes family bHLH transcription factor 1
ICR	imprinting control region
Igf1r	insulin like growth factor 1 receptor
Igf2	insulin like growth factor 2
iDISCO	immunolabeling-enabled three-dimensional imaging of solvent-cleared organs
IGF	insulin-like growth factor
INP	intermediate progenitor cell
iOSN	immature olfactory sensory neuron
IRES	internal ribosome entry site
ISH	insitu hybridization
Kir2.1	potassium inwardly rectifying channel subfamily J member 2
Kirrel2	kirre like nephrin family adhesion molecule 2

Kirrel3	kirre like nephrin family adhesion molecule 3
LacZ	an intracellular enzyme encodes β-galactosidase
LBR	lamin B receptor
LGN	lateral geniculate nucleus
LIN-41	lineage variant 41
lncRNA	long non-coding RNA
Lockd	lncRNA downstream of Cdkn1b
LSD1	lysine (K)-specific demethylase 1A
M71	olfactory receptor gene Olfr151
M72	olfactory receptor gene Olfr160
Malat1	metastasis associated lung adenocarcinoma transcript 1
Map1b	microtubule-associated protein 1b
Mash1	mammalian achaete-scute homolog 1
Meg3	maternally expressed gene 3
Miat	myocardial infarction associated transcript
miRNA	microRNA
MOB	main olfactory bulb
MOE	main olfactory epithelium
MOR28	olfactory receptor gene Olfr1507
mOSN	mature olfactory sensory neuron
Nanog	nanog homeobox
ncRNA	non-coding RNA
Neat1	nuclear paraspeckle assembly transcript 1
NeuroD1	neurogenic differentiation 1
Ngn1	neurogenin 1
Nrp2	neuropilin 2
OB	olfactory bulb
OMP	olfactory marker protein
OR	olfactory receptor
OSN	olfactory sensory neuron
Otx2os1	orthodenticle homeobox 2 opposite strand 1
Pantr1	POU domain, class 3, transcription factor 3 adjacent noncoding transcript 1
Pax6	paired box protein 6
PBS	phosphate buffered saline
PBST	phosphate buffered saline with TritionX-100

Chapter 1 Introduction

Brain development is a continuous process that involves complex interactions between genetic inheritance and environmental factors. To coordinate heritability with the changing environment, the nervous system exhibits plasticity in its inter-neuronal connectivity and can adapt to changes in environment and experience. Nonetheless, neuronal plasticity declines with age. For example, human language acquisition is progressively restricted when growing older. The early postnatal period is crucial for brain development as the neural system begins to experience environmental stimuli that eventually shape the neural connections. What are the neurophysiological mechanisms that underlie this critical period of heightened plasticity? To address this question, I employ the murine olfactory sensory neurons (OSNs) as a model and focus on the genetic traits that enable the plasticity of OSNs during the early postnatal period.

Olfaction is a major sense across species with a fundamental role in animals' social behaviors and survival. Although olfactory systems have evolved separately in different species, OSNs which initiate the olfactory input to the central nervous system (CNS), share similar properties. The general anatomical architecture of the olfactory system in different species is also shared, suggesting a common organizational principle (Ache and Young, 2005). The mouse OSNs express odorant receptors that detect odorants in the nose (Buck and Axel, 1991). One OSN only expresses one of ~1000 different OR genes (Malnic et al., 1999), and the axons of OSNs expressing the same type of OR converge to specific glomeruli at stereotyped positions in the olfactory bulb (OB) (Mombaerts et al., 1996; Ressler et al., 1994; Vassar et al., 1994). This convergence of olfactory axons into ~3000 glomeruli in each OB forms an olfactory map with spatial organization of the odorant receptors (Mori et al., 2006). As a consequence, odor information detected by ORs is topographically represented. This unique olfactory map provides great advantages to

study neural connections. OR identity can be used as a genetic readout to visualize the specificity of connection and to observe any alterations in axon projection in the stereotypic olfactory map. Characterizing the olfactory neuron development could provide clues to understand the mechanism of circuit formation in the neural system.

The olfactory sensory system has a lifelong regenerative capacity of OSNs. Whether there are critical periods in the development of the mammalian olfactory system has been not clear. Recently, two studies revealed a critical period in olfactory bulb development during which the glomerular map is established (Ma et al., 2014b; Tsai and Barnea, 2014). A follow-up study has shown that neurons generated during and after the critical period adopt different mechanisms in axon projection (Wu et al., 2018). A class of early-born neurons, the navigator cells, are able to set up convergent projection into single glomeruli and refine the innervating axons, whereas the late-born OSNs follow this existing projection track. In addition, the navigator neurons have a shorter life span, a faster turnover rate, and increased axon plasticity compared to the late-born neurons (Wu et al., 2018).

For the purpose of comprehensively understanding what factors were required for early glomerular map formation, whole-tissue and single-cell RNA sequencing were performed to discover the temporal transcriptome changes in different cell types of the main olfactory epithelium (Wu et al., 2018). From this dataset, we found a large set of long non-coding RNAs (lncRNAs) that were expressed in the olfactory epithelium. The majority of mammalian transcripts are non-coding RNAs (ncRNAs) (Roberts et al., 2014). The identification of lncRNAs in the OSNs raised the question of their function in OSN development. It was interesting to explore what the regulatory ncRNAs were and how they functioned in the olfactory system.

My thesis focuses on investigating the function of ncRNAs on OSN development. Numerous studies have shown that ncRNAs participate in diverse biological processes and

the development of disease (Slack and Chinnaiyan, 2019). In addition to ribosomal RNAs (rRNAs) and transfer RNAs (tRNAs), lncRNAs, microRNAs (miRNAs) and circular RNAs (circRNAs) are three groups of ncRNAs that play important roles in regulating the development of the nervous system (Kosik, 2006; Quan et al., 2017; Rybak-Wolf et al., 2015). Combining genetic tools and bioinformatic analysis, I studied the function of highly conserved maternally expressed lncRNA H19 and profiled circRNA species in OSN development.

In this chapter, I will review our current understanding of the development of the murine main olfactory system, neurogenesis of OSNs, axon guidance, olfactory regeneration, the discovery of the critical period, and the studies of functional ncRNAs in the neural system.

1.1 Development of the main olfactory system

In mice, there are several sensory organs capable of detecting odor and pheromones. Beside the main olfactory epithelium (MOE) and the vomeronasal organ (VNO), the Grueneberg ganglion (GG) (Grüneberg, 1973) and the septal organ of Masera (SOM) (Adams and McFarland, 1971) are also involved in detecting odorants.

Among these sensory organs, the MOE and VNO have been extensively studied. Both of these systems comprise of several subtypes of sensory neurons with specialized molecular and functional features. The MOE is a pseudostratified epithelium that predominantly consists of OSNs, which project to the main olfactory bulb (MOB) (Figure 1.1A-B). The VNO is located on both sides of the lower part of the nasal septum. The pseudostratified vomeronasal sensory epithelium contains at least two subtypes of vomeronasal sensory neurons (the apical and basal compartments), which express two classes of vomeronasal receptors (V1Rs and V2Rs, respectively) and project their axons to different portions of the accessory olfactory bulb (AOB) (Figure 1.1A) (Dulac and Axel, 1995; Herrada and Dulac, 1997; Matsunami and Buck, 1997; Ryba and Tirindelli, 1997).

The GG is located bilaterally to the anterior vestibule of the nasal cavity. The axons of GG neurons fasciculate into a few nerve bundles in the caudal OB which is a ring-like structure called necklace glomeruli (Figure 1.1A) (Fuss et al., 2005). The GG neurons express the mature sensory neuron marker Omp and a substantial portion of Omp-positive GG neurons are found to express Vmn2r83, a V2R subtype expressed in all basal VNO neurons (Fleischer et al., 2006), which supports the role of GG neurons in chemoreception.

The SOM is a small island of olfactory neuroepithelium lying bilaterally at the ventral base of the nasal septum. In terms of cellular composition, SOM resembles the MOE and is also composed of OSNs and supporting cells. The SOM expresses a few ORs at high densities and many other ORs sparsely. The axon bundles of SOM neurons project mainly to the posterior ventromedial MOB and converge mostly to a few glomeruli (Figure 1.1A) (Lèvai and Strotmann, 2003).

As my thesis study mainly focuses on the development of the OSNs in the main olfactory epithelium, I will review studies of the main olfactory system.

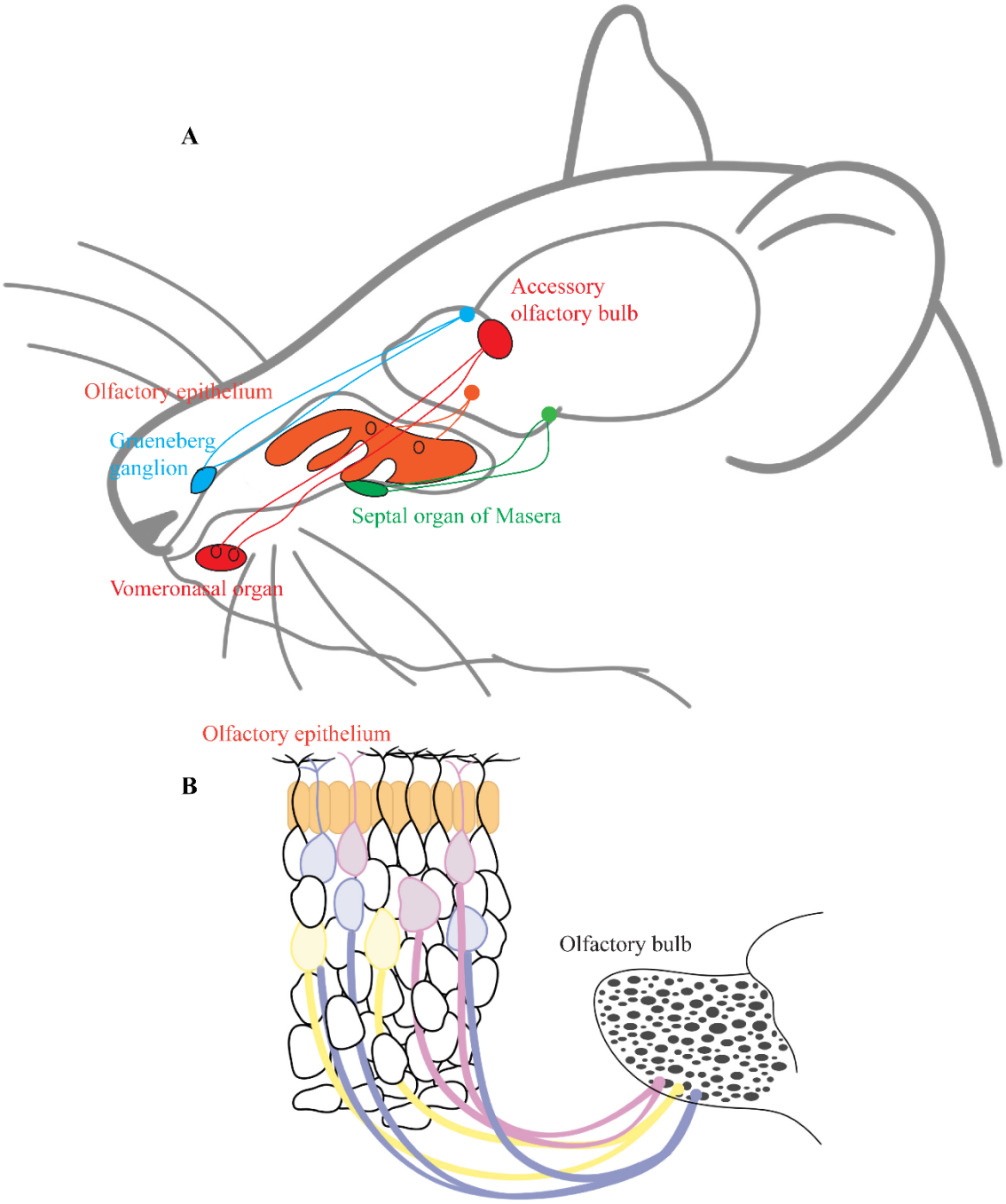

Figure 1. 1 The axon projection of neurons from different sensory organs in mice

(A) In the peripheral olfactory system, the GC cells (blue) project to the glomeruli in the caudal OB. The VNO neurons (red) project to the accessory olfactory bulb. The SOM neurons (green) project mainly to the posterior ventromedial OB. The OSNs in MOE project to the main olfactory bulb.

(B) The murine olfactory epithelium is a thin layer of pseudostratified cells covered in mucus that lines the nasal cavity. The olfactory bulb is an evaginated cortical structure with about 3000 glomeruli in each bulb and is located in the anterior region of the brain. OSNs in the epithelium detect odor molecules dissolved in the mucus and transmit odorant

information to the brain. Sensory neurons expressing the same OR (labeled with the same color) are locally scattered in defined zones within the olfactory epithelium. Their axons converge onto the same target glomeruli in the olfactory bulb. OSNs are continuously regenerated through the animal's lifespan. Newly generated OSN axons always converge onto the glomeruli of the same receptor type.

1.1.1 Embryonic development of MOE

The olfactory epithelia develop from the olfactory placodes, specialized areas of the cranial non-neural ectoderm in rostrolateral regions of the head that thicken as early as embryonic day 9 (E9) in mice (Cuschieri and Bannister, 1975). Following the transition from the olfactory pit to the nasal cavity structure, the MOE and VNO epithelia can be distinguished by E11.5 (Treloar et al., 2010). In contrast with other sensory placodes, the inductive events that initiate olfactory development are not well understood. It is partly because the olfactory placode is morphologically invisible until relatively late stages. Recent studies in zebrafish and chick have examined the origin of the olfactory placode at higher resolution and at intervening stages (Bhattacharyya and Bronner-Fraser, 2008; Whitlock and Westerfield, 2000). Some transcription factors, including Dlx3, Dlx5, and Pax6, are molecular markers for olfactory placode precursors at different stages (Bhattacharyya and Bronner-Fraser, 2008). Other transcription factors including Sox2 and Oct1work as combinatorial components to induce the olfactory placode (Donner et al., 2007). Following placode induction, the subsequent development of the nasal cavity involves signaling by retinoic acid (RA), fibroblast growth factors (FGFs), and bone morphogenetic proteins (BMPs) from the adjacent frontonasal mesenchyme and olfactory ectoderm (Balmer and LaMantia, 2005).

Although olfactory epithelium is a pseudostratified epithelium, the lining of the olfactory placode subsequently gives rise to three “layers” which consist of multiple cell types (Figure 1.2). Two types of stem cells, namely globose basal cells (GBCs) and horizontal basal cells (HBCs), are located at the inner basal layer and adjacent to the basal lamina. Most GBCs are mitotically active and are responsible for generating supportive sustentacular cells, OSNs, as well as the Bowman’s gland (Beites et al., 2005). A population of actively self-renewing GBCs give rise to transient amplifying cells (TACs), that express transcription factor achaete-scute homolog 1 (Ascl1, originally named *Mash1*

for mammalian achaete-scute homolog 1), which is essential for OSN development (Cau et al., 2002; Graziadei and Graziadei, 1979). The *Ascl1* expressing TACs differentiate into the intermediate neuronal precursors (INPs) that express transcription factors Neurog1 and Neurod1 (Cau et al., 2002; Packard et al., 2011). Following one or more divisions, the INPs exit the cell cycle and further differentiate into immature OSNs (iOSNs) in the intermediate layer where OSNs exhibit a basal to apical maturation gradient such that mature OSNs (mOSNs) are located closer to the apical layer. The mOSNs express a specific molecule olfactory marker protein (Omp) that is widely used as a molecular marker.

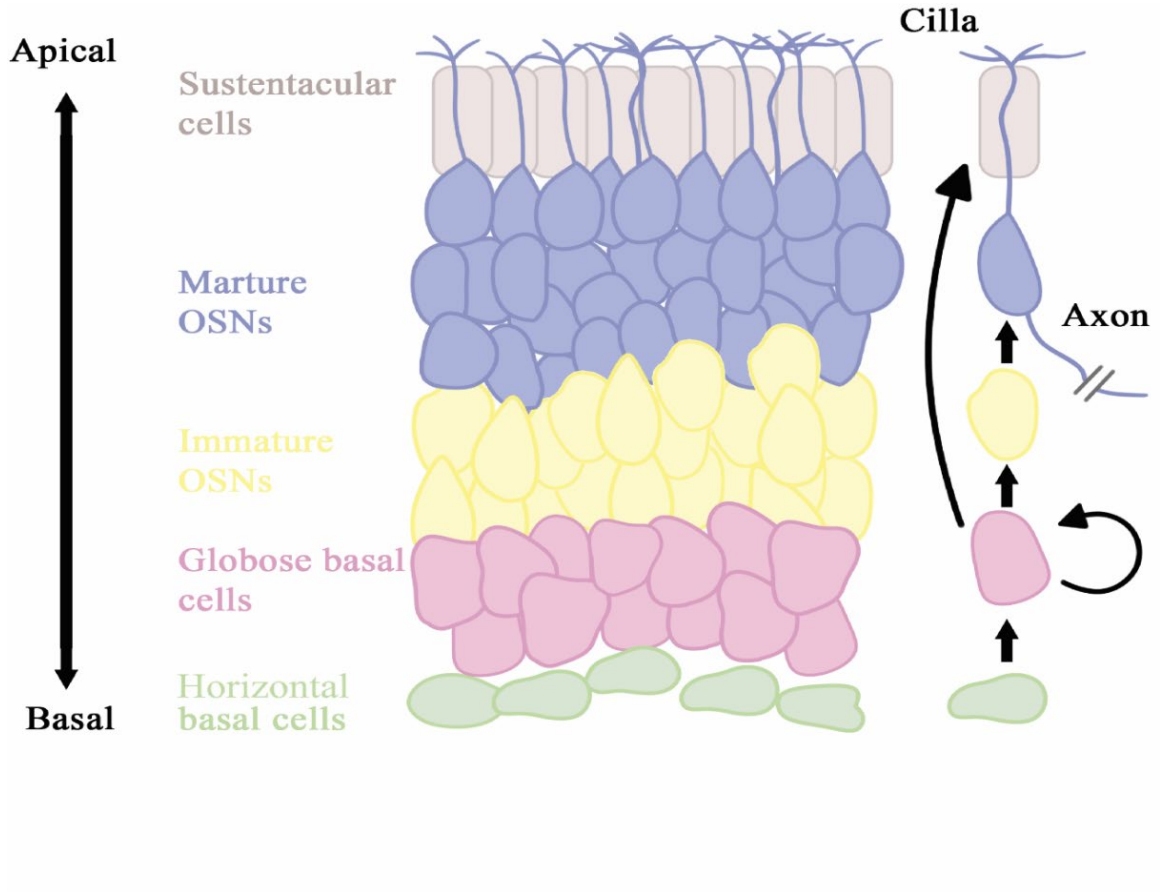

Figure 1. 2 Structure of the pseudostratified olfactory epithelium

The olfactory epithelium has a pseudostratified columnar organization and mainly consists of basal cells, olfactory neurons, and supporting cells. The stem cells of the olfactory epithelium lie along this basement membrane and are multipotent, able to reconstitute both the neural and nonneural elements of the olfactory epithelium. Quiescent HBCs (green color) differentiate into GBCs (pink color) when responding to injury. Mitotically active GBCs differentiate into sustentacular cells and OSNs during the continuous regeneration process.

1.1.2 Embryogenesis of OSN axons

Beginning at E10.5 in mice, the OSN axons extend across the basal lamina towards the developing telencephalon. By E11.5 the OSN axons contact the rostral-most tip of the telencephalon and innervate the presumptive olfactory bulb (Treloar et al., 2010). At the same time, molecularly defined subpopulations of axons show evidence of spatial segregation within the nascent nerve (Miller et al., 2010), indicating a pre-target OSN axon sorting is established at this moment. From E11.5 to E15, a majority of newly generated olfactory axons follow their primary trajectories and remain on the surface of the telencephalon. A subpopulation of axons, called pioneer olfactory axons, penetrate deeper into the presumptive olfactory bulb to establish synaptic connections and increases 40% in bulb volume, suggesting olfactory axons affect the development of the olfactory bulb (Gong and Shipley, 1995; Stout and Graziadei, 1980). The arrival of pioneer axons is thought to promote the precursor cell in the OB to exit the cell cycle (Gong and Shipley, 1995). A competing theory is that olfactory bulb development is induced by fibroblast growth factor signaling, via the interaction between Fgfr1 and Fgf8. Fgf8 is expressed at the anterior telencephalon, and Fgfr1 is expressed throughout the neuroepithelium lining the telencephalic ventricles (Hébert et al., 2003). Deficiency of either Fgfr1 or Fgf8 results in defects of olfactory bulb formation (Hébert et al., 2003; Meyers et al., 1998; Toyoda et al., 2010), suggesting that the interaction of Fgfr1 and Fgf8 plays a more important role in induction and morphogenesis of olfactory bulb.

The regulation of early olfactory nerve growth involves many transcription factors and guidance cues. For instance, inactivation of transcription factor Dlx5 prevents olfactory axons to contact the OB (Merlo et al., 2007). Loss of transcriptional regulator Gli3 alters the outgrowth and targeting to the telencephalon of OSN axons (Balmer and LaMantia, 2004). The deficits of some transcriptional factors, including Six1, Fez, Emx2, and Fgf8, have resulted in olfactory nerve defasciculate and project aberrantly near the forebrain

(Miller et al., 2010; Treloar et al., 2010). Additionally, it has been shown that OSNs expressing a mutated OR display poor outgrowth and fail to reach the OB (Feinstein et al., 2004). Despite these similar phenotypes seen in different knockout mice, the regulation of axon migration may not be completely cell autonomous since some of these cues are expressed outside OSNs. Moreover, OSN maturation and neuronal fate commitment are mostly not affected in these knockouts, which indicates that the olfactory nerve growth and the embryonic olfactory neurogenesis are two separated processes.

1.1.3 Signaling transduction in OSNs

Odorant signaling transduction begins with odorant binding to specific ORs located in the membranes of the cilia (Figure 1.3). The ORs are G protein-coupled receptors (GPCRs), and they are coupled with the G protein Gnal (G_{olf}), which activates adenylyl cyclase 3 (Adcy3) upon activation (Bakalyar and Reed, 1990). In turn, the activation of ACIII results in the generation of cyclic AMP (cAMP). The increase in cAMP concentration leads to the opening of cation-selective cyclic-nucleotide gated (CNG) channels, which then permits the influx of Na^+ and Ca^{2+} into the cytosol (Kurahashi and Yau, 1993; Reed, 1992). The entry of Na^+ brings about a first reduction in membrane potential, whereas the entry of Ca^{2+} affects a second channel, Anoctamin 2 (ANO2), which is a Ca^{2+}/calmodulin-sensitive Cl^- channel (Stephan et al., 2009). Activation of ANO2 further provides an amplified membrane depolarization (Brunet et al., 1996; Mombaerts, 2004; Stephan et al., 2009).

GPCRs are often depicted as bimodal switches with inactive and active states (Kobilka and Deupi, 2007). In the absence of odorant molecules, ORs produce a baseline level of cAMP by spontaneously flipping between active and inactive conformations. Each OR possesses a unique level of baseline activity and generates a specific amount of cAMP using another G protein alpha subunit, Gnas (G_s), which is structurally similar to G_{olf} (Nakashima et al., 2013; Reisert, 2010). The expression of G_s precedes that of G_{olf} during

development and CNG channels are not yet expressed in iOSNs (Nakashima et al., 2013). However, in the G_{olf} knockout animal, the existence of G_s doesn't rescue the signaling, suggesting that G_s is not sufficient to mediate odor detection (Belluscio et al., 1998). It is likely that G_s mediates signaling in the iOSNs. The differential activation of the G-proteins has implications in their role in axon projection.

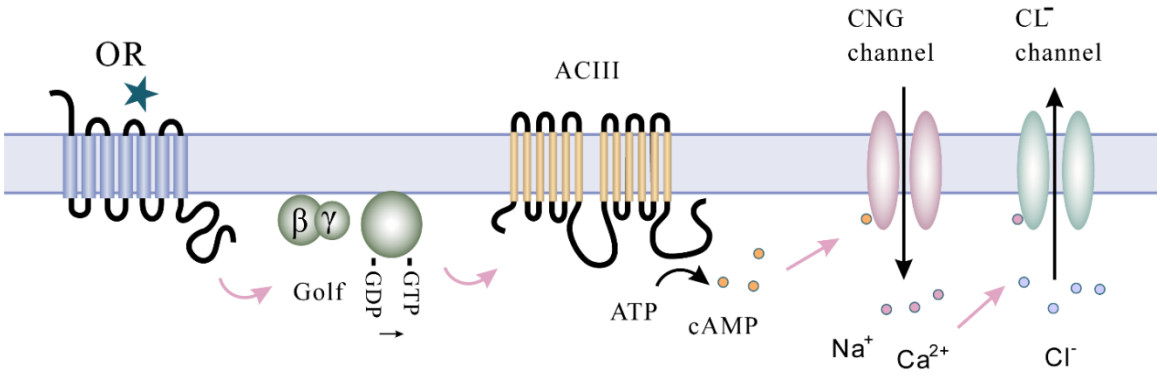

Figure 1. 3 Signal transduction in the OSNs

Odorant molecules bind directly to OR located in the membrane of the cilia. This association activates successively olfaction-specific G protein G_{olf} (green color), which in turn activates ACIII (yellow color), resulting in the generation of cAMP. The increase in cAMP opens CNG channels (pink color), allowing both Ca^{2+} and Na^{+} to enter the cell, leading to membrane depolarization. This depolarization is further amplified by Ca^{2+} activated Cl^{-} current, which generates action potentials carrying the odor information to the olfactory bulb.

1.1.4 OR choice

The olfactory system is able to discern tens of thousands of different odorants and their mixtures. One remarkable feature is that each OSN expresses a single OR gene out of the complete repertoire of genes. In mouse genome, there are approximately 1,100 functional OR genes (Zhang and Firestein, 2002). These OR genes are scattered in clusters across most chromosomes with the largest gene cluster on mouse chromosome 7 (Clowney et al., 2011). How is the singular expression of ORs regulated in OSNs?

In each OSN, only one of the two homologous alleles, either the maternal or paternal, of a given OR gene type is stochastically expressed (Chess et al., 1994; Takeuchi et al., 2010). Evidences point towards repressive heterochromatin marks, H3K9me3 and H4K20me3, widely cover the OR genes (Magklara et al., 2011). In contrast, one active OR allele is labeled with the H3K4me3 euchromatin histone mark (Magklara et al., 2011). It is proposed all OR genes are repressed in constitutive heterochromatin in basal cells, then a single OR locus is derepressed through demethylation of H3K9me3 during neuronal differentiation and goes through transcription (Lyons et al., 2013). In this scenario, the monoallelic expression of OR could be achieved since only one allele can be activated at a time. It is suggested that OR silencing is regulated by an integral membrane protein lamin b receptor (LBR) (Clowney et al., 2012; Ye et al., 1997). The reconstitution of OSN nuclear architecture is synchronous with the downregulation of LBR, and ectopic expression of LBR in mOSNs disrupts the aggregation of OR genes (Clowney et al., 2012).

Lomvardas and colleagues have elucidated that OR gene activation involves the transient expression of lysine-specific demethylase 1 (LSD1) (Figure 1.4) (Lyons et al., 2013). LSD1 acts directly on OR chromatin and derepress a previously silenced OR gene, allowing transcriptional activation in iOSNs. The expressed OR requires proper folding and posttranslational processing in the endoplasmic reticulum (ER), generating unfolded

protein response (UPR) through activating PKR-like ER kinase (PERK). PERK then phosphorylates the translation initiation factor Eif2a, leading to selective and transient translation of activating transcription factor 5 (ATF5). ATF5 induces the transcription of Adcy3, which leads to ER stress alleviation and LSD1 downregulation, allowing for terminal OSN differentiation and stabilization of the chosen OR (Dalton et al., 2013). This negative feedback mechanism enforces the singular OR expression triggered by LSD1.

The mechanism of OR gene choice initiation is not completely understood. It has been identified that specific DNA motifs like Olf-1/EBF-like family and homeodomain transcription factors are commonly shared in OR gene promoters (Clowney et al., 2011; Hoppe et al., 2006; Rothman et al., 2005). Transcription factor Lhx2 is shown to bind to the homeodomain site in the promoter region of some ORs like M71, which is required for the expression of these OR genes (Hirota and Mombaerts, 2004; Rothman et al., 2005). Another transcription factor, Emx2, binds to the putative OR promoter and is necessary for the expression of some OR genes (Hirota and Mombaerts, 2004; McIntyre et al., 2008). The transcription factors binding to the common DNA motifs is involved in the regulation of OR expression, but they do not explain the monogenic expression of OR genes. In addition, ORs are controlled by enhancer elements in *cis*, including H element (Serizawa et al., 2003), P element (Khan et al., 2011), and the “Greek islands” (Monahan et al., 2019).

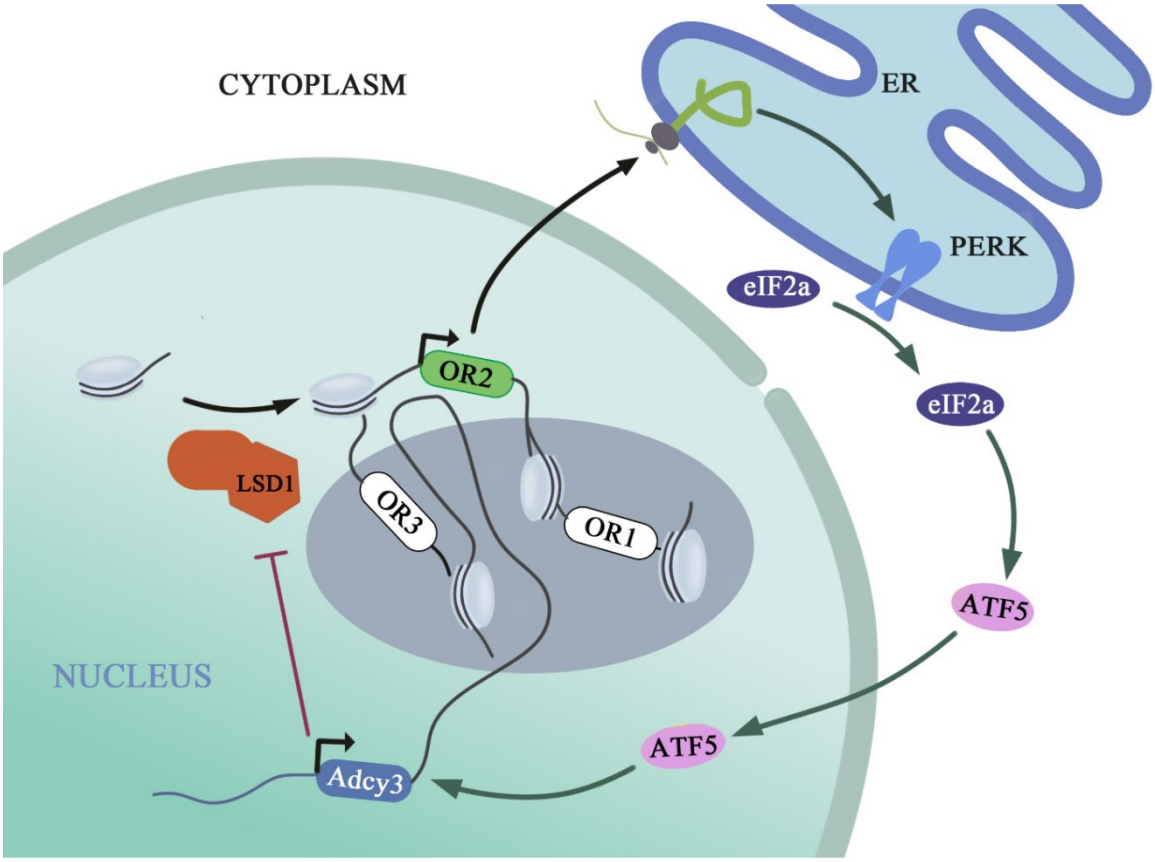

Figure 1. 4 Single OR gene choice in OSNs

Most OR genes are embedded with repressive histone marks. OR activation involved the derepression of a single OR gene by the histone demethylase LSD1 and unidentified chromatin-modifying enzymes. OR transcription triggers negative feedback mechanism through inducing transcription of Adcy3, and Adcy3 prevents derepression of additional OR genes by downregulating LSD1.

1.2 Olfactory sensory axon projection

In mice, each glomerulus is innervated by axons from sensory neurons expressing the same OR. Since an odorant molecule can interact with multiple OR species, odor signals are converted into a topographic map of multiple glomeruli activated with varying magnitudes. This olfactory map presents a practical model for investigating mechanisms involved in patterning connections between peripheral sensory neurons and central targets.

1.2.1 The olfactory sensory axon projection in olfactory bulb

OSNs extend their axons solely to the olfactory bulb, the first center dedicated to odor information processing. The olfactory bulb is divided into multiple layers with different types of neurons. The axons of OSNs make synapses in the glomerular layer where they make contact with dendrites of periglomerular cells, mitral cells, and tuft cells (Mori et al., 1999).

In addition to these broad connections, the zonal organization seen in the epithelia appears to be maintained in the olfactory bulb (Miyamichi et al., 2005). OSNs located in the dorsal nasal cavity converge to the glomeruli in the dorsal olfactory bulb, and ventrally located OSNs project their axons to the ventral glomeruli. However, each of the four broad zones is represented in the OB without distinct zonal boundaries (Miyamichi et al., 2005).

1.2.2 Olfactory axon sorting

The neural map is a fundamental brain architecture, forming the connections that transfer information from one area of the nervous system to another in a continuous or discrete manner. Unlike the continuous map of visual projection from the retina to the lateral geniculate nucleus, the olfactory map is a discrete topographic map. With individual glomerulus corresponds to a specific odorant receptor, the map converts odor activity into discrete spatial representations. How is this convergence established? A key observation is that substituting the coding region of an OR with another gene results in axons projecting

to a different glomerulus position (Wang et al., 1998). Also, based on the observation that OR proteins are expressed at the axon terminus (Barnea et al., 2004), it was once thought that the OR itself acts as an axon guidance molecule detecting the target cues in the olfactory bulb (Feinstein and Mombaerts, 2004). Although this model is attractive, there is no direct evidence for this yet. ORs are important in instructing the targeting of axons, but they are not adequate acting as axon sorting molecules based on their structure (Hall et al., 2004).

OR-instructed axonal fasciculation is also activity-dependent. Genetic manipulation of cAMP levels shifts the glomerular target of OSNs posteriorly or anteriorly, suggesting that OR-derived cAMP signals can direct glomerular positioning along the anterior-posterior (A-P) axis (Imai et al., 2006). The difference in OR identity results in different levels of cAMP, and thus downstream transcription of axon guidance molecules are differentially regulated. For instance, homophilic adhesion molecules Kirrel2 is expressed in the OSN with higher activity. Kirrel3 is expressed in the OSN with lower activity (Serizawa et al., 2006). Cell repulsive ephrinA5/EphA5 also regulates axon sorting correlated with OR species in an activity-dependent manner (Serizawa et al., 2006).

Several guidance molecules have been identified to be expressed along the dorsal-ventral (D-V) axis or A-P axis, which are not OR-dependent. For instance, in mice deficient with Robo2 and Slit1, a subset of OSN axons that normally project to the dorsal region of the OB mistarget and form glomeruli in the ventral region (Cho et al., 2007). Axon guidance receptor Nrp2 and its repulsive ligand Sema3F are expressed by OSNs in a complementary manner along the D-V axis. The sequential arrival of $Nrp2^{+}$ and $Sema3F^{+}$ axons in the OB forms a gradient, which contributes to the axon projection along the D-V axis (Takeuchi et al., 2010).

One interesting feature is that the identified D-V and A-P positioning, as well as axon sorting mechanisms, appears not to involve target-derived cues. Consistent with this idea,

it has been shown by surgical and genetic methods that convergence and sorting of OSN axons occur even independently of the olfactory bulb (St. John et al., 2003). This autonomous target-independent mapping could be an adaption to better shape the downstream information processing, and an advantage for establishing discrete connections.

1.2.3 Neural activity is required for axon guidance

In OSNs, neural activity is not only the way for communicating with each other, it is also required for olfactory map refinement. Blocking neuronal spontaneous activity by the overexpression of an inward rectifying potassium channel, Kir2.1, severely affects axonal convergence, indicating that the spontaneous activity is required for axon targeting (Yu et al., 2004). More recently, it is shown that the spontaneous firing of OSNs can modulate the whole topographic organization of glomeruli and intra-bulbar connections using the same Kir2.1 mouse (Lorenzon et al., 2015). Since different ORs have different spontaneous activity patterns, it is also demonstrated that temporal spike patterns of spontaneous firing may regulate OR-specific differential expression of glomerular segregation molecules (Nakashima et al., 2019). However, it remains unclear about what molecules are regulating this spontaneous activity.

Compare with spontaneous activity, the odorant evoked activity plays a distinct in axon guidance. This odorant dependent activity is induced by the signaling transduction described previously (Figure 1.3). Both Cnga2 knockout and G_{olf} knockout mice are anosmic but form a normal olfactory map (Belluscio et al., 1998; Brunet et al., 1996; Nakashima et al., 2013). In contrast, mice deficient for Adcy3 and G_s form diffused clusters of glomeruli (Nakashima et al., 2013). Since both Adcy3 and G_s are involved in maintaining singular OR regulation, the knockout phenotype may not be a direct consequence of altering ligand-dependent activity pathway. Another study using unilateral naris occlusion to block odorant from contacting the epithelium found a delayed single

glomerulus convergence recovery (Cummings and Belluscio, 2010). This could also be explained by the downregulated proliferation but increased turnover of OSNs (Suh et al., 2006).

1.3 Adult regeneration and developmental critical period in OSNs

Neurogenesis in adulthood occurs in three primary areas in the mammalian nervous system: the subgranular zone, which supplies new granule cells to the dentate gyrus of the hippocampus; the subventricular zone, which supplies new interneurons to the olfactory bulb; and the olfactory epithelium. Among these three areas, the OSNs are the only neurons in the mammalian nervous system that not only project to specific targets in the brain, but also regenerate naturally and in response to injury through the animal's life span. This unique and remarkable capacity for continuous regeneration provides a great *in vivo* model to study how neurons generated at different stages respond to different environments and how the neurons maintain specific connectivity when the circuit is fully developed or in response to damage.

1.3.1 Regeneration of OSNs

The OSNs are directly and constantly exposed to environmental insults like harmful chemicals or biological agents that cause inflammation. They have a considerably shorter lifespan than other neurons. In the 1970s, the life span for OSNs was measured as 30 days (Graziadei and Graziadei, 1979). It was later verified rodent OSNs have a lifespan of average of 30-90 days and up to one year in a clean environment (Mackay‐Sim and Kittel, 1991; Yu and Wu, 2017). Adult neurogenesis is needed to maintain the population of OSNs under constant environmental insult. The stem cell populations in the olfactory epithelium, HBCs, and GBCs, are critical for generating neurons. HBCs are mitotically quiescent and are not normally activated without extensive damage to the epithelium(Iwai et al., 2008). Upon severe damage, HBCs differentiate into GBCs and other cell types, including sustentacular cells and Bowman's gland (Brann et al., 2015; Leung et al., 2007).

On the contrary, most GBCs are mitotically active and are believed to be responsible for OSNs regeneration under most circumstances (Yu and Wu, 2017).

Despite the continuous turnover of OSNs, the convergent projection pattern of the olfactory map is consistently maintained. Studies using nerve damage experiments to trace the regeneration of single OR type axons have found that the newly generated olfactory axons project to multiple different locations (Costanzo, 2000; John and Key, 2003), indicating the olfactory axon mapping is significantly altered following nerve injury. Since these studies result in the destruction of neurons, axonal wiring may not be normal after massive lesions. The conclusion was challenged by another study using transgenic mice carrying a tet-operator driving diphtheria toxin A (DTA) to genetically kill cells, which has also examined the newly generated axon convergence and found the spatial map is fully restored (Gogos et al., 2000). However, induction of DTA expression does not result in the complete elimination of the targeted OSNs. A residual population of ~10% of original neurons remains, raising the possibility that these neurons are sufficient to guide reinnervation of the glomeruli. In summary, it remains to be seen if the mechanisms that dominate the glomerular map establishment also support its maintenance during adult OSN neurogenesis.

1.3.2 An olfactory critical period

The mechanism controlling neurogenesis is not clearly defined, perhaps it is because those that govern embryonic, juvenile, and adult neurogenesis are overlapping but not identical. Recent studies using a genetic approach to disrupt the glomerular map have identified regulation for early postnatal olfactory axon projection may be distinct from that in subsequent maintenance of the olfactory map (Ma et al., 2014b; Tsai and Barnea, 2014). These results indicate that the perinatal stage, recognized as a “critical period”, is crucial for olfactory development.

The concept of a sensitive period was first introduced in the 1930s (Kennard, 1938), to illustrate that there are periods of higher susceptibility to alterations by experience during brain development. The concept was further refined by David Hubel and Torsten Wiesel to define the critical period. Their experiments showed that if a kitten is deprived of normal visual experience during the critical period at the start of its life, the circuitry of the neurons in its visual cortex is irreversibly altered. Only the open eye that experienced visual stimulation had a fully developed vision (Wiesel and Hubel, 1963). No changes were seen when activity was deprived in adult cats or adult monkeys because they had fully developed their vision during their critical period (Hubel and Wiesel, 1970; Wiesel and Hubel, 1963).

Neuronal activity usually shapes the developmental refinement, and it is reasonable that most sensory systems with neurons that do not regenerate exhibit “critical periods” of heightened sensitivity to sensory experience. It is interesting to find such a critical period in the OSNs, which continue to regenerate throughout the lifespan of the animal. It is of interest to find out the molecular mechanism underlying high levels of plasticity.

1.4 Non-coding RNAs

The critical period is programmed to be opened and closed in a precise time sequence, which requires the execution of a complex developmental program. What are the genetic inheritances that cause the olfactory system to be plastic during the critical period? My research work focuses on one class of regulatory molecules, ncRNAs, which are involved in both transcriptional and translational controls.

The ncRNAs are functional RNA molecules that lack protein-coding capacity. In the past few decades, next-generation deep sequencing technologies have revealed that most of the mammalian genome is transcribed into RNAs, whereas less than 5% of human genome transcripts encode proteins (Consortium, 2012), less than 6% of transcripts from the FANTOM3 set are functionally annotated as protein-coding genes (Maeda et al., 2006),

and the majority of transcripts are ncRNAs. Further, plenty of studies have revealed ncRNAs participate in multiple biological and physiological networks via transcriptional, post-transcriptional, and epigenetic regulation (Li et al., 2019). The continuing discovery of regulatory function suggests that ncRNAs are important players in gene regulation. In addition, the regulation through ncRNAs is especially important in CNS because neurons are highly transcriptionally active, exhibiting robust expression of ncRNAs (Quan et al., 2017).

ncRNAs can be broadly classified into small ncRNAs (sncRNAs) and lncRNAs taking 200 nucleotides as a cutoff value. sncRNAs include functional RNAs such as tRNAs and rRNAs which are involved in transcriptional and translational regulation. They also include regulatory RNAs such as miRNAs and piwi-interacting RNAs (piRNAs) (Siomi et al., 2011) that are well-characterized in regulating gene expression. In contrast to sncRNAs, the lncRNAs are a group of large, heterogeneous ncRNAs of largely unknown function.

In this chapter, I will focus on the knowledge about the regulation and function of both lncRNAs and circRNAs. Also, particular emphasis is given to lncRNA H19 for its potential cellular functions at different levels of gene expression.

1.4.1 The unique features and general functions of lncRNAs

LncRNAs are produced in a similar way as that of mRNAs: they are usually transcribed by polymerase II and undergo post-transcriptional modifications such as capping, polyadenylation, and splicing. These lncRNAs do not exhibit coding potential and have generally fewer, but longer exons than protein-coding RNAs (Cabili et al., 2011). The primary sequences of lncRNAs are less conserved compared to protein-coding genes (Guttman et al., 2009). However, there is still evolutionary conservation in lncRNA promoter regions between vertebrates (Guttman et al., 2009). Notably, lncRNA genomic

position and secondary structure are conserved across organisms, indicating that functional structures can be maintained during evolution (Diederichs, 2014; Ponting et al., 2009; Ulitsky and Bartel, 2013). Another remarkable feature for lncRNAs is their discrete localizations in different cellular compartments, which is informative regarding their function. The nuclear enrichment of lncRNAs may suggest increased stability and function in the nucleus. The latter may account for relative lncRNA enrichment at the chromatin but depletion in the nucleoplasm compared with mRNAs (Schlackow et al., 2017). The cytoplasmic lncRNAs could act as miRNA sponges, protein scaffold and translation regulator, and nuclear lncRNAs are capable of interaction with DNA or chromatin-modifying complexes (Mercer et al., 2009).

The functional roles of lncRNAs initially have been studied in cell-based *in vitro* systems using gene knockdown and high-throughput transcriptome analysis. Recently, increasing numbers of studies have investigated the functions of lncRNAs using gene-targeted mouse models, largely verifying the physiological importance of lncRNA-mediated regulation. Considering that the majority of knockout mice do not show lethal phenotypes, it is proposed that most lncRNAs are generally involved in modulatory functions and only a few specific lncRNAs are essential for basic cellular functions (Nakagawa, 2016). The lncRNA Neat1 is a representative example of essential functions. The fertility of Neat1 knockout female mice was found to be severely decreased, and nearly half of the mice failed to become pregnant due to the severe defect in forming functional corpus luteum during pregnancy (Nakagawa et al., 2014). On the other hand, the effects and actions of lncRNA Hotair have been controversial. The human Hotair, expressed from the HoxC cluster, was proposed to attenuate the expression of genes in the HoxD cluster via association with chromatin modification factors, such as polycomb repressive complex 2 (PRC2) (Rinn et al., 2007). Currently, there are two generated Hotair knockout mouse lines. In the first mouse model that the entire HoxC cluster including Hotair is deleted,

neither the expression of HoxD genes nor chromatin marks at that locus are significantly affected (Schorderet and Duboule, 2011). However, the trans-acting de-repression of multiple members of the HoxD cluster and homeotic transformation phenotypes are observed in the second Hotair knockout mouse (Li et al., 2013). This transcriptomic difference may be caused by that these two studies used similar but different tissues for their analyses, in which direct comparison of RNA-seq reads mapping patterns show a similar trend of gene expression changes without statistically significant difference in the former study (Li et al., 2013; Schorderet and Duboule, 2011). Additional studies in the first group agree to a subtle anterior transformation in caudal vertebrae but this phenotype cannot be isolated from Hotair deletion itself or cis-regulatory alterations in HoxC expression (Amandio et al., 2016).

Considering that the expression of many lncRNAs is highly tissue-specific and is modulated under certain stress conditions (Connerty et al., 2020), these lncRNAs may not be essential for life, and instead, they are required in response to certain changes or function as biomarkers in particular tissues. One of best-known application of lncRNAs in diagnosis is the detection of PCA3 (Prostate Cancer Antigen 3, also known as DD3), a prostate-specific lncRNA that is upregulated by 60-fold in >90% of prostate tumors compared to benign prostatic tissue (Hessels et al., 2003) and is undetectable in other tumor types (Bussemakers et al., 1999). The urinary PCA3 test is now used for prostate cancer detection approved by the US Food and Drug Administration (FDA) (Groskopf et al., 2006).

Taken together, functional studies in knockout mouse models have provided compelling evidence that lncRNAs play central roles in mammalian development and physiology. It also should be stressed that some lncRNAs only induce minor modifications of development or behavior without causing deleterious drastic changes to core biological processes.

1.4.2 Functions of lncRNAs in neural development

The mammalian brain represents the complexity comprising hundreds of billions of cells of neuronal and glial origin with hundreds of trillions of synaptic interactions between these cells. The intricate development of this highly ordered complexity depends upon exquisite spatiotemporal control of gene expression in the cellular architecture. A great number of lncRNAs are specifically expressed in the developing brain, often exhibiting precise subcellular localization, suggesting they play key roles in neuronal development and function. In a recent study, Sauvageau et al. developed linc-Brn1b knockout mutants which showed a reduction in the number of intermediate progenitor cells in the subventricular zone, suggesting that linc-Brn1b plays a key role in the developing cortex (Sauvageau et al., 2013). Importantly, linc-Brn1b expression is primarily restricted to specific brain regions like telencephalon and subventricular zone and shows spatiotemporally regulated patterns during cortical development. These findings are encouraging as they suggest that lncRNAs may function depending on tissue-specific and regulated expression patterns.

A series of neural developmental events occur in embryonic and adult brains throughout life including precursor expansion, fate specification, differentiation, and maturation. The lncRNA Evf2 is a prime example illustrating the importance of lncRNA in neuronal differentiation. Evf2 is transcribed from the intergenic region between the Dlx5 and Dlx6 loci, and is overlapped by the Dlx5/6 intergenic enhancer (Feng et al., 2006). In the developing mouse forebrain, Evf2 recruits DLX and MECP2 transcription factors to Dlx5/6 intergenic enhancers and control Dlx5/6 expression through both trans and cis-acting mechanisms (Bond et al., 2009). Early transcription termination of Evf2 also reduces the transcription of glutamate decarboxylase 1 (Gad1), leading to a decreased number of GABAergic interneurons in early postnatal hippocampus and dentate gyrus and reduced synaptic inhibition in the adult hippocampus (Bond et al., 2009), which suggests

that Evf2 balanced gene regulation in embryonic GABAergic interneurons is critical for GABA-dependent connectivity in the adult brain. Another lncRNA Dlx1 antisense (Dlx1as) transcript, localized in the Dlx1/2 locus and overlapping with the conserved enhancer between the convergently transcribed Dlx1/2 genes (Dinger et al., 2008), has been shown to involve in neural lineage specification through negative regulation of Dlx1 (Kraus et al., 2013). Mice devoid of Dlx1as RNA are viable and fertile, but display an increased Dlx1 expression and changed neuronal lineages in subventricular zone neurogenesis (Kraus et al., 2013), suggesting Dlx1as functions potentially through antisense inhibition.

The role of lncRNAs may contribute to presynaptic function and activity regulation. A neuron-specific nuclear lncRNA "uc003wst.1"/neuroLNC was recently identified regulating presynaptic activity by Keihani and colleagues (Keihani et al., 2019). In primary rat hippocampal cultures, manipulating neuroLNC expression influences Ca^{2+} influx, suggesting neuroLNC is linked to neuronal activity (Keihani et al., 2019). Moreover, neuroLNC downregulation decreases the migration of cortical neurons from the ventricular zone to the cortical plate (Keihani et al., 2019). The effects of neuroLNC on synaptic vesicle release require interaction with the RNA-binding protein TDP-43 and the selective stabilization of mRNAs encoding for presynaptic proteins (Keihani et al., 2019), indicating neuroLNC possibly functions as a scaffold for the assembly of macromolecular complexes. The long noncoding RNA Gomafu/Miat/Rncr2 is a lncRNA involved in the regulation of the mesolimbic pathway (Ip et al., 2016). Gomafu knockout mice lack obvious phenotypic defects but exhibit hyperactive behaviors and increased responsiveness to methamphetamine, which is associated with increased extracellular levels of dopamine in the nucleus accumbens after injection with methamphetamine (Ip et al., 2016). However, it remains unclear how Gomafu affects dopamine transmission (Ip et al., 2016).

Some lncRNAs are also involved in neuronal degeneration and apoptosis. In the rat acute spinal cord injury (ASCI) model, the expression of lncRNA BDNF antisense RNA (BDNF-AS) is significantly upregulated (Zhang et al., 2018). Meanwhile, PRDM5 and c-caspase 3 protein levels are increased, which the same expression changes are observed in neuronal cell lines AGE1.HN and PC12 after hypoxia treatment (Zhang et al., 2018). In these neuronal cells, it is found that BDNF-AS positively regulates PRDM5 via sponging mir-130b-5p to facilitate neuronal apoptosis (Zhang et al., 2018), indicating a potential role of BDNF-AS in the progression of ASCI.

It has been well accepted that lncRNAs play important roles in regulating nervous system development. Given that many lncRNA knockout mice appear normal and are viable and, the association of lncRNAs and specific neurological processes still requires comprehensive investigation. Moreover, further exploration on mechanisms of lncRNA function will continue to add to our appreciation of the complex development of the nervous system.

1.4.3 The history of lncRNA H19

In my research, I find lncRNA H19 to be one of the most abundant transcripts in the early postnatal olfactory epithelium. Part of this research work focuses on understanding the physiological function of lncRNA H19 in OSN development. Here I review our current understanding of H19 regulation and function.

In the 1980s, H19 RNAs were found to be abundant in the developing mouse embryo (Pachnis et al., 1984; Pachnis et al., 1988) and H19 RNA lack conserved ORFs in both human and mouse even though it is transcribed by RNA polymerase II, polyadenylated and spliced (Brannan et al., 1990). During mouse embryogenesis, H19 is strongly expressed in endodermal and mesodermal tissues, and it is mainly found in skeletal muscle and heart in adults (Poirier et al., 1991). H19 is also found to be expressed from the

maternal allele (Bartolomei et al., 1991), and it is closely linked with paternally expressed insulin-like growth factor 2 (Igf2) in a reciprocally imprinting manner (Zemel et al., 1992). The imprinted H19-Igf2 locus is subject to complex regulation involving several differentially methylated regions (DMRs) in the Igf2 gene and at the imprinting control region (ICR) located immediately upstream of the H19 promoter, and enhancers downstream of the H19 gene (Ripoche et al., 1997; Thorvaldsen et al., 1998). The ICR contains four methylation-sensitive CCCTC-binding factor (CTCF) binding-sites mediating the assembly of a chromatin insulator that blocks interactions between the Igf2 promoter and enhancers downstream of the H19 gene, thereby silencing Igf2 expression and stimulating the transcription of H19 on the unmethylated maternal allele (Hark et al., 2000).

The regulatory functions of H19 are found to have three major components (Figure 1.5). First, H19 can serve as a direct or indirect regulator for IGF2/Igf2 (Figure 1.5A-B) (Gabory et al., 2010; Runge et al., 2000). In two types of H19 mutant mice, either deletion of 3-kb H19 transcription unit or deletion of total 13-kb including upstream ICR, there are loss of imprinting on the maternal allele and biallelic expression of Igf2 (Figure 1.5A), revealing a *cis* effect of H19 gene locus on Igf2 expression (Leighton et al., 1995; Ripoche et al., 1997). It is proposed that H19 RNA can bind to the Igf2 mRNA binding-protein 1 (IMP1) (Runge et al., 2000). IMP1 can bind to the 5'-UTR of Igf2 mRNA and maintain the stability of this mRNA (Hansen et al., 2004), suggesting that H19 could interfere with the post-transcriptional regulation of Igf2 through competing for the same IMP1 molecules (Figure 1.5B) (Hansen et al., 2004; Runge et al., 2000). The secreted protein IGF2 is highly expressed in the embryo and is a major driver of fetoplacental growth and development, and specifically controls the supply of maternal nutrients to the developing fetus (Constância et al., 2002; DeChiara et al., 1990). In contrast, IGF2 generally decreases to very low levels in most adult tissues, with notable exceptions including some

brain regions and the intestine (Bracko et al., 2012; Stewart and Rotwein, 1996; Stylianopoulou et al., 1988). IGF2 has been proposed as a critical component in memory enhancement and consolidation via promoting survival and maturation of hippocampal neurons (Chen et al., 2011). Moreover, in the hippocampal subventricular zone and subgranular zone, IGF2 is necessary for the maintenance of distinct adult epithelial stem cells, thus making it an essential factor for these stem cell niches (Ziegler et al., 2019).

Second, H19 is a developmental reservoir of miR-675-3p and miR-675-5p as both miRNAs are embedded in the H19 exon (Figure 1.5C) (Cai and Cullen, 2007; Keniry et al., 2012). H19 is also the only primary precursor of miR-675 that will in turn, post-translationally regulate a number of targets involved in cellular process, including tumor suppressor retinoblastoma (RB) and Runx1, cell growth regulator Igf1r, anti-differentiation transcription factors Smad1 and Smad5, DNA replication initiation factor Cdc6, and nodal signaling antagonist Nomo1 (Figure 1.5C) (Dey et al., 2014; Gao et al., 2012; Tsang et al., 2010; Wang et al., 2018; Zhuang et al., 2014).

Third, H19 can serve as a sponge or scaffold of micro-RNAs or proteins via direct binding (Figure 1.5C) (Kallen et al., 2013; Keniry et al., 2012). The multifaceted action of H19 may not be independent. For example, H19 interacts with HuR which has been shown to inhibit the processing of miR-675 from H19 in placenta, which decreased miR-675 and suppressed placental growth (Keniry et al., 2012). Silencing of H19/miR-675 results in placental overgrowth and HuR closely regulates the fluctuant processing of miR-675 during gestation (Keniry et al., 2012). Maternal-specific inactivation of H19 leads to reduced adult hematopoietic stem cells through Igf2 up-regulation and increased translation of Igf1r (Venkatraman et al., 2013). And upregulation of Igf2-Igf1r signaling mediates the translocation of inactive phosphorylated Foxo3, which further involved in cell-cycle arrest, resulting in increased proliferation, and eventual exhaustion of adult hematopoietic stem cells (Venkatraman et al., 2013). H19 modulates mir-let-7 family

members through harboring both canonical and noncanonical let-7 binding sites (Figure 1.5C) (Kallen et al., 2013; Ma et al., 2014a). Overexpression of let-7 could recapitulate precocious muscle differentiation cause by the H19, revealing the mutual functional interaction between H19 and let-7 (Kallen et al., 2013). H19 has been shown to guide chromatin-modifying enzymes to specific loci. In particular, H19 has been shown to bind to and recruit the histone methyltransferase EZH2 from PRC2 complex at the E-cadherin promoter, leading to an increase in H3K27me3 repressive marks and the silencing of the E-cadherin gene in bladder cancer (Luo et al., 2013). PRC2 protein members are not the only chromatin-modifying factors interacting with H19 since it has been shown that H19 physically binds to the methyl-CpG-binding domain protein 1 (MBD1) (Monnier et al., 2013). The H19-MBD1 complex is then recruited at several imprinted genes including Igf2, Slc38a4, and Peg1 (Monnier et al., 2013). This recruitment induces H3K9me3, probably via the additional interaction with H3K9 histone methyltransferase (Monnier et al., 2013).

Despite the emerging functional roles of H19, the only obvious phenotype of H19 targeted deletion mice is an increase in placental and fetal weight (Leighton et al., 1995; Ripoche et al., 1997). Whether the H19 regulatory function is specific to some tissues or cell types requires further investigation. Whether there are other tissue-specific H19 targets and their underlying mechanisms also remain to be deciphered. Similarly, the description of an H19 antisense RNA, named 91H, in both human and mouse tissues, whose characterization and function are still not fully understood (Berteaux et al., 2008; Tran et al., 2012). Therefore, it is interesting to determine whether the dynamic expression of H19 and its associative protein partners at different development periods are related to the development of olfactory epithelium and OSN projection.

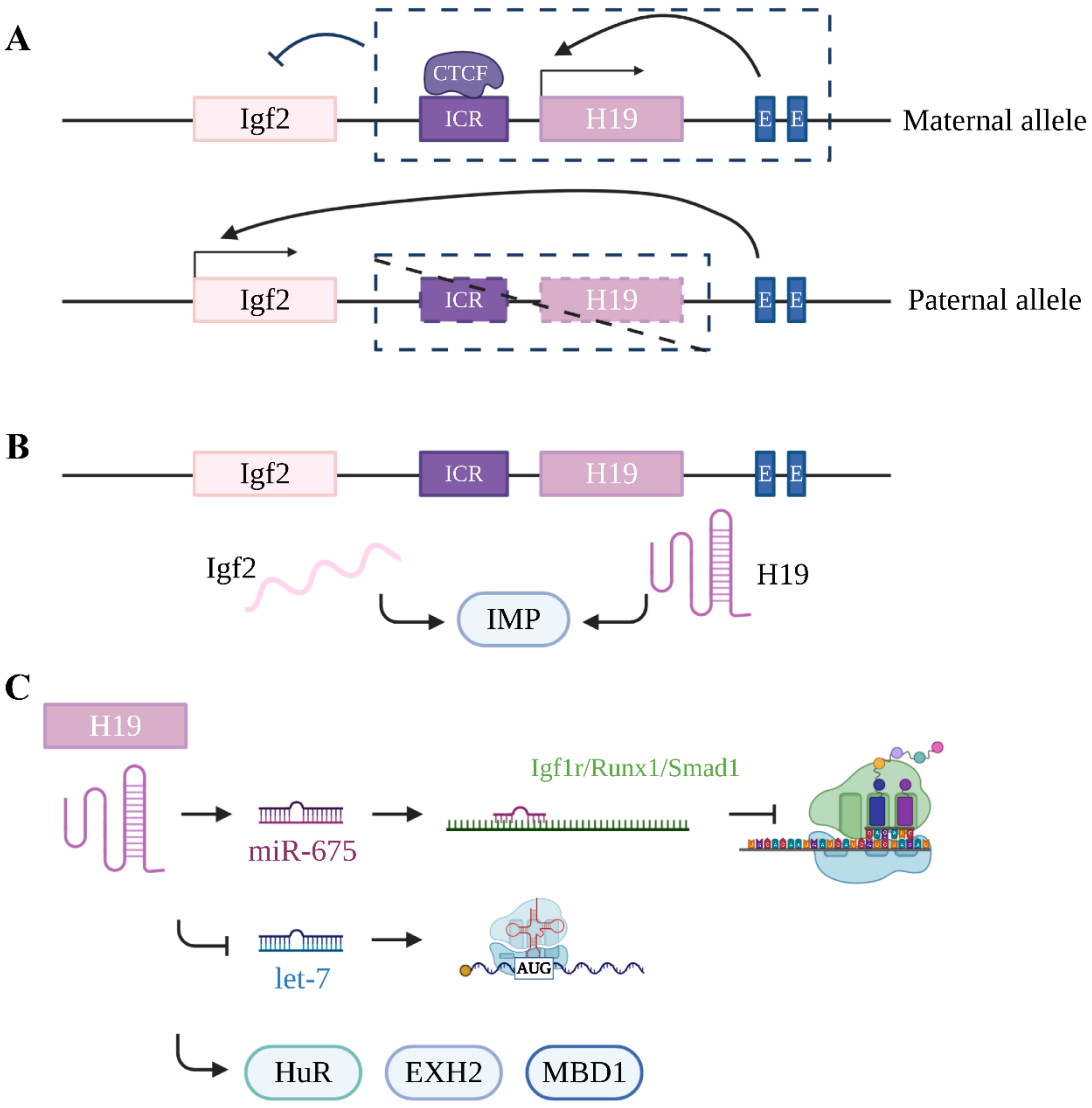

Figure 1. 5 The multifaceted action of the lncRNA H19

(A) H19 serves as a direct or indirect regulator for Igf2. Because deletion of 3-kb H19 transcription unit itself or even with ICR results in the biallelic expression of Igf2.

(B) H19 RNA competes with Igf2 mRNA for binding to IMP1 protein.

(C) H19 acts as a precursor for miR-675-5p and miR-675-3p. H19 also serves as a sponge of miRNA let-7 or as a scaffold of some proteins.

1.4.4 Role of circRNAs in neuronal development

CircRNAs are a unique class of RNA with a stable structure formed by special loop splicing. Once considered a rare event, few examples of circRNAs were described decades ago, including spliced circular transcripts from Dcc gene (Nigro et al., 1991) and circular transcript from mouse testis-determining gene Sry (Capel et al., 1993). Like the deep mining of ncRNAs, the advances in sequencing technology also enables the discovery of thousands of circRNAs, with tissue-specific and spatiotemporal expression patterns across many species like human, mouse, Drosophila and C. elegans (Memczak et al., 2013; Rybak-Wolf et al., 2015; Westholm et al., 2014). The sequencing data of ribosome-depleted RNA convincingly shows that human fibroblasts accommodate more than 25,000 unique and stable circRNAs originated from 14,4% of the expressed genes (Jeck et al., 2013). The massive sequencing data confirms that circRNAs is not a rare phenomenon and circRNAs may account for about 1% of total RNA in human (Salzman et al., 2013). Moreover, these studies have demonstrated the evolutionary conservation of circRNAs. Although most circRNAs are lowly abundant, some circRNAs are ubiquitously expressed at a higher level as compared to their linear transcripts. And the transcription of circRNAs sometimes is independent of their corresponding linear mRNAs (You et al., 2015), indicating circRNAs may possess important physiological functions.

The average length for circRNAs is 500 nucleotides (Salzman et al., 2013), and it is thus classified as lncRNA. Multiple mechanisms have been proposed for circRNA biogenesis. A commonly accepted model is circRNAs are generated from spliceosome-mediated backsplicing (Lasda and Parker, 2014). Since the circRNAs population is diverse, their biogenesis can also be through spliceosome-mediated intronic circularization (Zhang et al., 2013), and exon skipping, driven by lariat or intron-pairing mechanisms (Lasda and Parker, 2014). In addition, intronic complementary repetitive sequences and the adenosine deaminase, RNA-specific (Adar1) are linked to the circularization of exons (Ivanov et al.,

2015; Zhang et al., 2014). A remarkable feature of circRNAs is that they do not show typical features of mRNA processing, such as capping and polyadenylation, making them highly resistant to degradation by exonucleases.

CircRNAs appear to be specifically enriched in the brain. They are present abundantly in neuron cell bodies and mostly derived from synapse-related genes (Rybak-Wolf et al., 2015). At a time corresponding to synaptogenesis, many circRNAs change their abundance abruptly, suggesting circRNAs might regulate synaptic function (You et al., 2015). Analysis of 20 clinically-relevant tissues from a single human donor, 141 circRNAs are identified unique to the cortex compared to 19 other tissues (Maass et al., 2017). And several circRNAs are derived from host genes that regulate brain function. For instance, one circRNA host gene is RTN4, which encodes an inhibitor of axonal sprouting and regulates disease progression related to Alzheimer's disease (Masliah et al., 2010).

The first demonstration of circRNA function is circRNA CDR1as, which harbors over 70 binding sites for the miR-7, working as a microRNA sponge to sequester miRNAs and prevent their interactions with target mRNAs (Hansen et al., 2013; Jeck and Sharpless, 2014). However, the notion that circRNA serves as a microRNA sponge as a general mechanism of function is challenged by the fact that only a few out of thousands of circRNAs harbor multiple computer-predicted binding sites for individual microRNAs (Guo et al., 2014). Furthermore, in silico analyses suggest that circRNAs may not be more efficient than linear RNAs in binding miRNAs or RNA binding proteins (Memczak et al., 2013).

Recently, the investigation of circRNAs in the nervous system is gaining momentum. For instance, the circRNA Cdr1as knockout mice display behavioral and physiological phenotypes with neuropsychiatric disorders, indicating Cdr1as may play roles in neurodegenerative diseases (Piwecka et al., 2017). Another circRNA circHomer1 was upregulated after synaptic plasticity induction in primary hippocampal neuron culture, and

the elevated circHomer1 expression decreases the expression of the host gene Homer1b/c by competing for transcription and then inhibits plasticity (You et al., 2015).

1.5 Problem statement

Although lncRNAs, miRNAs, and circRNAs have been implicated in regulating nervous system development, very little is known about their specific mechanism. The function of lncRNAs in regulating developmental plasticity in the nervous system is unknown. I set out to study lncRNA function in the development of the mammalian olfactory system. The mouse olfactory system is characterized by "one-neuron-one-receptor" rule and is amenable to genetic manipulation *in vivo*. The OR identity can be adopted as a genetic readout to address the specificity of connection. OSN has the unusual capacity to generate new neurons throughout the lifespan. The regenerative capacity makes it possible to study how the neurons maintain specific connectivity after the circuit is fully developed. Due to the stereotypy in the axon projection, it is possible to observe any alterations by genetic manipulation of lncRNAs or circRNAs in the system. Additionally, since there are striking similarities among different species in the olfactory circuits (Ache and Young, 2005), the regulation and mechanisms of lncRNAs and circRNAs displayed in the olfactory system may be conserved across species. Considering the functional roles of ncRNAs in transcription regulation and their abundance in the neuronal system, I hypothesize ncRNAs are involved in modulating olfactory neuron development and shaping their unique molecular characteristics.

Chapter 2 Methods

2.1 Experimental Animals

All animals were maintained in Lab Animal Services Facility of Stowers Institute with a 14:10 light cycle and provided with food and water. Experimental protocols were approved by the Institutional Animal Care and Use Committee at Stowers Institute and in compliance with the NIH Guide for Care and Use of Animals. Both male and female mice were used in the experiment without discrimination. DOX treatment was performed by either weaning the pups onto DOX diet or by fostering the pups to CD1 moms fed with DOX diet at least 48 hours earlier.

C57BL/6J mice and CD1 females were obtained from Lab Animal Services Facility of Stowers Institute.

2.1.1 Transgenic mice

For tetO-H19-IRES-tdTomato transgene, the DNA fragment of H19 genomic locus was PCR-amplified from Mouse Genomic DNA (Promega, Cat#G3091).

For tetO-Adar1p150-IRES-tdTomato and tetO-Adar1La-IRES-tdTomato transgenes, the DNA fragment of Adar cDNA isoforms were PCR-amplified from a cDNA library generated from RT-PCR of mouse olfactory epithelium tissues in the lab.

For tetO-AdarE861A-IRES-tdTomato transgene, the plasmid vector was cloned from plasmid tetO-Adar-IRES-tdTomato using Gibson Assembly Protocol.

2.1.2 Mutant mice strains

The OMP-IRES-tTA (JAX:017754 B6;129-*Omp*$^{tm1(tTA)Gogo}$/J), tetO-tTA*/LacZ (JAX:008344 Tg(tetO-lacZ,tTA*)1Mmay/J), M72-IRES-tauGFP (JAX:006678 *Olfr160*^{tm6Mom}/MomJ), Ago2 (JAX: 016520 B6.129P2(129S4)-*Ago2*$^{tm1.1Tara}$/J),

ADAR1$^{flox/flox}$ (JAX: 016160 B6.129(Cg)-*Adar*$^{tm1.1Phs}$/KnkMmjax) mice were purchased from the Jackson laboratory.

H19 knockout mice are generous gifts provided by Luisa Dandolo and imported to Stowers Institute by Linheng Li.

Mice containing individual alleles were maintained by breeding with C57BL/6J strain and were mated with mice carrying other alleles for experiment.

2.2 RNA-seq library preparation and Illumina sequencing

2.2.1 Small RNA Sequencing

Mice were sacrificed using CO_2 followed by cervical dislocation. The main olfactory epithelium was dissected in ice-cold PBS and homogenized in 1 mL Trizol (Thermo Fisher Scientific). Total RNA was extracted by adding 200 µL chloroform, vortexing for 15 s, incubating at room temperature for 2 minutes, then centrifugation at 13,000 rcf for 15 minutes at 4°C. The aqueous phase was collected, and RNA was precipitated with isopropyl alcohol. The RNA pellet was washed twice with 75% ethanol, dried, then resuspended in nuclease free water. With rRNA depletion using Ribo-Zero rRNA Removal Kit (Human/Mouse/Rat) (Epicentere), RNA was subjected to indexing and library preparation using TruSeq Small RNA Library Preparation Kits (Illumina). All libraries were sequenced on an Illumina HiSeq 2500 Rapid flowcell.

2.2.2 Fluorescence activated cell sorting and RNA Sequencing

For fluorescence activated cell sorting (FACS), mice were sacrificed using CO_2 followed by cervical dislocation. The main olfactory epithelium was dissected and transferred to ice-cold PBS. The epithelium tissue was cut into small pieces with a surgery scissor, and then dissociated in 0.25% Trypsin-EDTA solution (Thermo Fisher Scientific) with 10 U/mL DNase I (New England Biolabs) and incubated for 10 minutes at 37°C with gently pipetting. After 10 minutes, the tissue was washed once with PBS (0.1 M) and 2% Fetal

Bovine Serum. the dissociated cell suspension was filtered with Filcon Sterile 30 µm syringe-type filter (BD Medimachine) and transferred to a flow cytometry tube staining with 10 µg/mL of 7-AAD in PBS. For the FACS, live cells were selected by gating out 7-AAD positive cells.

Live sorted cells were pelleted (5 minutes, 400 rcf, 4°C), the supernatant was aspirated until 250 µL of media remained, and then the cell pellet was resuspended in 750 µL Trizol. Total RNA was extracted by adding 200 µL chloroform, vortexing for 15 s, incubating at room temperature for 2 minutes, and then centrifugation at 13,000 rcf for 15 minutes at 4°C. The aqueous phase was collected, and RNA was precipitated with isopropyl alcohol with 10 µg/mL RNase-free glycogen (Thermo Fisher Scientific) added as a carrier. The RNA pellet was washed twice with 75% ethanol, dried, then resuspended in nuclease free water. After rRNA depletion using RiboGone- Mammalian Kit (Clontech), RNA-seq libraries were generated using HiSeq Rapid Cluster Kit v2 (Illumina). Sequencing libraries were profiled on Bioanalyzer 2100 using a high sensitivity DNA kit (Agilent) The libraries were sequenced on Illumina HiSeq 2500 Rapid flowcell with 100-bp single-end.

2.2.3 Bulk RNA Sequencing

RNA was extracted from mouse main olfactory epithelium using Trizol (Thermo Fisher Scientific) following the manufacturer's instructions. RNA was subjected to rRNA depletion using Ribo-Zero rRNA Removal Kit (Human/Mouse/Rat) (Epicentere) and preparation using TruSeq RNA Library Prep Kit (Illumina). Libraries were sequenced in two runs on Illumina HiSeq 2500 Rapid flowcell (Illumina) in the 100-bp single-end reads.

2.3 Single-cell RNA library preparation and sequencing

The single-cell RNA-seq (scRNA-seq) was performed with the 10x Genomics Chromium Single Cell Kit (v3.1, 10x Genomics). Approximately 50,000 single cells consisting of 10 samples were collected as previously described (Wu et al., 2018), with the number of cells recovered per samples ranging from 4,270 to 7,770. The reverse transcription, cDNA synthesis/amplification, and library preparation were performed according to the manufacturer's instructions (10x Genomics, Illumina). All samples were sequenced in two runs on NovaSeq S1 flowcell (Illumina) with 150-bp paired-end reads.

2.4 qRT-PCR

The mice olfactory epithelium was dissected, cut into small pieces, and then added to 1 mL of Trizol. Samples were vortexed for 15 s, and then incubated for 5 minutes at room temperature. Total RNA was extracted by adding 200 µL chloroform, vortexing for 15 s, incubating at room temperature for 2 minutes, then centrifugation at 12,000 rcf for 15 minutes at 4°C. The aqueous phase was collected, and RNA was precipitated with isopropyl alcohol. The RNA pellet was washed twice with 75% ethanol, dried, then resuspended in nuclease free water. 800 ng of total RNA was treated with DNase I (Ambion) and subjected to reverse transcription with SuperScriptIII (Thermo Fisher Scientific) according to manufacturer's instructions with miRNA specific primers. qPCR was performed using the second set of miRNA specific primers. Fold change was calculated using the ΔΔCT approach, using small nucleolar RNA as a reference gene to normalize between different miRNA species and expressing fold change relative to the small nucleolar RNA level at each time point.

2.5 RNA *in situ* hybridization

2.5.1 RNA fluorescent *in situ* hybridization

RNA fluorescent *in situ* hybridization was carried out according to published protocols (Ishii et al., 2004). Regions of Omp and H19 were cloned and verified by Sanger

sequencing. DNA for *in vitro* transcription was generated by PCR from these templates using an antisense primer bearing the T7 promoter. RNA probe was generated by *in vitro* transcription of 1 µg of PCR product with T7 polymerase and DIG RNA Labeling Mix (Roche). The second probe used Fluorescein RNA Labeling Mix (Roche). Probe RNA was ethanol precipitated and resuspended in 50 µL of hybridization buffer (50% formamide, 5X sodium chloride sodium citrate (SSC), 5X Denhart's, 250 µg/mL Yeast tRNA, 500 µg/mL Salmon Sperm DNA). Prior to hybridization, probe was diluted 40X in hybridization buffer and was denatured at 85°C for 5 minutes.

For RNA fluorescent *in situ* hybridization, whole olfactory epithelium was dissected, embedded and then frozen in OCT (Thermo Fisher Scientific). Coronal cryosections were taken at a thickness of 14 µm and then were dried at 95°C for 2 minutes. Slides were fixed with 4% PFA in PBS for 10 minutes. After fixation, slides were rinsed 3 times with PBS, and then washed with PBST (PBS with 0.1% Triton X-100) for 10 minutes. Slides were then rinsed once with PBS and then incubated for 15 minutes in Acetylation Buffer (0.021 N HCl, 1.2% triethanolamine (v./v.), 0.25% acetic anhydride (v./v.)). After acetylation, slides were rinsed 3 times with PBS, then probe was added and hybridized overnight at 65°C in a humid chamber. Following hybridization, slides were washed twice for 15 minutes with 0.2% SSC at 65°C, rinsed three times with PBS, and then blocked for 1 hour with TNB (0.1M Tris pH 7.5, 0.15M NaCl, 0.05% Blocking Reagent; Perkin Elmer). After blocking, slides were stained overnight at 4°C with anti-DIG-AP antibody (Roche) and anti-FLU POD antibody (Roche) diluted to 1:100 in TNB. The next day, slides were rinsed twice with TNT buffer (0.1M Tris pH7.5, 0.15M NaCl, 0.1% Tween 20) and then washed in TNT buffer for 30 minutes. Slides were then treated HNPP/Fast Red and TSA amplification with fluorescent labeling, and then washed 3 times for 10 minutes with TNT buffer. DAPI was included in the 3 times of TNT washing at a concentration of 1 µg/mL.

Slides were then mounted with Vectashield Antifade Mounting Medium (Vector Laboratories) for imaging.

2.5.2 Third-generation *in situ* hybridization chain reaction

Third-generation *in situ* hybridization chain reaction was carried out according to published protocols (Choi et al., 2018). For each target mRNA, a set of 20 DNA probe pairs was designed and purchased from Integrated DNA Technologies. For each target miRNA, one pair of DNA probes was designed and purchased.

The DNA HCR amplifier, and hybridization, wash and amplification buffers were purchased from Molecular Technologies.

Coronal cryosections were taken at a thickness of 14 µm and then 95°C dried for 2 minutes. Slides were fixed with 4% PFA in PBS for 60 minutes and then were treated with EDC for 60 minutes. After fixation, slides were rinsed 3 times with PBS, and then incubated with 1 mL of pre-heated 30% probe hybridization buffer at 37°C for 5 minutes. Slides were then treated with probe solution (30% formamide, 5X SSC, 9 mM citric acid (pH 6.0), 0.1% Tween 20, 50 µg/mL heparin, 1X Denhardt's solution, 10% dextran sulfate) by adding 4 pmol of each probe mixture (odd & even: 2 µL of 2 µM stock per probe mixture) to 1 mL of 30% probe hybridization buffer at 37°C overnight. The excess probes were removed by washing slides for 15 minutes with 1 mL of pre-heat 30% probe wash buffer (30% formamide, 5X SSC, 9 mM citric acid (pH 6.0), 0.1% Tween 20, 50 µg/mL heparin) at 37°C. The process was repeated 4 times. Following the first washing, slides were again washed twice with SSCT at room temperature and then incubated with 500 µL of amplification buffer (5X SSC, 0.1% Tween 20, 10% dextran sulfate) containing 30 pM of each fluorescently labeled hairpin. After amplification, slides were washed with 1 mL of 5X SSCT at room temperature for 5 minutes. This process was repeated 5 times. DAPI was included in the 5X SSCT wash at a concentration of 1 µg/mL. Slides were then mounted with ProLong Gold Antifade Mountant (Thermo Fisher Scientific) for imaging.

2.6 Immunohistochemistry

Immunohistochemistry was carried out according to published protocols (Ma et al., 2014b). Mice were intracardially perfused with 10 mL PBS and followed with 10 mL 4% PFA in PBS. The main olfactory epithelium and olfactory bulb were dissected and post-fixed in 4% PFA in PBS at 4°C overnight. Prior to being embedded in OCT, the olfactory epithelium was incubated in 10 mL 20% w./v. sucrose and 0.5 M EDTA overnight at 4°C.

For olfactory epithelium tissue, coronal cryosections were taken at a thickness of 14 µm and then dried at 95°C for 2 minutes. Slides were stained overnight with primary antibody in PBST (PBS with 0.1% Triton X-100) at room temperature and washed with PBST 15 minutes for 3 times on next day. Slides were then stained overnight with secondary antibody and DAPI in PBST at room temperature and washed with PBST 15 minutes for 3 times. Finally, slides were mounted with ProLong Gold Antifade Mountant for imaging.

For olfactory bulb tissue, coronal free-floating sections were taken at a thickness of 35 µm and floating staining was performed overnight with primary antibody in PBST at room temperature in a shaking platform. Slides were then washed, stained with DAPI (1 µg/mL) and secondary antibody in PBST overnight at room temperature. Following the DAPI staining, the slides were re-washed, and mounted with ProLong Gold Antifade Mountant for imaging.

Antibodies used are listed as under:

Antibodies	Source	Identifier
Goat anti-Omp	Waco	Cat#544-10001
Rabbit anti-Gap43	Novus	Cat#NB300-143
Chicken anti-β-galactosidase	Abcam	Cat#Ab9361
Chicken anti-GFP	Abcam	Cat#Ab13970
Mouse anti-Vglut2	Millipore	Cat#MAB5504

Rabbit anti-RFP	MBL	Cat#PM005
Donkey anti-goat Alexa Fluor 568	Thermo Fisher Scientific	Cat#A-11057
Donkey anti-rabbit Alexa Fluor 488	Thermo Fisher Scientific	Cat#A-21206
Donkey anti-rabbit Alexa Fluor 594	Thermo Fisher Scientific	Cat#A-21207
Donkey anti-mouse Alexa Fluor 647	Thermo Fisher Scientific	Cat#A-31571
Donkey anti-chicken Alexa Fluor 488	Jackson ImmunoResearch Laboratories	Cat#703-545-155
Donkey anti-chicken Alexa Fluor 594	Jackson ImmunoResearch Laboratories	Cat#703-585-155

2.7 iDISCO brain clearing

The iDISCO immunolabeling and tissues clearing was carried out according to published protocols (Renier et al., 2014).

2.7.1 Adenovirus production

The AdV5-CMV-mGFP was generated in the lab (Wu et al., 2018).

The AdV-shRNA-GFP was first constructed containing shRNA and GFP form shuttle vector pADTrack-CMV (Addgene plasmid #16405) using Gibson Assembly (NEB). Production of recombinant adenovirus vector AdV-shRNA-GFP was conducted by recombination of modified shuttle vector and pADeasy-1 vector (Addgene #16400) in BJ5183 cells (Agilent). The first step was to electroporate pADeasy-1 vector into BJ5183 cells, and select the clones carrying pADeasy-1 by restriction digestion mapping and sequencing. Then pADeasy-1 positive cells were made electrocompetent by washing the cells with 10% glycerol at 4°C and then transformed with linearized vector carrying shRNA and GFP. Correctly recombined plasmid was selected by kanamycin resistance and the digestion patterns of restriction enzymes PacI and NcoI. It was further confirmed

by DNA sequencing and was amplified in One Shot TOP10 Electrocomp E. coli (Thermo Fisher Scientific). Then at least 3 μg of plasmid DNA was digested with PacI and transfected into HEK293 cells using Lipofectamine 3000 (Thermo Fisher Scientific). After the formation of fluorescent plaques, adenovirus was released from the infected HEK293 cells. The collected cells and culture medium were subject to 3 freeze and thaw cycles using ethanol dry ice bath and 37°C water bath, respectively. After removing the cell pellet through centrifugation, the released viruses in the medium were further purified by polyethylglycol-8000 (PEG 8000; Sigma) precipitation. Subsequently, titer of the virus was determined by infection efficiency in Neuro-2a cells.

2.7.2 Adenovirus labeling

The noses of P0 pups were infected with the adenovirus (1 μL, 10^7-10^{13} infectious particles/mL) by inhaling the solution. After 72 hours, P3 pups with adenovirus sparse labeling were anesthetized on ice in latex gloves for perfusion with 10 mL PBS and then 10 mL 4% PFA in PBS.

2.7.3 iDISCO tissue clearing

The harvested olfactory bulb tissue was postfixed overnight at 4°C in 4% PFA in PBS, and then washed sequentially in PBS for 1 hour twice, 20% methanol (in PBS) for 1 hour, 40% methanol for 1 hour, 60% methanol for 1 hour, 80% methanol for 1 hr and 100% methanol for 1 hour twice. Samples were then washed in 2:1 dichloromethane (DCM) (Sigma)/methanol (2 volume DCM and 1 volume methanol) overnight at room temperature. The next day, samples were washed in 100% methanol for 1 hour twice, and then bleached with 5% H_2O_2/methanol (1 volume 30% H_2O_2 and 5 volume methanol, ice cold) at 4°C overnight. After bleaching, samples were washed sequentially in methanol for 1 hour twice, 80% methanol for 1 hour, 60% methanol for 1 hour, 40% methanol for 1 hour, 20% methanol for 1 hour, PBS for 1 hour twice and finally in PBS/0.2% Triton X-100 for 1 hour twice before further staining procedures.

The pretreated samples were incubated in Permeabilization Solution (PBS, 0.2% Triton X-100, 20% DMSO, 0.3 M glycine) at 37°C overnight. Then samples were incubated in primary antibody solution (primary antibody 1:1000 dilution in Permeabilization Solution and 3% donkey serum) at 37°C overnight. Following primary antibody staining, samples were washed in PBST for overnight before incubated in secondary antibody dilutions (secondary antibody 1:1000 dilution in Permeabilization Solution and 3% donkey serum, 1 µg/mL DAPI) at 37°C overnight. The immunostainings against GFP and Vglut2 were performed, and samples were finally washed in PBST for overnight before clearing and imaging.

Immunolabeled tissues were washed sequentially in PBS for 1 hour twice, 20% methanol for 1 hour, 40% methanol for 1 hour, 60% methanol for 1 hour, 80% methanol for 1 hour and 100% methanol for 1 hour twice at room temperature. Samples were then washed in 2:1 DCM/methanol for 3 hours and DCM 15 minutes at room temperature. Finally, samples were incubated in 5 mL of dibenzyl ether (DBE) (Sigma) without shaking until they became clear and then stored in DBE at room temperature until imaging.

2.8 Microscopy

All images were acquired with LSM-700, LSM-710 and LSM-780 confocal system (Zeiss).

Whole mount images of the olfactory bulb were acquired by spectral imaging. Animals were sacrificed by cervical dislocation. The skin and skull on the dorsal head were removed to expose the olfactory bulbs. Spectral imaging was conducted on LSM-710 and LSM-780. Samples were excited using 488 nm and 561 nm excitation laser and 32 channels of the detector were used, spanning 411-965 nm. Linear unmixing was conducted in the microscope software Zen (Zeiss).

The iDISCO imaging was conducted on LSM-700 and LSM-780. The sample was incubated in a glass bottom petri dish covered with DBE.

2.9 Tissue Culture

Neuro-2a cells obtained from ATCC were inoculated on 6-well plate dish and incubated with Dulbecco's modified Eagle medium (DMEM) (Invitrogen) supplemented with 10% heat-inactivated fetal bovine serum (Sigma-Aldrich) at 37°C in 5% CO_2 humidified incubator.

Transfection was performed when cells were at < 50% confluency with each construct (5 µg/dish) mixed with Lipofectamine 3000 (Invitrogen) in Opti-MEM I (Invitrogen). Media was changed after 4 hours and cells were sampled two days later.

2.10 Bioinformatic analysis

The RNA-seq aligner, Spliced Transcripts Alignment to a Reference (STAR) was used to align the sequencing reads to the mouse reference genome (mm10). Detection of circRNA was done with CIRCexplorer2 and DCC. The pipeline was run as suggested by the developers, except for an increased filtering stringency, requiring only circRNAs with one or more supporting reads within single samples to be kept.

For scRNA-seq analysis, initial gene expression tables for individual barcodes were generated using the cellranger pipeline (v3.0.0) according to instructions provided by 10x Genomics. The mean reads per cell varied from 51,345 to 69,320 with median UMI ranging from 1,773 to 12,824 per cell. All gene expression matrices were imported into R and analyzed with Seurat (v.3.2) (Stuart et al., 2019). Low-quality cells were discarded if the number of expressed genes was smaller than 200. Cells were also removed if their mitochondrial gene counts were larger than 2.5%. Doublets were detected and removed using computational tool DoubletFinder (McGinnis et al., 2019). The DoubletFinder predicts doublets according to each real cell's proximity in gene expression space to artificial doublets created by averaging the transcriptional profile of randomly chosen cell pairs, which enhances the identification of differentially expressed genes (McGinnis et al., 2019). Gene expressions of each cell were normalized by total number of molecules,

multiplied by a scale factor (10,000) per cell, and log-transformed. Highly variable genes were identified and used as input for dimensionality reduction via principal component analysis (PCA). The resulting PCs were then used as input for clustering analysis.

Chapter 3 LncRNA H19 regulates mammalian OSN development

Genetic manipulation was performed to perturb axon projection for varying lengths of time after pups were born. Perturbation beyond postnatal day 7 permanently disrupts the targeting specificity of sensory neurons (Ma et al., 2014b). In addition, the establishment of the convergence map requires perinatal sensory neurons. Late-born neurons were not able to restore convergence after perturbation (Ma et al., 2014b). Therefore, I hypothesize that a switch between the perinatal neurons and the late-born neurons results in the transcriptome change of the olfactory epithelium during the critical period. Profiling the transcriptome of the olfactory epithelia will help understand the genetic machinery utilized by the perinatal neurons, and therefore elucidate a genetic mechanism for the critical period.

Through RNA sequencing (RNA-seq) and *in situ* hybridization, I found that lncRNA H19 is one of the most abundant transcripts in the early postnatal olfactory epithelium, but its physiological function is unknown in the olfactory system. As a long non-coding RNA and the primary precursor of miR-675, H19 could work through multiple mechanisms. To probe the role of H19 function in OSN plasticity, we examined the M72 (MOR171-3, Olfr160) olfactory axon projection in H19 knockout mice. Mice deficient in H19 form a normal olfactory map, suggesting H19 is not required for axon projection. However, when the H19 knockout mice were chronically exposed to acetophenone during the critical period, the OSNs lost the ability to prune the misrouted axons. This result indicates H19 is required for early olfactory neuron plasticity. In transgenic mice that extend the expression of H19 into later stages of development, I find the induction of H19 disrupts the singular projection pattern of OSN axons and extends the lifespan of early generated OSNs, which indicates H19 may affect the longevity of OSNs and thereby affect their axon targeting.

Interestingly, I observe that overexpression of H19 in mature OSNs also results in an increased number of immature OSNs and a reduced number of mature OSNs. Nevertheless, the ectopic expression of H19 also induces the upregulation of miR-675, the miRNA embedded in the first exon of H19 locus. To determine the effect of miR-675 on this H19 overexpression phenotype, I generate a transgenic mouse line with ectopic expression of truncated H19 transcript without miR-675, which I find to display normal targeting pattern as in wild-type mice. These results suggest that H19 may function through regulating microRNAs during OSN development to influence the development of OSNs and their axon targeting.

3.1 LncRNA H19 is downregulated during postnatal development

3.1.1 RNA-seq analysis identifying differentially regulated lncRNAs during postnatal development

To identify functional lncRNAs in the olfactory transcriptome, I adopt a two-step pipeline to leverage existing RNA-seq data in the lab. First, I analyzed the whole tissue RNA-seq to broadly classify lncRNAs with dynamic expression. Next, I evaluated OSN-specific RNA-seq data to exclude transcripts that are only expressed in the mature neurons.

In order to profile the dynamically expressed lncRNAs during postnatal olfactory development, I performed bioinformatic analysis of the existing data in the lab. This whole-tissue dataset contained transcriptome sequencing data of olfactory epithelial tissues of wild-type mice at postnatal day 0, 3, 5, 7, 10, 14 and 21. Each time point had at least three biological replicates and all samples were prepared using both rRNA depletion and poly-A selection treatment.

The RNA-seq data was aligned using STAR aligner (Dobin et al., 2013) and DESeq2 package (Love et al., 2014). This method outputs the normalized counts which represent the relative expression level of each gene. To characterize the differentially expressed

lncRNAs across different time points, ANOVA analysis was used to screen for the candidates where the normalized counts between any two time points had an adjusted p-value less than 0.05. Given this criterion, we uncovered a total number of 499 lncRNAs that we defined as significantly differentially expressed ones from the RNA-seq data (Figure 3.1).

To group these lncRNAs with similar expression patterns, I performed hierarchical clustering by first calculating the spearman distance of the mean, then linked the distance using Ward.D method. To define the major clusters, I cut the dendrogram tree into 3 big branches according to their expression changes (Figure 3.1). The first cluster showed a decreasing level of expression from P0 to P21. The second cluster maintained an increasing pattern which reached a peak at P21. The lncRNAs from the last cluster had a general increasing expression with the lowest level around P7 (Figure 3.1). To further understand the genes in the three clusters, I examined the individual lncRNAs and found 244 out of 499 were annotated transcripts with little known function. Nevertheless, some well-studied lncRNAs were highly enriched at specific developmental stage (Figure 3.1). For instance, Meg3, an imprinted gene belonging to the imprinted Dlk1-Meg3 locus, was overall expressing at a relatively low level and was rapidly downregulated after P0 (Figure 3.2). Inhibition of Meg3 has been shown to reduce neuronal apoptosis through the activation of the Wnt/β-catenin signaling pathway (You and You, 2019). The downregulation of Meg3 after P0 coincides with the observation that the turnover of perinatal OSNs is faster than that of late-born OSNs (Wu et al., 2018). LncRNA Pantr1 has a similar expression pattern to Meg3 (Figure 3.2), which may be related to the proposed function of Pantr1 on regulating the differentiation of neuronal progenitors through *trans*-mediated effect on some neuronal progenitor markers (Fan et al., 2018). The Dbpht2, Neat1 and Malat1, among the most abundant lncRNA in the nervous system, were conspicuously upregulated during postnatal olfactory development (Figure 3.2)

(Clemson et al., 2009; Hutchinson et al., 2007; Nakagawa et al., 2012). In the mammalian brain, Neat1 is enriched in the nucleus and essential for nuclear paraspeckle formation (Clemson et al., 2009; Hutchinson et al., 2007). Neat1 is also an activity-dependent transcript and may control the transcription of genes encoding ion channel proteins, acting as a negative regulator of neuronal excitability (Barry et al., 2017). Moreover, the same study reports that Neat1 can directly bind to potassium channel-interacting protein KCNAB2 and KCNIP1, which modulates the excitatory response of neurons (Barry et al., 2017). Malat1 is located in nuclear foci and appears to control genes regulating synapse formation in cultured hippocampal neurons (Bernard et al., 2010). However, Malat1 knockout mouse does not give rise to any obvious prenatal and postnatal phenotype or physiological abnormalities (Eißmann et al., 2012; Nakagawa et al., 2012; Zhang et al., 2012). The exact mechanisms of Malat1 activity remain to be determined. Miat, Lockd, and H19 were significantly downregulated during postnatal olfactory development (Figure 3.2). Miat, also known as Gomafu or Rncr2, was first described in the retina where it was suggested to be primarily expressed in neurons and localize in nuclear subdomains (Blackshaw et al., 2004). The physiological role of Miat is demonstrated in cell fate commitment of progenitors and survival of newborn neurons (Aprea et al., 2013). Miat controls proliferation versus differentiation by regulating splicing of cell fate determinant Wnt7b (Aprea et al., 2013). It will be interesting to address the role of Miat in alternative splicing in the olfactory development. On the mouse genome, Lockd (lncRNA downstream of Cdkn1b) is named as it lies immediately downstream to Cdkn1b, a gene whose protein product plays a key role in regulating cell division (Toyoshima and Hunter, 1994). The promoter of Lockd locus contains binding sites for multiple transcription factors. In addition, the promoter of Lockd gene comes into direct physical contact with the promoter of Cdkn1b, and in that way acts as an enhancer to stimulate Cdkn1b's transcription (Paralkar et al., 2016). This study suggests a functional role of Lockd through its transcription and supports a paradigm that simply deleting a lncRNA locus may not be

sufficient for understanding its function. As one of the first identified imprinted lncRNAs, H19 is highly expressed in embryogenesis but is barely detectable in most tissues after birth (Gabory et al., 2010). Heretofore, H19's effect on sensory neuron function has remained enigmatic.

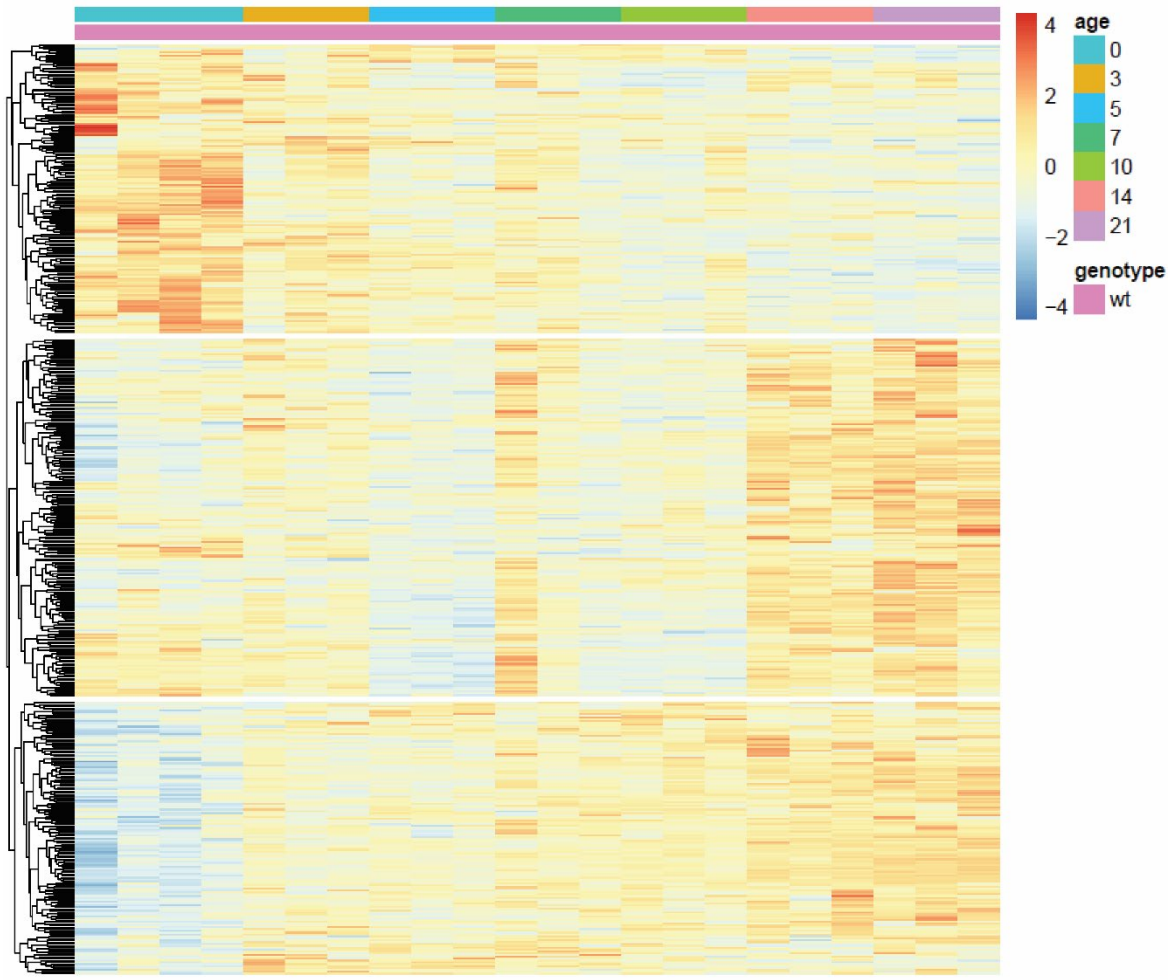

Figure 3. 1 Whole olfactory epithelia RNA-seq profile of differentially expressed lncRNAs

Heat map of differentially expressed lncRNAs. The olfactory epithelia tissues are collected from mice at P0, P3, P5, P7, P10, P14 and P21. The input materials for RNA-seq are the whole olfactory epithelia without cytometry sorting. Three major lncRNA clusters are separated by white lines. All time points are composed of three or four biological replicates. The heatmap is visualized as a Z-score matrix. The x-axis labels different postnatal time points with different colors and the y-axis lays out total 499 lncRNAs. There are three major clusters of lncRNAs according to their expression changes. Biological replicates N=3-4.

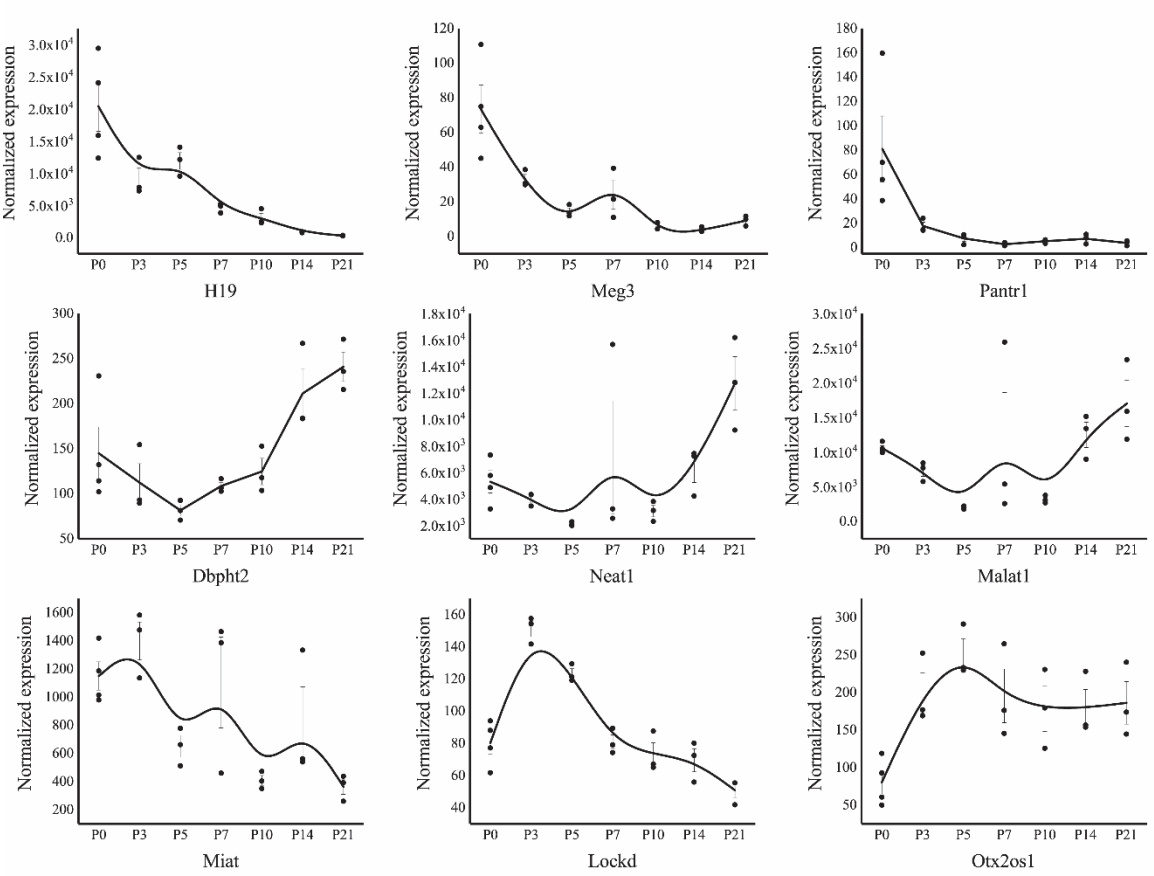

Figure 3. 2 Representative differentially expressed lncRNAs in olfactory epithelia

Normalized counts (from DEseq output) of some interesting lncRNAs across different postnatal time are plotted. The x-axis labels different postnatal time points and the y-axis lays out the normalized counts. The lncRNA H19, Meg3, Pantr1, Miat, Lockd, and Otx2os1 showed a generally decreasing pattern. The lncRNA Dbpht2, Neat1, and Malat1 were upregulated during postnatal development. Black line indicates the expression changes using a spline function (B-spline). Each dot represents a normalized count value from one RSA-seq sample.

3.1.2 H19 is the only downregulated lncRNA from FACS-seq analysis

A major caveat of whole tissue RNA-seq is the lack of robustness of detecting transcripts from a heterogeneous cell population. To resolve specific gene expression profiles in OSNs, I analyzed a parallel sequencing dataset which used fluorescence activated cell sorting (FACS-seq) to isolate specific cell types. The cell population used in FACS-seq were collected from GFP positive cells from OMP-IRES-GFP animals, which represents the mature sensory neurons.

The FACS-seq data was collected from two time points postnatal day 2 (P2) and P16. Comparing differentially expressed transcripts between the two time points showed only one lncRNA that was differentially expressed between P2 vs P16, the lncRNA H19 (Figure 3.3A). The miR-675 is not expected to be present in poly-A selected sequencing data; nevertheless, its expression can be accounted for, as reads from the precursor miR-675 sequence contained within H19 will map to miR-675 annotations. Further, the predicted genes Gm5797, Gm8246, Gm3115 and Gm6337 are actually protein coding genes with annotated protein products. In accordance with the RNA-seq data, it is reasonable to consider that H19 functions in olfactory neurons, especially in perinatal stage.

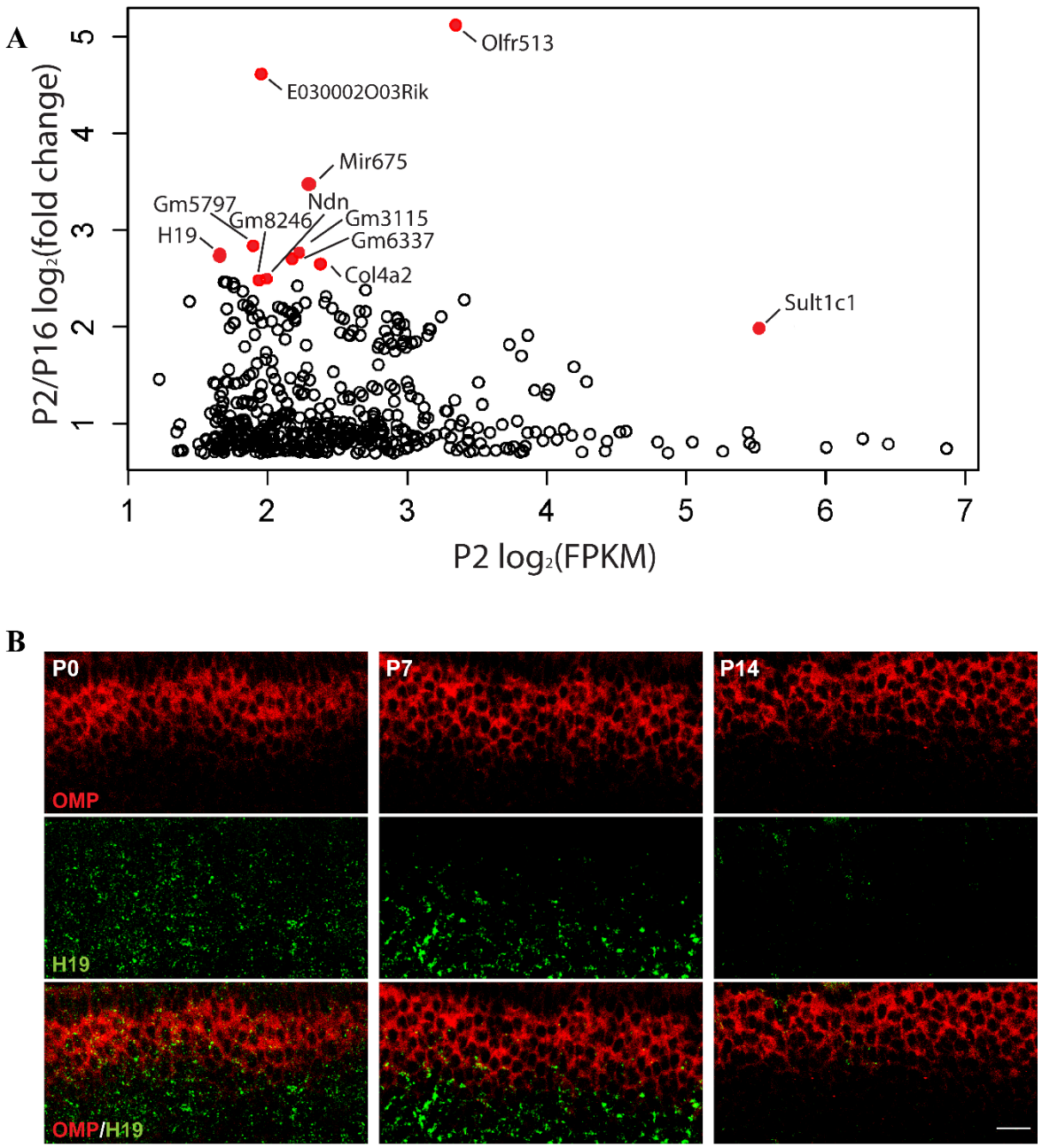

Figure 3. 3 H19 is the only downregulated lncRNA from FACS-seq analysis

(A) MA plot of downregulated transcripts in P16. The x-axis labels relative expression of each transcript and the y-axis fold change of expression between P2 and P16 for each transcript. The transcripts with a cutoff of 4-fold difference are highlighted. FPKM stands for fragments per kilobase of transcript per million mapped reads. The reads from miR-675 precursors are detected but the expression of the precursors could not to be correlated to the miR-675 expression.

(B) Two-channel confocal micrographic detection of H19 (green) and Omp (red) mRNAs in the olfactory epithelium. Scale bar, 20 μm.

3.1.3 H19 has a decreasing expression pattern during postnatal development

To reveal the subcellular location of H19 in the olfactory epithelium, I performed both fluorescence *in situ* hybridization (FISH) (Ishii et al., 2004) and single-molecule hybridization chain reaction (smHCR) (Choi et al., 2018) to visualize and quantitate H19 expression. Consistent with RNA-seq data, H19 showed a decreasing expression pattern from the FISH images (Figure 3.3B). At P0, the H19 signal overlapped with mature neuron marker Omp, indicating that H19 is highly expressed in mOSNs. However, H19 RNA was barely detected in mOSNs at P7. H19 signals were detected in the cytoplasm (Figure 3.4A), consistent with those shown in other tissue (Brannan et al., 1990). There were also some signals overlapping with DAPI (Figure 3.4A), representing either the nascent transcript or some specific function in chromatin modification. By quantifying H19 molecules (Figure 3.4B) in individual OSNs, it is clear that H19 is downregulated in mOSNs. This result matches that from the FACS-seq analysis that H19 experiences at least a four-fold decrease in expression from P0 to P21.

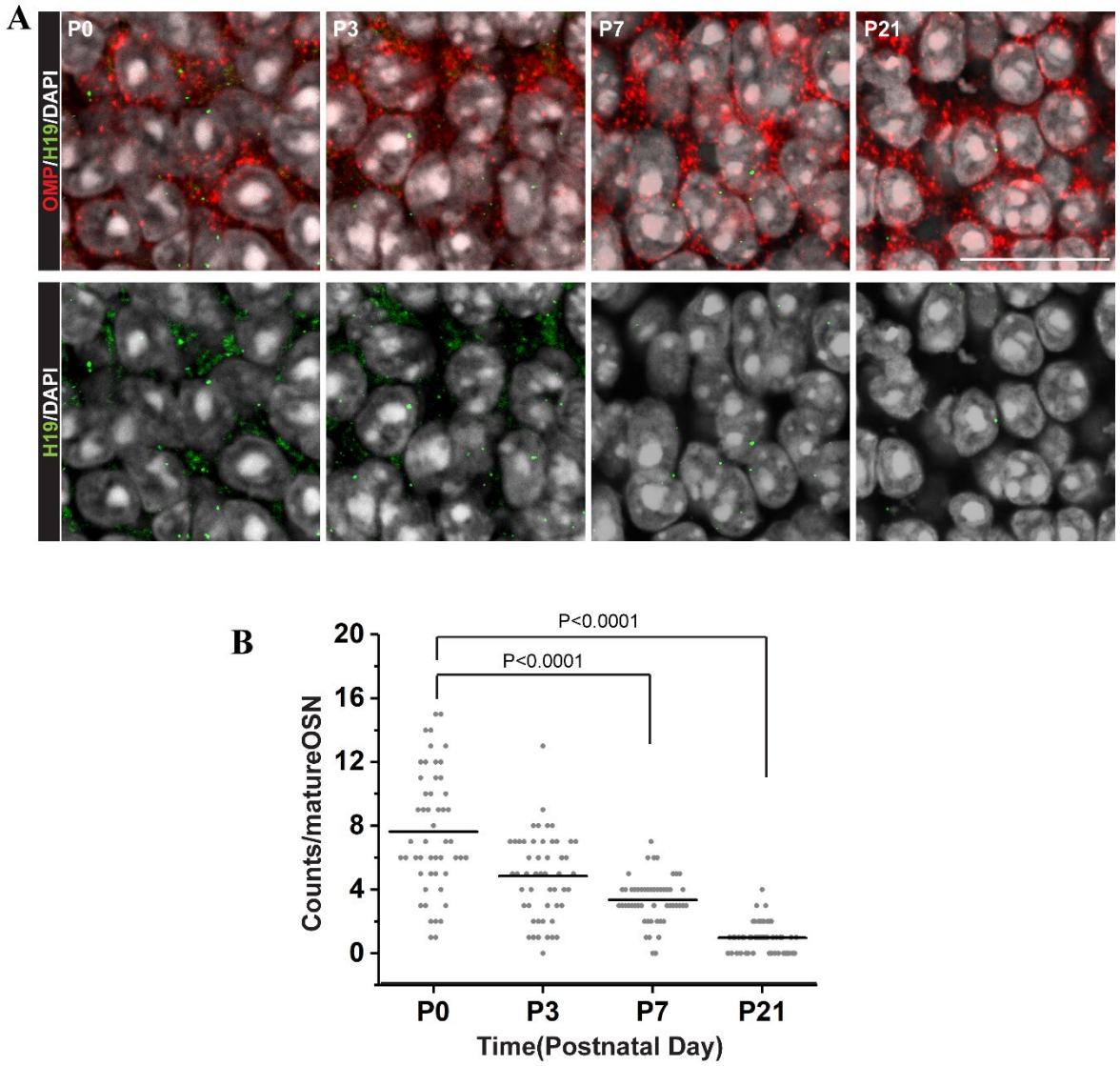

Figure 3. 4 smHCR of H19 in the mOSNs.

(A) Detection of H19 and Omp with smHCR probes separately targeting the Omp mRNA sequence (Alexa Fluor 594) and H19 RNA (Alexa Fluor 488) in the OSNs. Probe sets for H19 and Omp: 20 probes per set, each addressing 52 nucleotides target subsequence. Scale bar, 20 μm. DAPI is in white.

(B) Quantification of H19 mRNA per mOSN. Each dot represents one H19 molecule in mOSN. The horizontal bar represents the mean value. For each postnatal time point, there are three C57BL/6J mice used as biological replicates. N=36-48 (cells).

3.2 Characterization of olfactory axon projection in H19$^{mat-/-}$ mice

H19 function is closely linked to IGF signaling, as the transcription of H19 itself regulates Igf2 (Zemel et al., 1992) and miR-675 derived from H19 suppresses Igf1r in embryonic development (Keniry et al., 2012). During embryonic olfactory development, it is reported that both Igf1 and Igf2 are expressed by cells in and surrounding the olfactory bulb, whereas their receptor Igf1r is expressed in a complementary fashion on olfactory sensory axons (Scolnick et al., 2008). Igf1 serves as a chemoattractant for axon growth cones of olfactory neurons. Deletion of Igf1r results in a shift in glomerular positions in the olfactory bulb (Scolnick et al., 2008). This suggests IGF signaling is required for the normal embryonic projection of olfactory axons in the olfactory bulb.

3.2.1 Normal glomerular map is observed in adult H19$^{mat-/-}$ mice

To examine the possibility that the H19 RNA regulates OSN development, I studied an H19 mouse model (H19$^{mat-/-}$ mice) carrying a 3-kb deletion covering just the H19 transcription unit including miR-675, which specifically ablated the H19 RNA without affecting the imprinting control element (Ripoche et al., 1997). However, since H19 has never been studied in OSNs, I first performed smHCR and found that H19 was maternally expressed in the olfactory neurons (Figure 3.5A).

I sought to test whether deletion of H19 could alter the general projection of olfactory axons. I generated mice H19$^{mat-/-}$;M72-IRES-tauGFP carrying both H19 deletion alleles and an allele with OR gene M72 labeled with GFP (Potter et al., 2001) to examine the projection pattern of the M72 OSNs. Compared to the M72-IRES-tauGFP (control) animals, there was no significant change in the number and the relative target site of glomeruli in adult (P21) H19$^{mat-/-}$;M72-IRES-tauGFP animals (Figure 3.5B). Quantification of major and minor M72 glomeruli numbers also showed no significant difference (Figure 3.5C). This result indicates that H19 does not affect targeting specificity of olfactory sensory axon. Nevertheless, the interaction between H19 and IGF signaling

does not persist into adulthood since H19 is barely detected at P21 (Figure 3.4C). Therefore, it is more appropriate to examine the projection patterns of axons during the perinatal period. However, the inherent variability of axon projection pattern during this developmental stage makes it difficult to determine whether the expression of H19 could influence the axon pathfinding process of early olfactory neurons. During early development, olfactory axons project exuberantly and some glomeruli are heterogeneously innervated by more than one OSN population (Zou et al., 2004). At the same time, the ectopic innervation by the stray axons is pruned during the critical period (Ma et al., 2014b). Stray axon projection in the $H19^{mat-/-}$ mice may not be distinguishable from those normally found in the controls. If H19 does not impact the timing of the critical period, we may not observe changes that last into adulthood, either. Therefore, we opt to study this problem using odor stimulation assay.

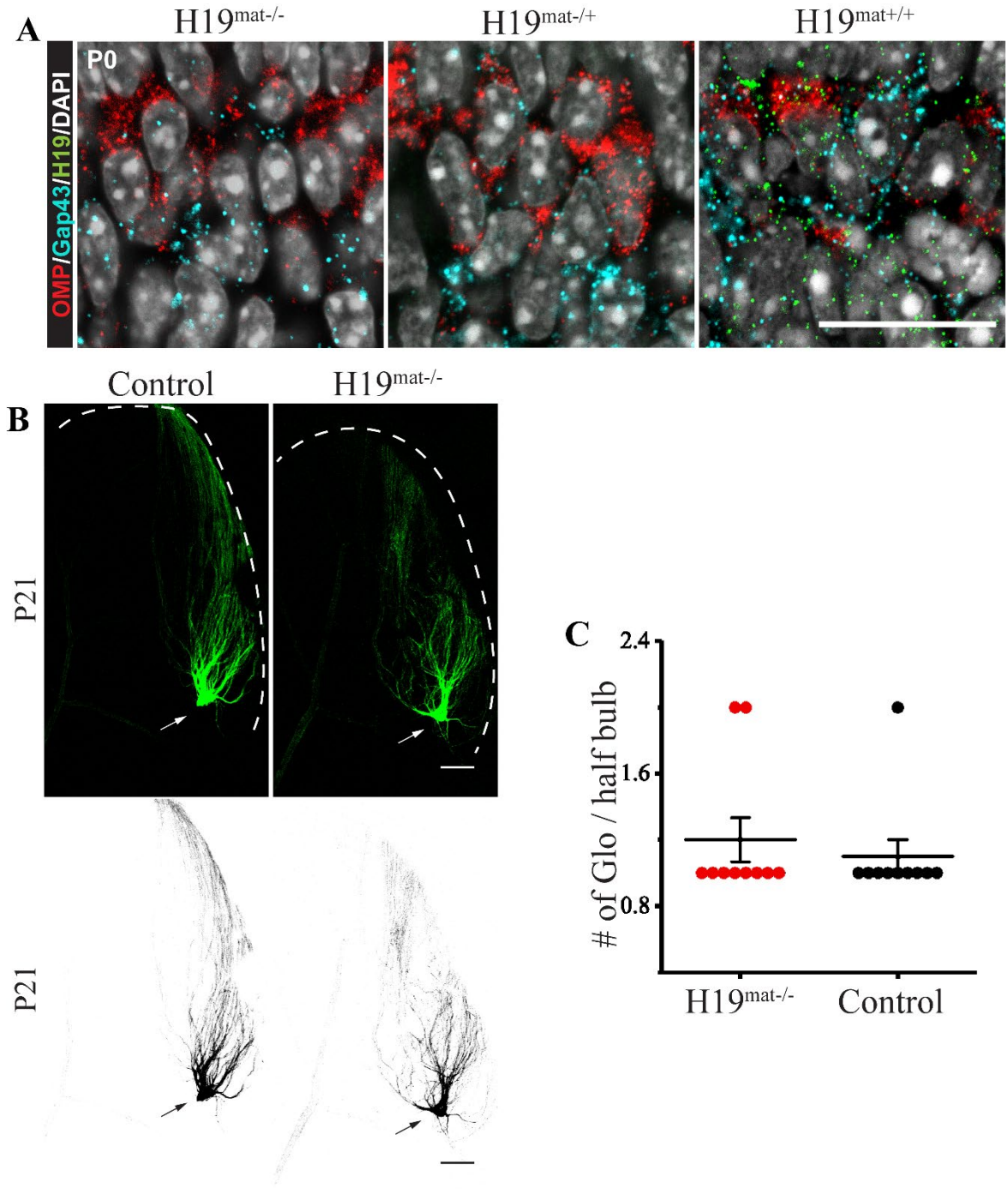

Figure 3. 5 Normal glomerular map is observed in adult H19$^{mat-/-}$ mice

(A) Identification of H19 in P0 H19$^{mat-/-}$, H19$^{mat+/-}$, H19$^{mat+/+}$ olfactory neurons. And H19 is only detected in H19$^{mat+/+}$ tissue. Three different sets of smHCR probes are applied separately targeting the Omp mRNA sequence (Alexa Fluor 594, red), H19 RNA (Alexa Fluor 488, green), and Gap43 (Alexa Fluor 647, cyan). Probe sets for H19, Omp, and Gap43: 20 probes per set, each addressing 52 nucleotides target subsequence. Scale bar, 20 μm. DAPI is in white.

(B) Whole-mount images of M72 glomeruli in M72-IRES-tauGFP (control) and $H19^{mat-/-}$; M72-IRES-tauGFP mice. The GFP signal is shown in green on the upper panel. Only the dorsal M72 glomeruli are shown here. Arrowheads indicate major glomeruli containing M72-GFP axons. Scale bar, 200 μm. The same image of upper panel is represented in gray color on the bottom panel which helps visualize the partially innervated axons or the minor glomerulus.

(C) Quantification of the number of M72 glomeruli in control (black circle) and $H19^{mat-/-}$ (red circle) mice. Each dot represents a half bulb and horizontal bars represent mean ± SEM n = 4–5 mice. one-tailed Student's t-test, no significance. Glo, glomeruli.

3.3 Knockout of H19 affects the refinement of glomerular map

To probe the necessity of H19, I used the acetophenone assay (Figure 3.6A). Acetophenone is a volatile ketone compound, which can be detected by the M72 receptor. It is shown that chronic postnatal exposure to acetophenone from birth to 20 days induces the formation of odor-specific supernumerary glomeruli. Our lab tested this assay on M72-IRES-tauGFP mice and found that if the chronic exposure to acetophenone was removed within the critical period (before P7), the singular projection of M72 axons was recovered. This is due to the heightened plasticity of OSNs during the critical period (Ma et al., 2014b; Wu et al., 2018). Following this protocol, I exposed the $H19^{mat-/-}$;M72-IRES-tauGFP to acetophenone from birth for 3 days and evaluated the M72 glomeruli in the olfactory bulb. I observed multiple partially innervated M72 glomeruli in the olfactory bulb of M72-IRES-tauGFP (control) mice 2 days after removing acetophenone. A slow refinement proceeded and by P21, there was a single M72 glomerulus each half bulb as observed in the control mice. However, in the $H19^{mat-/-}$;M72-IRES-tauGFP mice, most of the partially innervated M72 glomeruli could not be pruned and thus remained up to and after P21 (Figure 3.6B-C). This result demonstrates H19 functions in early postnatal OSNs development and is required for the refinement of exuberant axons.

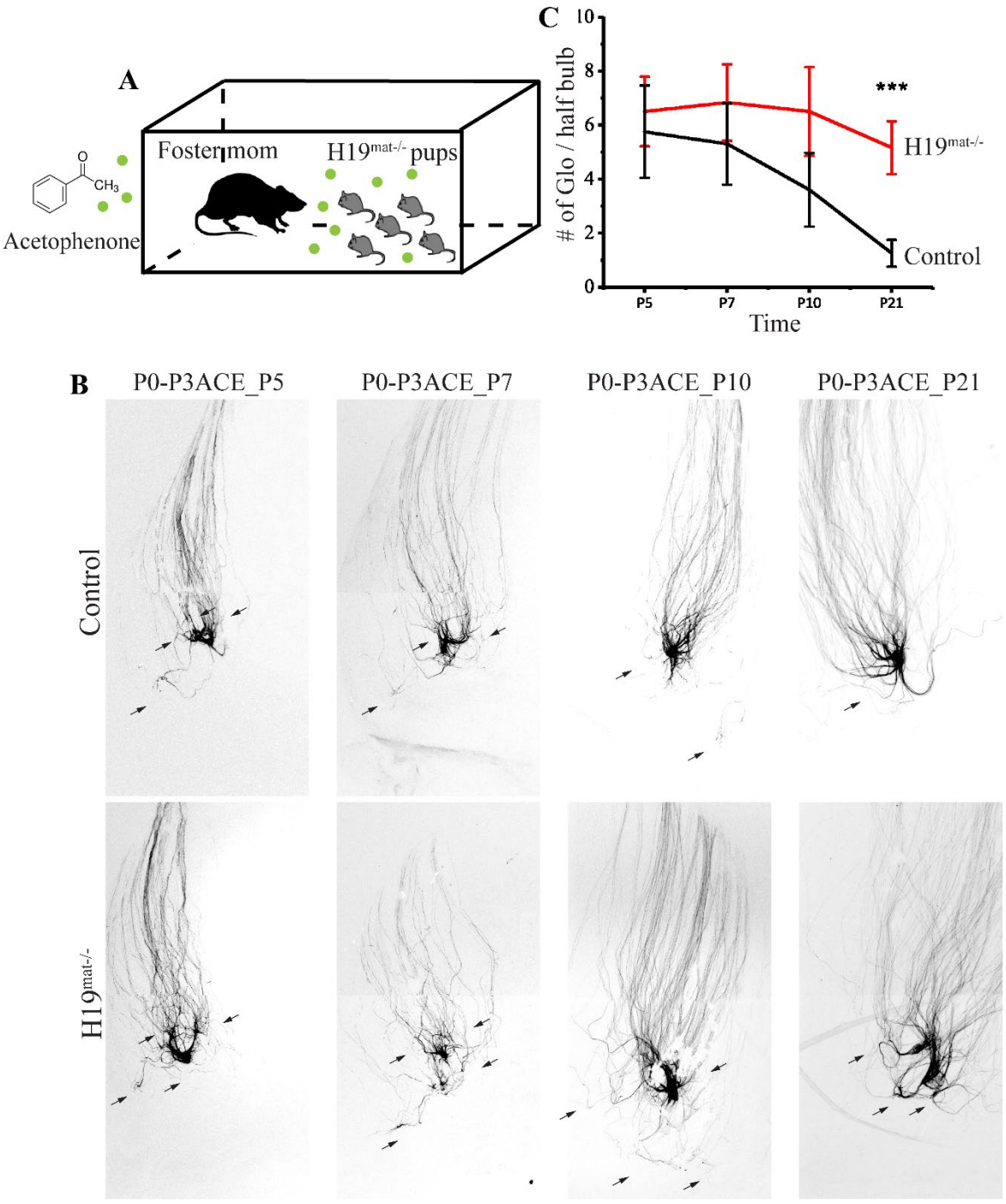

Figure 3. 6 Loss of H19 prevents the recovery of glomerular map

(A) Schematic illustration of acetophenone assay. The H19$^{mat-/-}$;M72-IRES-tauGFP mice pups are raised in cage filled with the odorant acetophenone. After P3, the acetophenone was removed.

(B) Representative images of M72 glomeruli in control and H19$^{mat-/-}$ mice after smelling acetophenone. Arrowheads represents quantified major and partially innervated glomeruli in half olfactory bulb.

(C) Quantification of the sum of major and partially innervated M72 glomeruli. M72 glomeruli in control mice, black line; $H19^{mat-/-}$ mice, red line. The bars represent mean ± SEM with p-value calculated from one-tailed Student's t test, $***p < 0.001$.

3.3.1 The perinatal OSNs are less dynamic in the absence of H19

In M72-IRES-tauGFP mice, all M72 OSNs are labeled with GFP. To explore how individual OSNs grow in $H19^{mat-/-}$ mice, I adopted recombinant adenovirus carrying CMV-membrane GFP, AdV5-CMV-mGFP (Wu et al., 2018), to sparsely label individual OSNs (Figure 3.7A). Combined with the tissue-clearing technology immunolabeling-enabled three-dimensional imaging of solvent-cleared organs (iDISCO) (Renier et al., 2014), I was able to investigate individual OSN axon paths in the olfactory bulb. For both $H19^{mat-/-}$ and wild-type control pups, I administered AdV5-CMV-mGFP at P0, and perfused the pups at P3 to allow the optimal expression of membrane GFP inside the OSN. After applying the immunostaining and iDISCO method, the labeled olfactory axons were image and traced (Figure 3.7B).

I found that the in control mice imaged at P3, olfactory axons labeled at P0 traversed along a twisting and winding path before arriving at the final glomerulus, with some branching axons were observed along with their migration (Figure 3.7C-D). By contrast, axons of $H19^{mat-/-}$ generally went directly to their destination without circling or branching out to other glomeruli (Figure 3.7C-D). This result reveals that in the absence of H19, olfactory axons are less dynamic and migrate close to a direct line.

Why do wild-type perinatal axons grow circuitously? It is identified that a group of perinatally born OSNs, called navigator neurons, undergoes a phase of exuberant axon growth during the critical period. The navigator cells are required to establish and refine a convergent glomerular map (Wu et al., 2018). From these results, P0 sensory neurons in $H19^{mat-/-}$ mice did not exhibit these navigator neuron-like properties. This raises the possibility that deletion of H19 affects, or even diminishes the navigator neuron population. Alternatively, H19 deletion may abolish the ability of the navigators to grow exuberant axons.

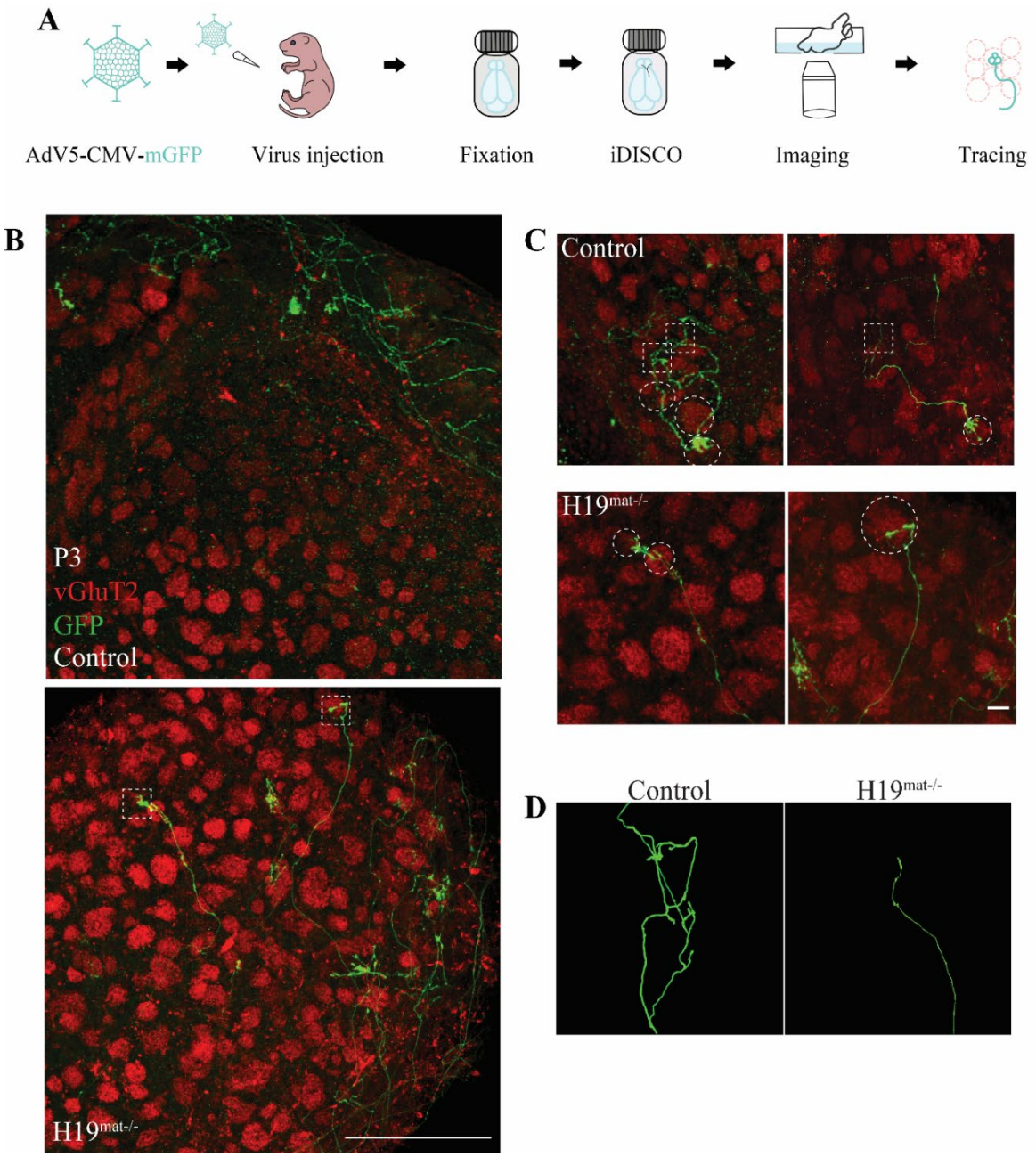

Figure 3. 7 Tracing of individual OSN axons in the olfactory bulb

(A) A schematic of the individual axon tracing method in cleared olfactory bulb. Recombinant adenovirus carrying membrane GFP is applied to label individual OSNs. The olfactory bulb is subject to tissue-clearing treatment with iDISCO and antibody staining of GFP and Vglut2 (vesicular glutamate transporter 2, for labeling individual glomerulus) at 72 hours after nasal infection. The cleared bulb is embedded and imaged using Zeiss confocal microscope. Modified from the published schematic (Wu et al., 2018).

(B) Confocal micrographs of how P0-labeled OSN axons imaged at P3. GFP, green. Vglut2 (red), which mediate the packaging of the excitatory neurotransmitter glutamate into synaptic vesicles, is strongly expressed in axon terminals of OSNs. Here the staining of Vglut2 is to label individual glomerulus. Scale bar, 200 μm.

(C) Representative confocal micrographs of individual OSN axon. The site of an axon entering a glomerulus is labeled with a circle. The branching site is labeled with square. Scale bar, 20 μm.

(D) 3D rendering of individual OSN axon. The imaged axon is processed in ImageJ using the Fiji package Simple Neurite Tracer, which semi-automatic tracing of axon structure. The path labeled in green which represents the actual axon projecting path.

3.4 Ectopic expression of H19 dramatically disrupts OSN targeting

There two possible explanations for the observation that perinatal OSNs are less dynamic in $H19^{mat-/-}$ mice. One is the deletion of H19 directly affects the navigator neuron population to prevent exuberant growth. Second, H19 is required to make OSNs retain navigator fate. These two possibilities are not mutually exclusive. It has been shown that navigator neurons do not last in the olfactory epithelium and are eliminated from the circuitry after the critical period (Wu et al., 2018). Therefore, I hypothesize extending H19 expression after the critical period in the OSNs would lead to prolonged exuberant axon growth.

To test whether ectopic expression of H19 enables prolonged navigator characters, I generated mice expressing tetO-H19-IRES-tdTomato (Figure 3.8A). This transgenic mouse line contains a tetO promoter that drives the expression of un-spliced H19 RNA (2.6 kb), as well as the fluorescent protein marker tdTomato. IRES, the internal ribosome entry site, allows for translation initiation of tdTomato in the transgene cassette. In mice carrying OMP-IRES-tTA;tetO-H19-IRES-tdTomato (tetH19 mice), the Omp promoter drives the expression of tetracycline-controlled transcription activator (tTA), and tTA binds to tetO, resulting in H19 RNA being ectopically expressed in the OSNs. The expression of H19 in tetH19 mice was examined with smHCR targeting H19 and Gap43 mRNAs. I found that H19 RNAs were highly abundant in the transgenic mice and did not overlap with iOSN marker Gap43 (Figure 3.8B). Comparing the whole-mount images of M72 glomeruli in M72-IRES-tauGFP (control) and tetH19;M72-IRES-tauGFP mice, I observed a diffused projection pattern of M72 axons (Figure 3.8C). Instead of converging to a singular glomerulus, M72 axon fibers were dispersed in the vicinity of the control M72 glomerulus position, and several axons projected towards the medial side of the olfactory bulb in tetH19;M72-IRES-tauGFP mice (Figure 3.8C). This phenotype was observed for the dorsal M72 glomerulus on both medial and lateral halves of the OB

(Figure 3.8C). These results indicate H19 ectopically expression enables prolonged navigator characters after the critical period.

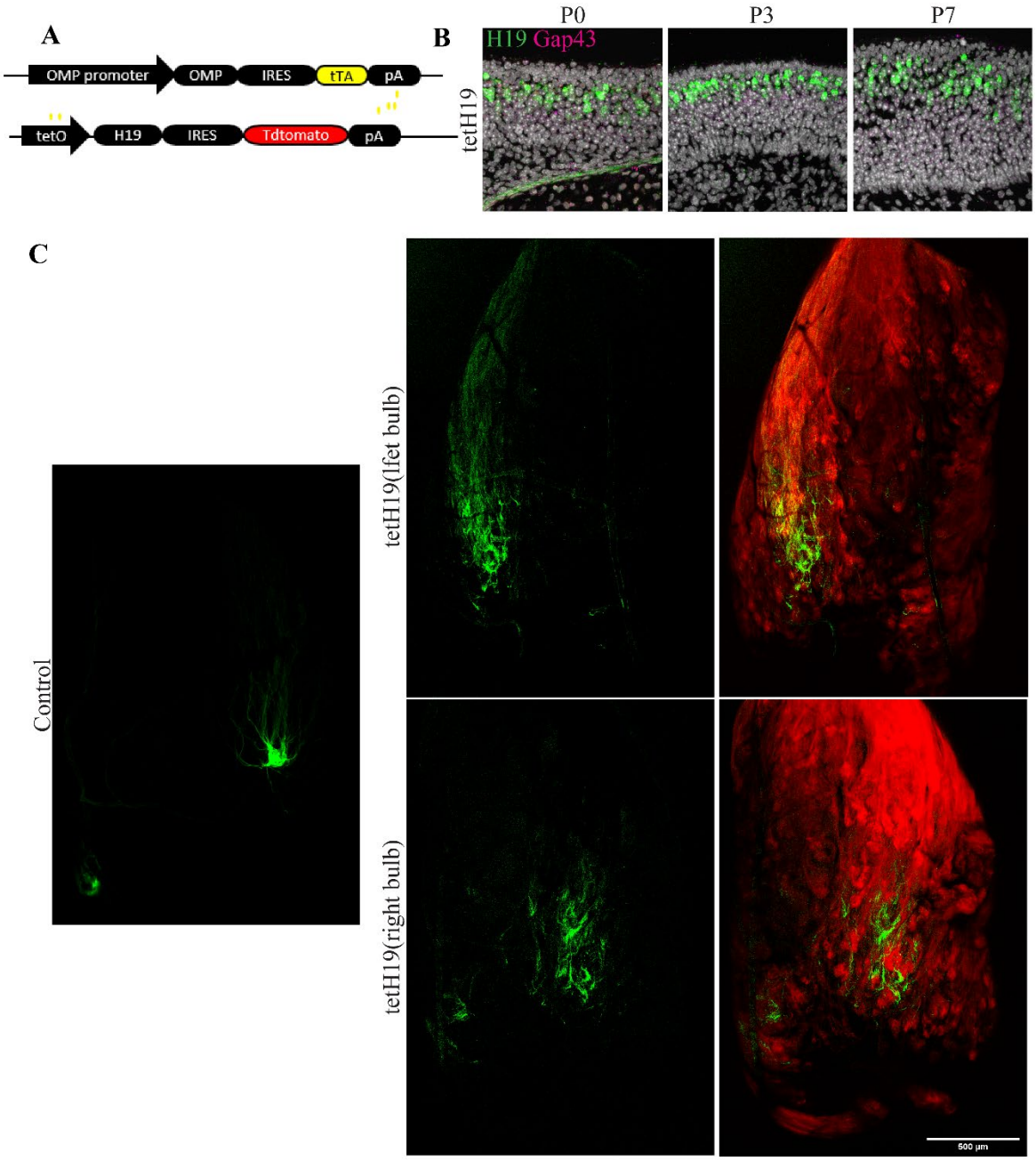

Figure 3. 8 Ectopic expression of H19 dramatically disrupts OSN targeting

(A) Schematic of ectopic expressing lncRNA H19 in mOSNs with tetH19 transgene. In the absence of DOX, Omp^{+} mOSNs express tTA which drives the expression of H19 and Tdtomato.

(B) Confocal micrographs of H19 and Gap43 in tetH19 transgene. Probes separately target the H19 RNA sequence (Alexa Fluor 488) and Gap43 mRNA (Alexa Fluor 647) in the olfactory epithelium. 20 sets of probes per gene, each addressing 52 nucleotides target subsequence. DAPI is in white.

(C) Whole-mount images of M72 glomeruli in M72-IRES-tauGFP (control) and tetH19;M72-IRES-tauGFP mice. GFP, green; tdTomato, red. Scale bar, 500 μm.

3.4.1 Early termination of H19 ectopic expression rescues OSN mistargeting

For tetH19;M72-IRES-tauGFP mice, the overexpression of H19 can be paused under doxycycline (DOX) treatment. I treated the tetH19;M72-IRES-tauGFP mice with DOX from P3, P7, or P14 to stop ectopic H19 expression (Figure 3.9A). I examined axon projections at P30. DOX administration from P3 nearly completely rescued the spreading projection of axon fibers. Discontinuing tetO-H19-IRES-tdTomato expression from P7 largely restored the diffusion of axon bundles. In contrast, the DOX diet beginning at P14 did not help for the disrupted axon convergence (Figure 3.9B). These results indicate disruption of H19 ectopic expression before the critical period restores the exuberant axon growth of OSNs.

Notably, H19 was downregulated during postnatal development and was barely detected in mOSNs at P7 (Figure 3.4A). The navigator axons are also eliminated after the critical period (Wu et al., 2018). This coincidence potentially offers a link that H19 retains the navigator neurons population before the critical period. In addition, deletion of H19 led to the loss of exuberance in OSNs (Figure 3.7C), and only ectopically expressing H19 after the critical period led to the exuberant axon growth of OSNs (Figure 3.9B). These results suggest H19 potentially affects the navigator neuron longevity to regulate axon projection.

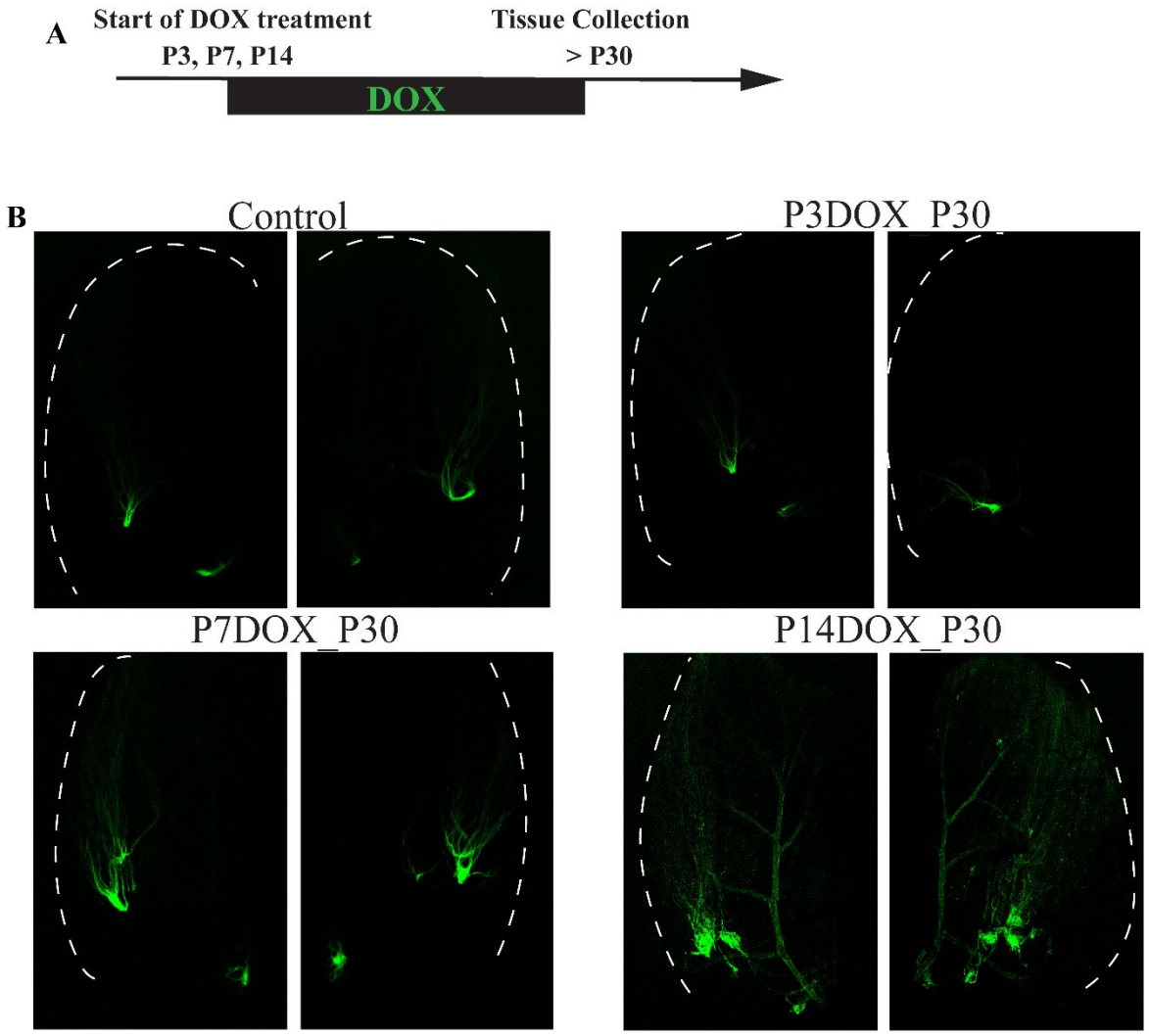

Figure 3. 9 Early termination of H19 ectopic expression rescues OSN mistargeting

(A) Schematic illustration of DOX treatment to stop ectopic H19 expression in tetH19; M72-IRES-tauGFP and control M72-IRES-tauGFP mice.

(B) Whole-mount images of M72 glomeruli in M72-IRES-tauGFP (control) and tetH19;M72-IRES-tauGFP mice treated with DOX food at different time point. DOX treatment prevents the ectopic expression of H19 and tdTomato. GFP, green. Both the dorsal and medial M72 glomeruli are shown.

3.5 Ectopic expression of H19 results in a longer lifespan of early OSNs

To test the hypothesis that overexpression of H19 leads to a longer lifespan in perinatal OSNs, I crossed tetO-H19-IRES-tdTomato transgene with OMP-TetTag (OMP-IRES-tTA: tetO-tTA*/LacZ) mice (Wu et al., 2018). The OMP-TetTag line is crossed from OMP-IRES-tTA and TetTag mice. The TetTag allele contains a bi-directional tetO promoter that can be activated by tTA to express LacZ and tTA*, a tetracycline insensitive variant (H100Y) of tTA (Reijmers et al., 2007). Thus, in OMP-TetTag mice, the mature neurons generated before DOX treatment were continuously labeled with LacZ (Figure 3.10A). When tetO-H19-IRES-tdT;OMP-TetTag mice are fed with a DOX diet, OSNs that are Omp^+ before DOX treatment will maintain LacZ/H19/tdTomato expression via the persistent activity of tTA*. With this chronogenetic tracking system, it is possible to determine the lifespan of perinatal neurons.

For both tetO-H19-IRES-tdTomato;OMP-TetTag (tetH19;OMP-TetTag) and control OMP-TetTag mice, I treated DOX at P0 and collected neuroepithelia from DOX-fed animals at P3, P7, P14, P28. P0-labeled cells were largely gone by P14 in the control mice, whereas moderate numbers of P0-labeled neurons were observed from tetH19;OMP-TetTag animals at P14 (Figure 3.10B). With the ectopic expression of H19, P0-labeled cells lived as long as 28 days (Figure 3.10B). The lifespan of navigator cells was expanded by the ectopic expression of H19 in tetH19;OMP-TetTag mice, indicating that H19 was involved in regulating neuronal lifespan.

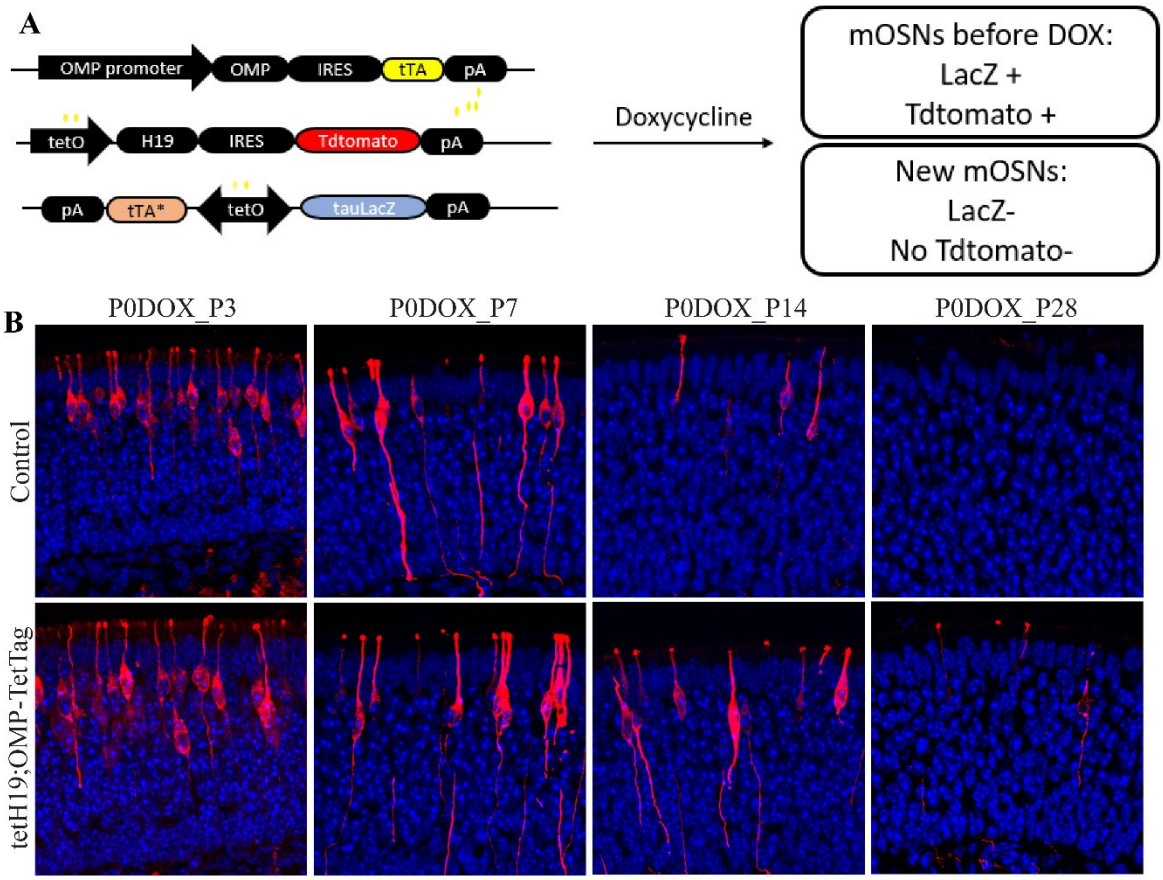

Figure 3. 10 Chronogenetic Tracing of H19 ectopically expressed OSNs

(A) Schematic illustration of labeling OSNs with tetH19;OMP-TetTag method. In the absence of DOX, Omp^+ mOSNs are labeled with both tdTomato and LacZ. When mice are fed with a DOX diet, mOSNs that are Omp^+ before DOX treatment will maintain LacZ expression via persistent activity of tTA^*. New mOSNs that become Omp^+ after DOX treatment will not express LacZ.

(B) Representative images of olfactory epithelium from P0-DOX-fed animals. Sections are stained with antibodies against β-gal (red) and DAPI (blue). OMP-TetTag and tetH19;OMP-TetTag pups are fostered starting at P0 with moms fed with DOX.

3.5.1 Overexpression of H19 leads to an increase of iOSNs

Previous study from the lab has reported that ectopic expression of anti-apoptotic gene Bcl2 also extends the survival of OSNs in the epithelium, which results in a phenotype of perturbed axon convergence (Wu et al., 2018). However, the altered olfactory axon projection pattern detected in tetH19 mice is visually different from that in Bcl2 mice, suggesting H19 may act on other aspects of OSN development. To evaluate the effect of overexpressing H19 in mOSNs, I performed immunostaining of mature marker Omp and immature maker Gap43 in olfactory epithelia sections from the transgenic mice. A difference in the ratio between Omp^+ and $Gap43^+$ neurons would indicate a change in OSN maturation. Although OSNs positive for Omp or Gap43 were still observed in the neuroepithelia of OMP-IRES-tTA;tetO-H19-IRES-tdTomato mice, there was an enrichment of immature cells that express Gap43 at P7 (Figure 3.11A). The increased number of iOSNs is thought to be associated with the apoptosis of mOSNs, which triggers the replenishment of the mOSN population. However, our tracking experiments have demonstrated an extended lifespan of mOSNs (Figure 3.11B), which is opposite to the existing hypothesis. One possibility is that the mOSNs with extended lifespan lose their mature properties and turns into “immature” neurons. To test this possibility, I performed Omp and Gap43 immunostaining in tetH19;OMP-TetTag mice at P7. I found that some P0-labeled mOSNs were still located in the mature neuron layer but were Omp-negative and Gap43-positive (Figure 3.11B). These results indicate some of the early marked OSNs have dedifferentiated to an “immature" state and resumed expressing Gap43.

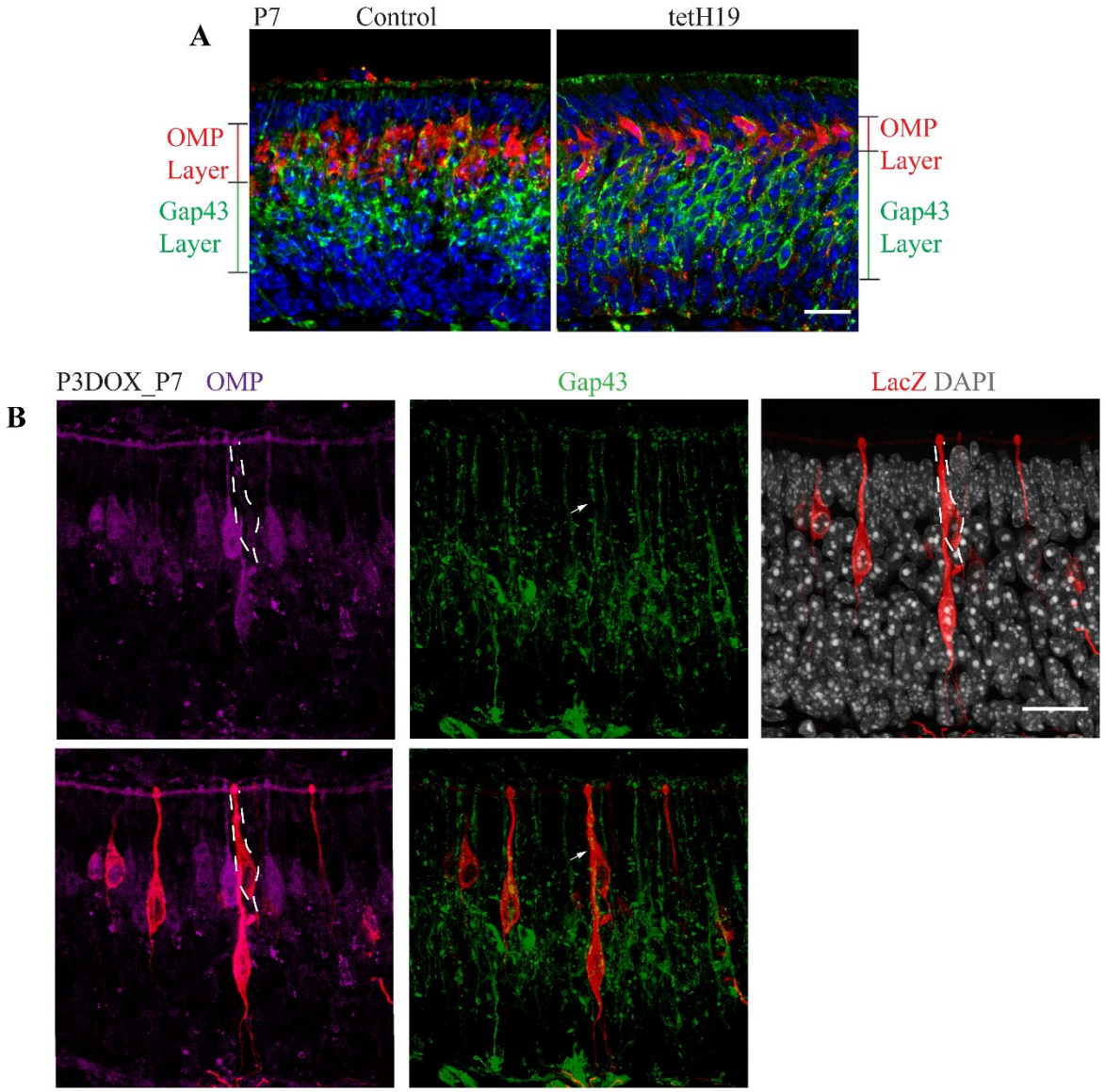

Figure 3. 11 Overexpression of H19 leads to an increase of iOSNs

(A) Altered thickness of Omp (red) layer and Gap43 (Green) layer in P7 olfactory epithelium. Sections stained with Omp and Gap43 showed a decreased amount of Omp^+ cells and an increased number of $Gap43^+$ in tetH19 mice as compared to control, indicating an increased number of immature neurons. The double-arrowhead indicates the thickness of Omp^+ neuron layer. DAPI, blue. Scale bar, 20 µm.

(B) P7 tetH19;OMP-TetTag olfactory epithelium section stained with Omp (magenta), GAP-43 (green), and LacZ (red). The white line and arrowhead indicate the P3-labeled mature $LacZ^+$ cell expresses Gap43 but not Omp in P7, suggesting it has turned into the immature neuron. DAPI, white. Scale bar, 20 µm.

3.6 Dissociation of H19 function in OSN development

What is the molecular basis of H19's function in OSNs? There are three major functional roles of H19. First, H19 can serve as a direct or indirect regulator for Igf2. Second, H19 serves as a sponge or scaffold of micro-RNAs or proteins via direct binding. Third, H19 is a reservoir of miR-675-3p and miR-675-5p and thereby determine the level of miR-675 to a certain extent.

H19/miR-675 signaling is known to inhibit Igf1r. During the embryonic stage, mutations that eliminate Igf1r cause axons destined for targets in the lateral bulb to shift to ectopic sites on the ventral-medial surface (Scolnick et al., 2008). It has been found that IGF is a chemoattractant cue for axon growth cones in primary cultures of the olfactory neuron (Scolnick et al., 2008). In mammalian adult stem cells, the Igf2-Igfr1 pathway regulates FoxO3-mediated cell cycle arrest (Venkatraman et al., 2013). Therefore, it is possible that H19 acts through miR-675 to repress Igf1r expression, which ultimately affects cell proliferation and axon targeting.

However, it remains unclear whether H19/miR-675 independently has this effect. H19 works as a sponge to soak miRNAs like the let-7 family. Let-7 inhibits the reprogramming of human cells to induced pluripotent stem cells by targeting LIN-41/TRIM71 (Worringer et al., 2014). LIN-41 further represses the translation of prodifferentiation transcription factor EGR1 to inhibit reprogramming (Worringer et al., 2014). In the mouse subventricular zone, expression of let-7 negatively regulates Lin28 to balance the fate choice of progenitor cells (Romer-Seibert et al., 2019). In *C. elegans*, the increasing level of let-7 contributes to a developmental decline in anterior ventral microtubule axon regeneration by down-regulating LIN-41 (Zou et al., 2013). Therefore, I sought to test whether H19 derives its functionality through regulating miRNAs.

3.6.1 The expression of miR-675 is positively corelated with H19

H19 produces two mature forms of miRNA-675, miR-675-3p and miR-675-5p, both of which have known functions, such as reducing cell proliferation rate by upregulating cell cycle negative regulator Rb1 (Keniry et al., 2012). However, miR-675-3p and miR-675-5p are biologically different in terms of functionality and stability. For instance, both miR-675-3p and miR-675-5p promote skeletal muscle differentiation (Dey et al., 2014). And miR-675-3p represses the BMP pathway by targeting anti-differentiation transcription factors, Smad1 and Smad5, whereas miR-675-5p represses Cdc6, a DNA replication initiation factor (Dey et al., 2014). Moreover, miR-675-3p seems to be dominantly expressed since it is more abundant than miR-675-5p during embryonic development (Keniry et al., 2012).

To identify the relationship between H19, miR-675 and the let-7 family, I first examined the expression profile of miR-675 and let-7 at different postnatal time (Figure 3.12A). I dissociated tissue from P0, P3, P7, and P21 olfactory epithelia and performed qRT-PCR of miR-675-5p and let-7 family. From a preliminary test result, 9 different species of let-7 family were detected in the OSNs. I took let-7a-5p, let-7b-5p and let-7i-5p for qRT-PCR since they each have an obvious decreasing expression during postnatal development. This method includes two steps: stem-loop reverse transcription (RT) and qPCR (Chen et al., 2005a). I used small nucleolar RNA sno202 as an endogenous control for normalization of miRNA levels. As expected, expression of miR-675-5p was highest at P0 and was remarkably reduced at P21 (Figure 3.12A), indicating a positive correlation with H19 level. The expression of the let-7 family was low at P0 but reached its peak at P21 and was anti-correlated with H19 expression. These expression patterns corroborate the proposed interaction between H19 and let-7 and provide support for the hypothesis that H19 performs its function through regulating miRNAs.

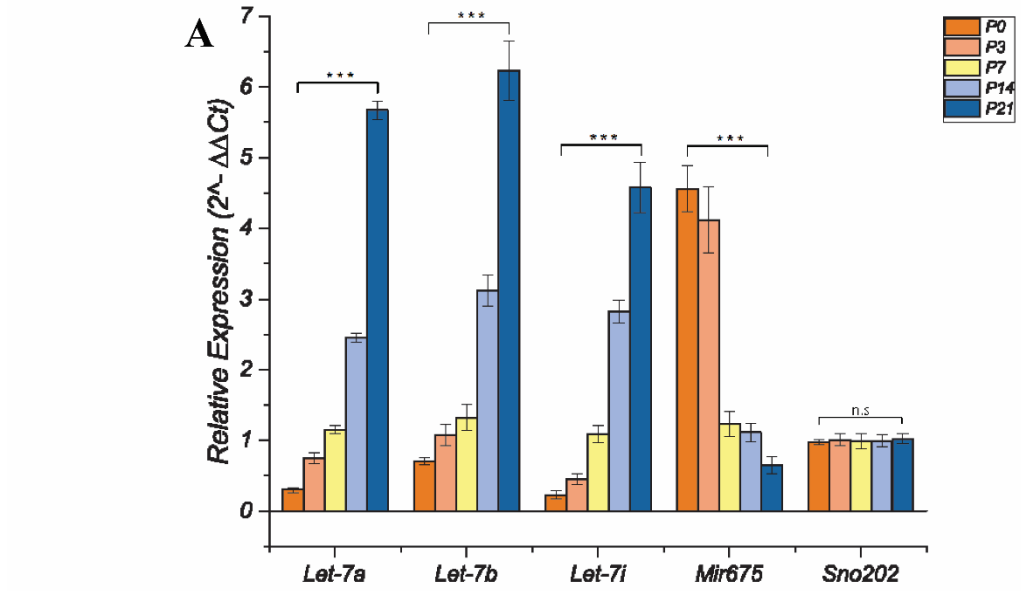
A
Relative Expression (2^- ΔΔCt)
P0
P3
P7
P14
P21
***
***
***
***
n.s
Let-7a
Let-7b
Let-7i
Mir675
Sno202

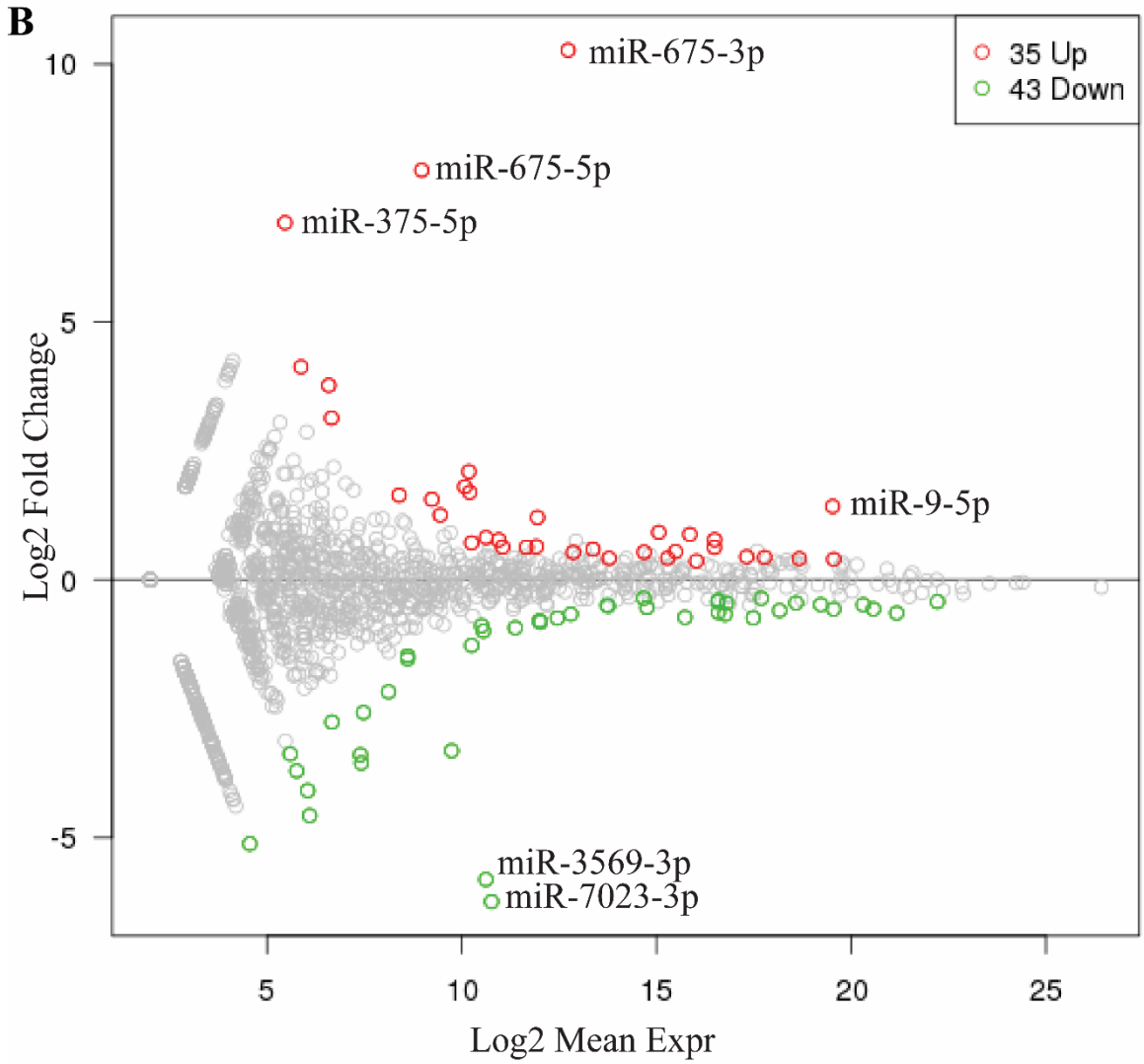
B
35 Up
43 Down
miR-675-3p
miR-675-5p
miR-375-5p
miR-9-5p
miR-3569-3p
miR-7023-3p
Log2 Fold Change
Log2 Mean Expr

Figure 3. 12 Ectopic expression of H19 remarkably induce miR-675

(A) Identification the expression of let-7a-5p, let-7b-5p, let-7i-5p and miR-675-5p by qRT-PCR in the developmental olfactory epithelia. Data are collected from 3 technical replicates and 3 biological replicates. The y-axis represents the relative expression in which each time point is normalized to the control small nucleolar RNA MBII-202 (sno-202).

(B) MA plot of total miRNAs identified in control and H19 overexpression olfactory epithelium. Small RNAs were size selected and sequenced. Each experiment has four biological replicates. The x-axis displays the normalized expression of individual miRNA in wild-type calculated by log2(meanRPKM+1), and the y-axis shows the log2 fold change of tetH19/wild-type. Red dots represent miRNAs with significant expression change (FDR >0.05; ∗∗∗p < 0.001).

3.6.2 Ectopic expression of H19 induces miR-675

As H19-miRNA interaction seems to be present in the olfactory epithelium, I dissociated olfactory epithelial tissues and performed miRNA sequencing (miRNA-seq) to compare the expression difference of miRNAs in adult OMP-IRES-tTA;tetO-H19-IRES-tdTomato and control mice. Species of miR-675 were detected to be highly upregulated with the overexpression of H19 (Figure 3.12B). The expression of both miR-675-5p and miR-675-3p were low in the wild-type epithelium (Figure 3.13), which is consistent with the qRT-PCR result that the level of miR-675-5p is low at P21 (Figure 3.12A).

I also examined the expression of let-7 in the tetH19 olfactory epithelia. Unexpectedly, among the 9 different let-7 species detected in the OSNs, let-7b-5p and let-7c-5p were upregulated in tetH19 olfactory epithelia and the other 7 let-7 species were not differentially changed (Figure 3.13). The presence of increased H19 RNAs does not reduce let-7 levels. One possibility is that both let-7b-5p and let-7c-5p were highly expressed in the wild-type tissue (Figure 3.13), which may saturate the sponge effect from H19. Alternatively, let-7 RNAs that are absorbed by H19 are not degraded and can be detected by RNA-seq experiments. Thus, the effect of H19 overexpression on let-7 is inconclusive. More works are needed to test the availability of H19 soaking let-7 in the olfactory system.

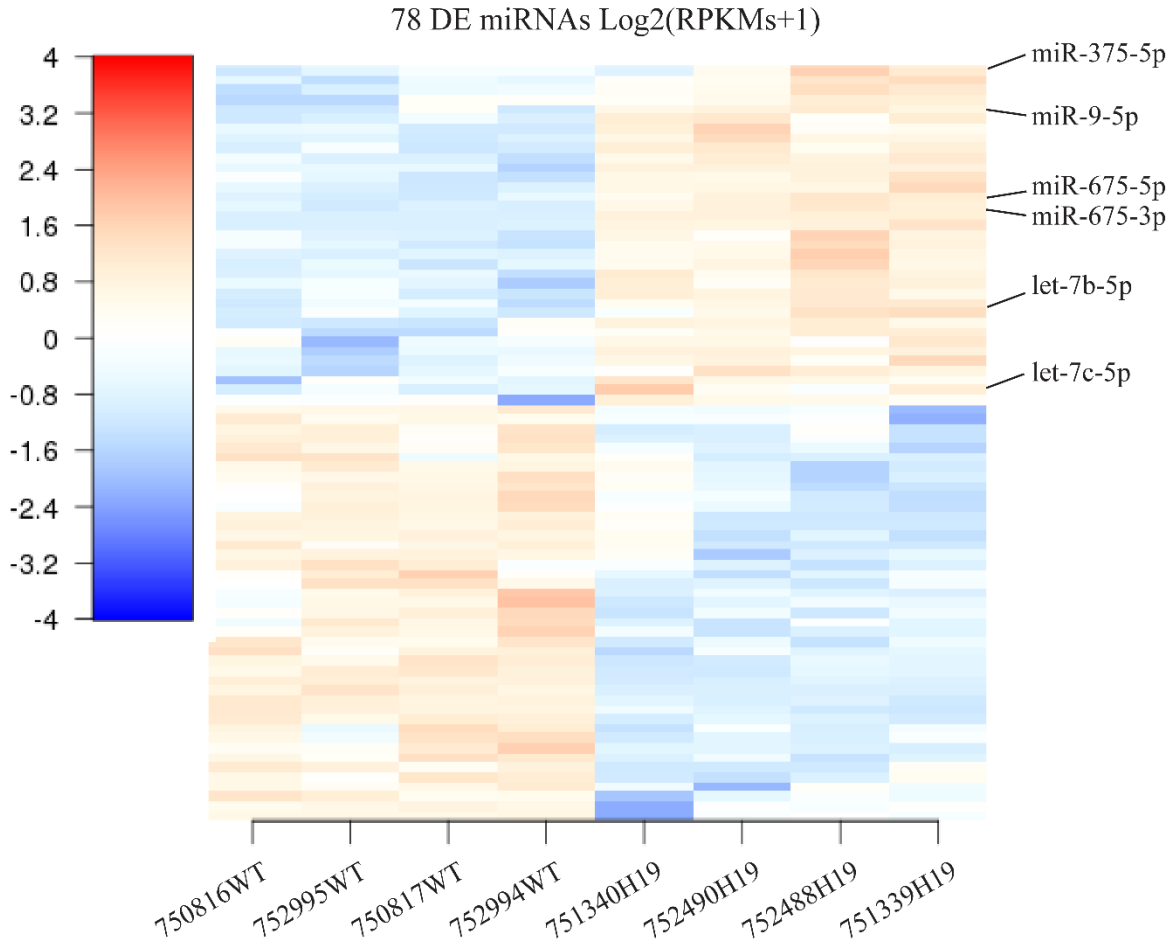

Figure 3. 13 Differentially expressed miRNAs identified in tetH19 olfactory epithelium

Heatmap of 78 differentially expressed miRNAs in OMP-IRES-tTA;tetO-H19-IRES-tdTomato and control olfactory epithelium tissue. The x-axis displays all the biological replicates. The heatmap colors represent the Z-score(log2(RPKM + 1)). Wald test of the negative binomial generalized linear model is applied.

3.6.3 Overexpression of H19 transcript without an embedded miR-675 shows normal single glomerulus pattern

Both miR-675-3p and miR-675-5p were massively induced in adult tetH19 mice (Figure 3.12B). To study miR-675 independently of H19, I generated transgenic mice expressing H19 transcript without an embedded miR-675 ($H19^{\Delta675}$), tetO-$H19^{\Delta675}$-IRES-tdTomato (Δ675 stands for deletion of miR-675 precursor), which contains a truncated H19 where an 86bp deletion removes the miR-675 precursor. I crossed the OMP-IRES-tTA:tetO-$H19^{\Delta675}$-IRES-tdTomato ($tetH19^{\Delta675}$ mice) mice with M72-IRES-tauGFP line and analyzed the whole-mount images of the olfactory bulb in $tetH19^{\Delta675}$;M72-IRES-tauGFP mice. It showed a singular glomerulus pattern, the same as in M72-IRES-tauGFP (control) adult mice (Figure 3.14A). An ideal explanation for this phenotype is that expression of miR-675 from H19 is required for H19 to result in the innervation of multiple glomeruli. However, there is another aspect deserving further attention: H19's function is structure-dependent, as H19 shows conservation in its secondary structure (Brannan et al., 1990). The ectopic expression of truncated H19 may result in the deprivation of functionality due to the change in secondary structure.

3.6.4 Ectopic expression of H19 also induces expression of miR-375 and miR-9

Notably, there were other highly differentially regulated miRNAs identified from the miRNA-seq data (Figure 3.13), which suggests miR-675 may not be sufficient to do the job of H19. Therefore, I searched the characterized functions of two new miRNAs, miR-375-5p and miR-9-5p, which were highly upregulated in tetH19 olfactory epithelium but have not been shown to be regulated by H19 (Figure 3.12B). In wild-type epithelium, it is clear that miR-375-5p was not detected (Figure 3.13). It is possible that H19 regulates the processing of miR-375. It is known that overexpression of miR-375 not only inhibits cell proliferation and differentiation, but also promotes apoptosis by binding the 3'-UTR of Notch2 and increasing Bax/Bcl2 ratio in P19 cells (Wang et al., 2016). It is also reported

that miR-375 inhibits differentiation of neurites by both destabilizing the mRNA of neuronal RNA-binding protein HuD and repressing HuD translation (Abdelmohsen et al., 2010). MiR-9 is one of the most highly expressed miRNAs in the developing and adult vertebrate brain, with identified direct targets like FoxG1, Hes1, and Tlx (Coolen et al., 2013). In spinal cord motoneurons, manipulating miR-9 levels impairs the differentiation and axonal projections of spinal motoneuron lineages, possibly through deregulation of FoxP1 protein levels (Otaegi et al., 2011). Moreover, inhibition of miR-9 in cultured neurons increased axonal length and reduced axonal branching by targeting microtubule-associated protein 1b (Map1b) (Dajas-Bailador et al., 2012). Since both miR-375 and miR-9 are involved in cell proliferation, it is necessary to explore the interaction between H19 and these miRNAs.

Due to the short length of miRNAs, it is extremely difficult to perform smHCR in the olfactory tissue sections. Thus, I transfected tetO-H19-IRES-tdTomato and tetO-H19$^{\Delta 675}$-IRES-tdTomato expression vectors along with VP22-tTA into Neuro-2a cells, and performed smHCR of miR-675, miR-375, and miR-9 *in vitro*. It is clear that transfection of tetH19 vector induced the expression of miR-675, miR-375, and miR-9 (Figure 3.14B).

In contrast, transfection of tetH19$^{\Delta 675}$ vector increased the level of miR-375 and miR-9 but not miR-675 (Figure 3.14C-D). These results confirm that ectopic expression of H19 causes the upregulation of miR-675, miR-375, and miR-9, and the overexpression of H19$^{\Delta 675}$ specifically impairs its processing of miR-675, but not of miR-375 and miR-9. Therefore, we conclude that processing to generate miR-675 is the most important aspect of H19's function in olfactory neurons.

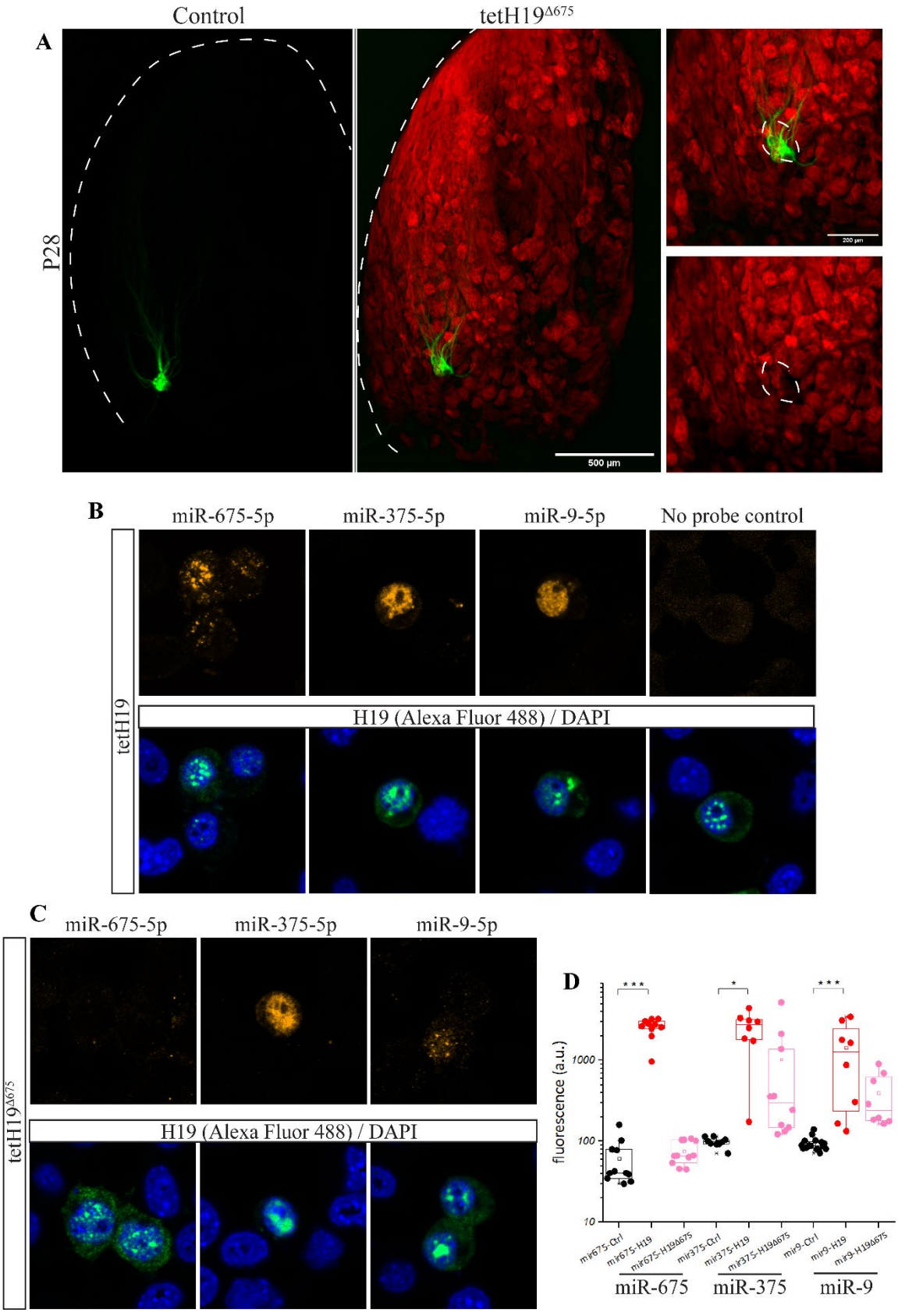
A
Control
tetH19Δ675
P28
500 µm
B
miR-675-5p
miR-375-5p
miR-9-5p
No probe control
tetH19
H19 (Alexa Fluor 488) / DAPI
C
miR-675-5p
miR-375-5p
miR-9-5p
tetH19Δ675
H19 (Alexa Fluor 488) / DAPI
D
fluorescence (a.u.)
1000
100
10
miR-675
miR-375
miR-9

Figure 3. 14 Overexpression of H19$^{\Delta 675}$ shows normal single glomerulus pattern

(A) Whole-mount images of M72 glomeruli in control and tetH19$^{\Delta 675}$ mouse. The axonal projection of mice overexpressing truncated H19 looks normal in the olfactory bulb. Scale bar, 500 μm. Mice at age P28 are shown.

(B) SmHCR detection of miR-675-5p, miR-375-5p and miR-9-5p in Neuro-2a cell with H19 transiently expressed. Only 1 probes smHCR set is used to target each miRNA (Alexa Fluor 594). The H19 RNA (Alexa Fluor 488) and DAPI (blue) are also examined in the same cell. Probe sets for H19: 20 probe sets, each addressing 52 nucleotides target subsequence. The florescence intensity is measured for quantification.

(C) SmHCR detection of miR-675-5p, miR-375-5p and miR-9-5p in Neuro-2a cell with H19$^{\Delta 675}$ transiently expressed.

(D) Quantification of florescence intensity of miR-675, miR-375 and miR-9 per cell. Each dot represents the arbitrary units (a.u.) of target miRNA smHCR signal per cell. The bars represent mean ± SEM with p-value calculated from one-tailed Student's t test, ***$p < 0.001$. N=20-25 (cells).

3.6.5 Knockdown of miR-675 in OSNs leads to the decreased exuberance of axons

To further probe the function of miR-675 independent of H19, I generated recombinant adenovirus expressing shRNA targeting miR-675 (AdV-shRNA-GFP). The knockdown efficiency was tested in Neuro-2a cells (Figure 3.15A). I administrated AdV-shRNA-GFP at P0 to wild-type pups and collected the fixed olfactory bulb tissue at P3 for immunostaining and iDISCO tissue clearing. I found that axons with miR-675 knocked down had a decreased exuberant property (Figure 3.15B) than the control pup which was administrated with AdV5-CMV-mGFP (Figure 3.7C). The olfactory axons with miR-675 knocking down were similar to the early $H19^{mat-/-}$ axons which moving along relatively straight paths (Figure 3.7C). These preliminary data show closely growing paths between knocking down miR-675 and knocking out H19 in mOSN, which suggests that H19 functions in olfactory axon projection through regulating miR-675.

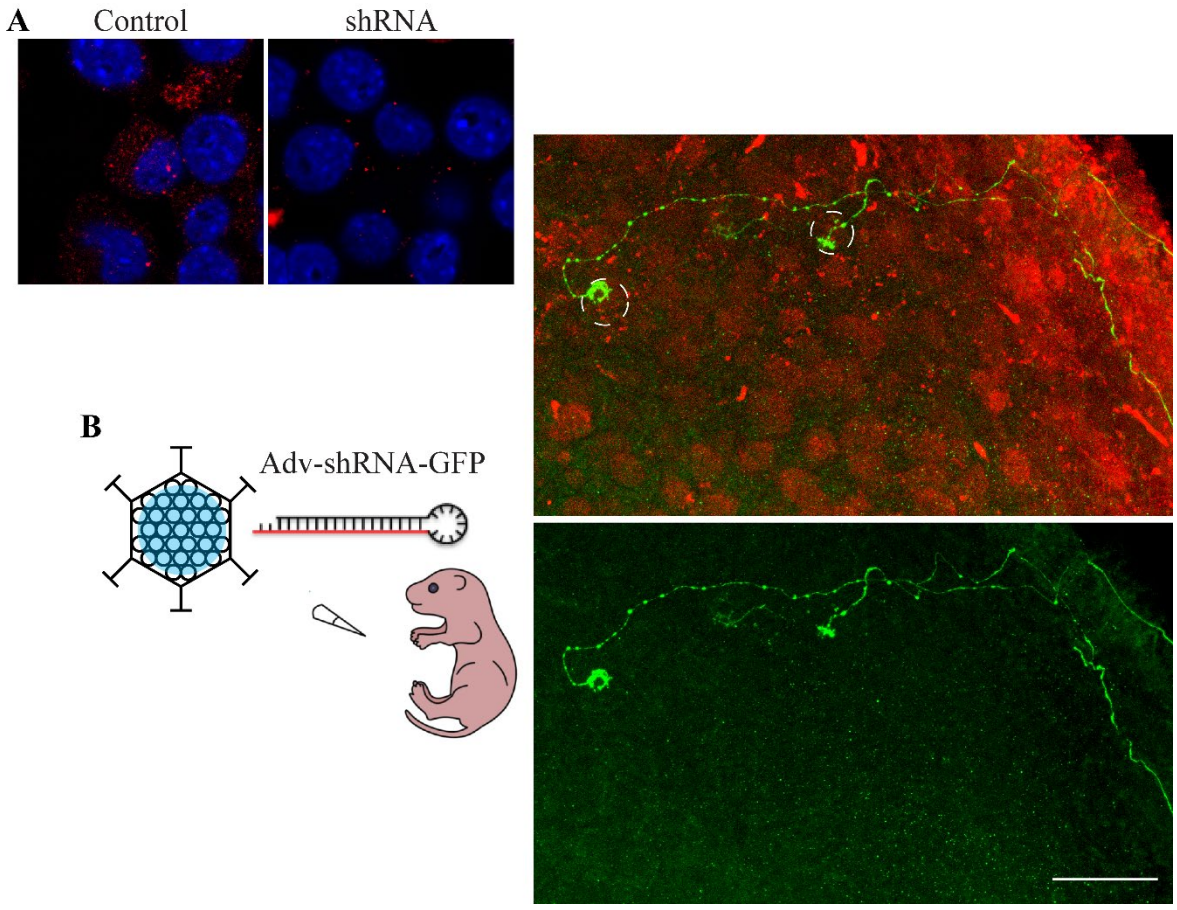

Figure 3. 15 Knockdown of miR-675 in OSNs leads to the decreased exuberance of axons

(A) SmHCR detection of miR-675-5p in Neuro-2a cells. Neuro-2a cells are fixed and subjected to smHCR 24 hours after transfection. Cells transfected with an empty vector are shown in the control panel and miR-675 shRNA transfected cells are shown in the shRNA panel. Only 1 probe smHCR set is used targeting miR-675-5p (Alexa Fluor 594). DAPI, blue.

(B) Tracing the growth of individual axons labeled with miR-675 shRNA. The left panel is schematic illustration of injecting recombinant adenovirus that expressing shRNA targeting to knock down miR-675. The right panel is the confocal micrographs the P0-labeled shRNA-miR-675 OSN axons projection trance at P3. The olfactory bulb cleared with iDISCO and stained with antibodies against GFP (green) and Vglut2 (red, labeling individual glomerulus) at 72 hours after nasal infection of AdV-shRNA-GFP. The entering glomerulus of axon terminal is labeled with circle. GFP, green; Vglut2, red. Scale bar, 50 μm

3.7 Transcriptomic analysis of potential target mRNAs of H19

It is notable that a given miRNA is often considered the master regulator of the genome as it can regulate several hundred transcripts belonging to different cellular pathways and networks. Given that H19 is a reservoir of miR-675 and both H19 and miR-675 reduction could decrease the exuberance of olfactory axons, I investigated the growth-suppressive role of miR-675 through regulation of its corresponding mRNA targets. To address the transcriptional cascades associated with H19/miR-675, I performed single-cell RNA sequencing (scRNA-seq) from $H19^{mat-/-}$ and tetH19 mutant pups as well as control littermates at P3, when H19 was downregulated during the critical period of olfactory neuron development (Figure 3.16A). Single-cell RNA sequencing could provide a comprehensive survey of cell populations in mutant mice, which improved the sensitivity to detect differentially expressed transcripts in small cell populations and resolved diversity within OSNs.

3.7.1 Transcriptomic analysis of mRNAs expression profiles in distinct mOSN populations

After doublets removal and filtration based on quality control metrics, 29,451 high-quality single cells were used to define clusters with a pipeline adopted from the published package Seurat (Stuart et al., 2019). Computational analysis using the first 35 principal components generated 29 molecularly distinct clusters. They were visualized in two dimensions via uniform manifold approximation and projection (UMAP) (Figure 3.16B). Initial inspection of the scRNA-seq data revealed subtype clusters corresponding to olfactory stem cells HBC, GBC derived cell population TAC and INP, iOSN, mOSN, microvillous cell (Mv), sustentacular cell (Sus), and other cell types on the basis of previous studies that have described marker genes (Figure 3.16B-C).

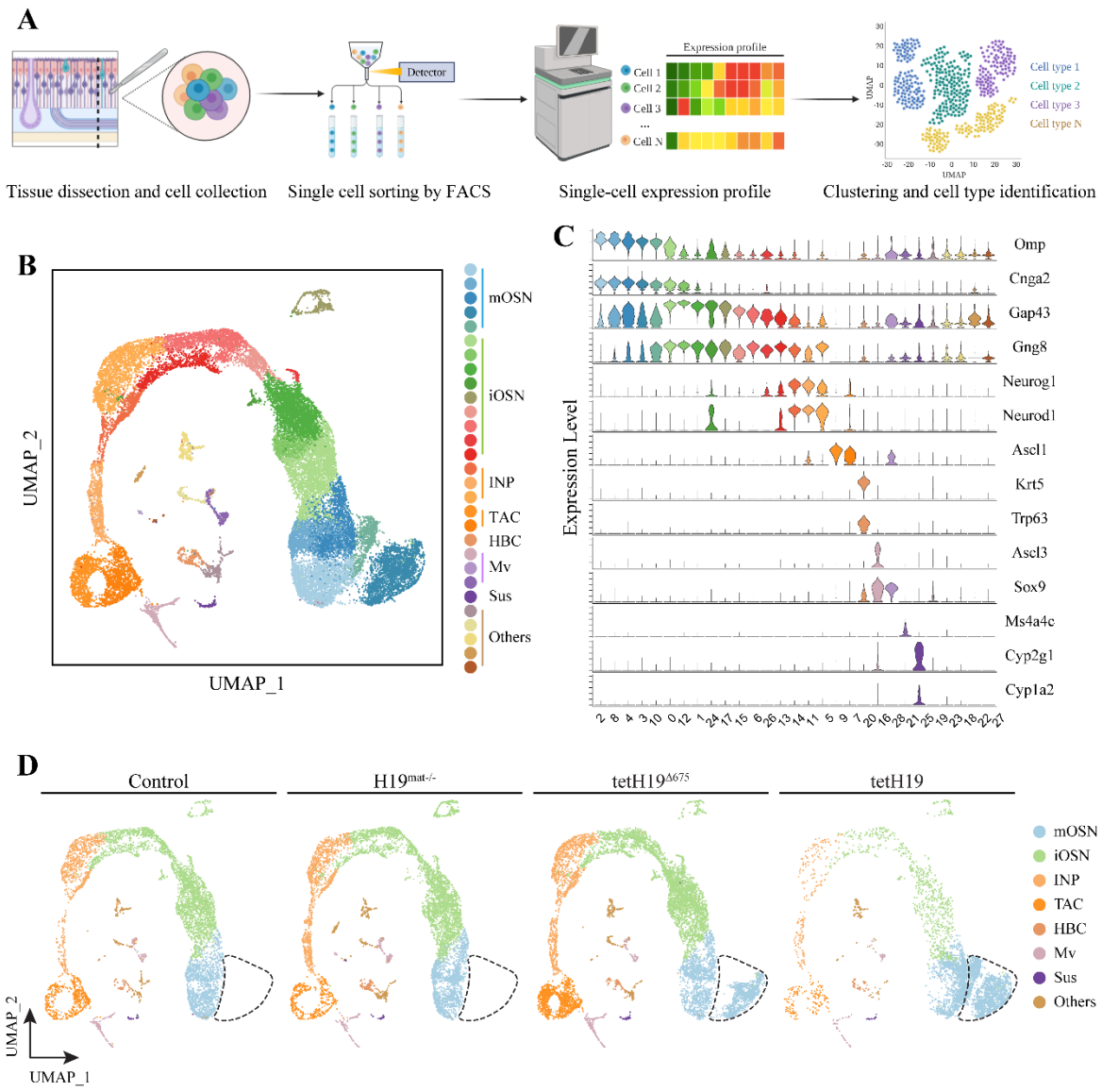

Figure 3. 16 Visualizations of scRNA-seq data for OE generated from H19$^{mat-/-}$, tetH19, tetH19$^{\Delta675}$ and control littermates

(A) Schematic presenting the scRNA-seq pipeline. OE tissue were dissociated for FACS sorting to capture live single cells. Resultant libraries were sequenced, mapped to the reference genome, and screened for doublet removal before clustering and classification.

(B) UMAP plot showing 29 clusters assigned by the expression of marker genes.

(C) Violin plots showing the expression levels of the known cell-type markers. Cell clusters are identical to those in (B).

(D) Cells from different genotypes of the animals are visualized in UMAP plots.

I first focused on the mOSNs group and found a distinct population predominantly containing P3 tetH19 mOSNs can be visualized without maximizing the cluster distance (Figure 3.16D), suggesting the variation in transcriptional programs of mOSNs ectopically expressing H19. These mOSNs were divided into two contiguous clusters (labeled with cluster 1 and cluster 2) (Figure 3.17A). Cluster 1 was found in tetH19$^{\Delta 675}$ genotype and tetH19 mice, suggesting the cells in this cluster highly are distinguished from others with or without miR675. Moreover, the most significantly differentially expressed gene in these mOSN predominant cluster 1 and cluster 2 was H19 (Figure 3.17B), further indicating this cell distribution is due to an increase in H19 level.

I next investigated the genes that were preferentially expressed in H19$^{mat-/-}$ mOSNs. Ribosomal protein L26 pseudogene Gm15772, Wdr17, and lncRNA E330020D12Rik were highly reduced in H19$^{mat-/-}$ neurons, whereas ribosomal protein S13 pseudogene Rps13-ps1 and GTPase-activating-protein Rap1gap were increased compared to controls (Figure 3.17C). A closer look indicated that cytosolic phosphoprotein Stmn1 which regulates cellular microtubule dynamics, actin monomer binding protein Tmsb10, transcription factor Fos and Junb also had a relatively lower expression when compared to wild-type mOSNs (Figure 3.17C). I performed gene ontology (GO) analysis to investigate whether these differentially expressed genes belonged to certain biological functional groups that were coordinately regulated. GO terms were predominantly associated with the microtubule-based process, especially with transport along the microtubule, cytoskeleton-dependent intracellular transport (Figure 3.17D), which is in accordance with downregulation of Stmn1, Tmsb10. Dynamic changes in the cytoskeleton are required to drive cell migration and proper axon projection in neurons (Menon and Gupton, 2016). Microtubules are composed of alpha and beta tubulin heterodimers, which form polarized linear protofilaments (Akhmanova and Steinmetz, 2008). Transcripts for three microtubule-associated proteins were downregulated (Figure 3.17C). Stmn1 encodes the

protein stathmin which participates in direct interactions of alpha/beta tubulin heterodimers (Gupta et al., 2013). Studies have demonstrated that actin filaments contribute to membrane protrusions, working in combination with stable microtubules to initiate neurite outgrowth (Dent et al., 2011; Sainath and Gallo, 2015). Tmsb10 is proposed to bind to actin monomers and function in actin polymerization (Sun et al., 1996; Yu et al., 1994). In addition, Dynlt1f is associated with cellular cargo transportation along microtubules (King et al., 1996) and actin remodeling during neurite outgrowth (Chuang et al., 2005). The reduction in cytoskeleton-associated genes in the absence of H19 may affect the dynamic properties of some intracellular filaments, which is consistent with the previous phenotype that the perinatal H19 knockout OSNs exhibit fewer dynamics (Chapter 3.3.1).

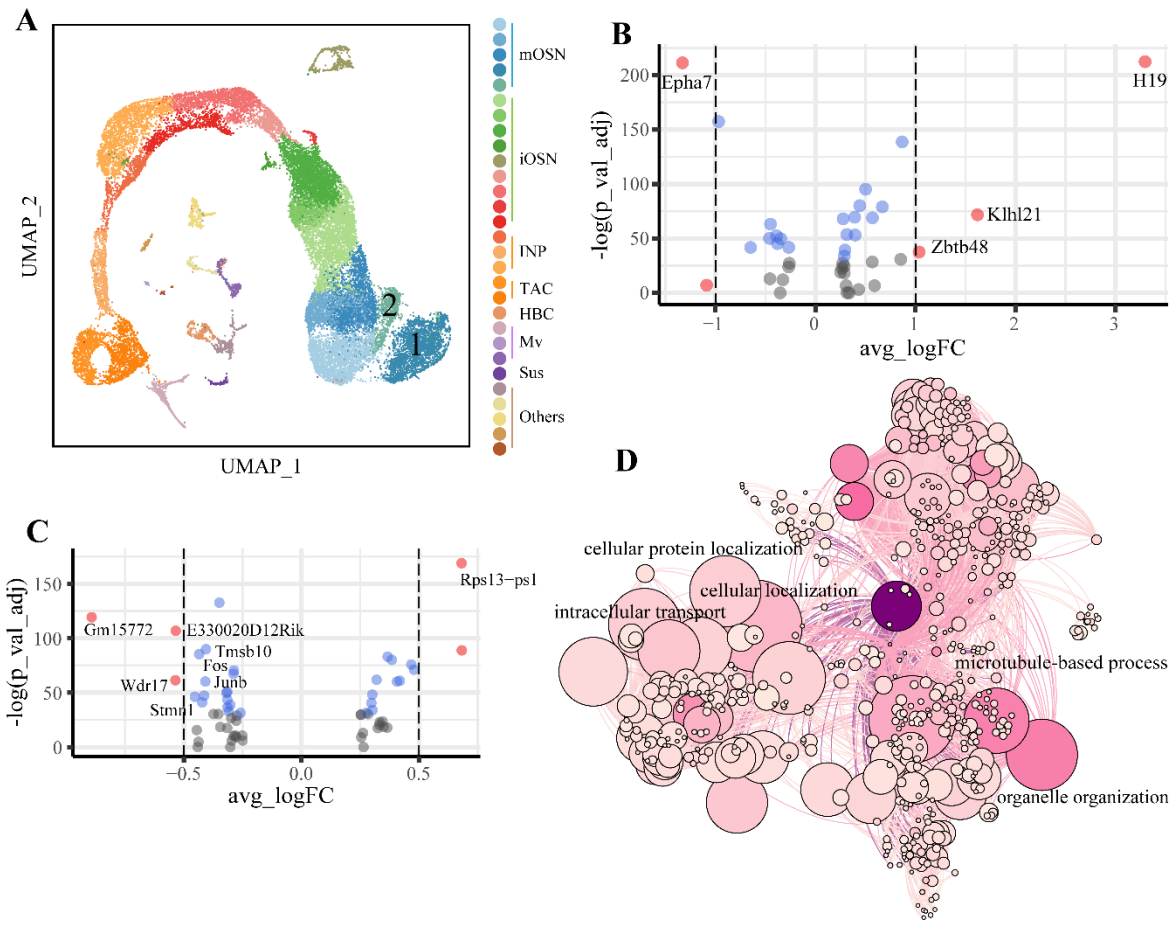

Figure 3. 17 Differentially expressed genes and GO term analyses of H19$^{mat-/-}$ mOSN populations

(A) UMAP visualization of scRNA-seq data of all genotypes. Cluster 1 and 2 label two mOSN clusters that are uniquely detected in the tetH19 mouse.

(B) Volcano plot of significantly differentially expressed genes (adjusted p-value < 0.001) from Cluster 1 and 2 mOSNs in panel (A). The average fold change in x-axis is comparing Cluster 1 to Cluster 2 mOSNs. Shades of red indicate significantly differentially expressed genes with natural log (ln) value of fold change more than 0.5, whereas blue shades represent differentially expressed genes with ln value of fold change less than 0.5.

(C) Volcano plot of significantly differentially expressed genes (adjusted p-value < 0.001) from H19$^{mat-/-}$ mOSNs compared to wild-type controls. The average fold change in x-axis is comparing H19$^{mat-/-}$ to wild-type mOSNs.

(D) GO term enrichment is represented as a hierarchical map built from differentially expressed genes in H19$^{mat-/-}$ mOSNs. The size of the circle represents the significance of enrichment using -log2 of the adjusted p-value. Color code indicates the level of

connectivity of a defined GO term. Only major GO terms are shown to simplify the graphs.

Notably, genes that were associated with immature neurons (Gap43 and Gng8) were upregulated in tetH19 mOSNs but had relatively lower expression in $H19^{mat-/-}$ mOSNs when compared to controls (Figure 3.18A), whereas the major mature markers (Omp, Cnga2, and Gnal) showed reduced expression in tetH19 mOSNs but remained upregulated in $H19^{mat-/-}$ mOSNs (Figure 3.18A), suggesting that H19 likely retains some premature neural differentiation characteristics in the OSNs. This is consistent with our finding that the ectopic expression of H19 affects the mature state of the OSNs (Chapter 3.5.1). Furthermore, manipulation of H19 altered the expression of OSN-specific transcription regulators (Figure 3.18A). Genes including Lhx2, Ebf1, and Hdac2 were upregulated in the tetH19 mOSNs, whereas activating transcription factor gene Atf5 was reduced (Figure 3.18A). Loss of Atf5 leads to a massive reduction in mature OSNs resulting from a differentiation defect and the induction of apoptosis (Wang et al., 2012). Lhx2 and Ebf regulate singular odorant receptor expression (Monahan et al., 2019; Monahan et al., 2017) which is an important function that permits OSNs maturity. Histone deacetylases Hdac2 is more specific to iOSNs in OE (Nickell et al., 2012) and is proposed to regulate olfactory activity (Tepe et al., 2018; Yamakawa et al., 2017). These results further suggest that H19 regulates terminal differentiation of OSNs.

Given our initial analysis of the graph-based representation of tetH19 mOSNs distribution, I also determined the consequences on the transcriptome. Although H19 knockout mainly affects microtubule-associated genes, many differentially expressed genes in tetH19 mOSNs were largely neuron-specific, such as neuronal intermediate filament protein Prph, neuronal vesicle trafficking-associated protein Nsg1 and Nsg2, neuronal leucine-rich repeat protein Lrrn3, calcyon neuron-specific vesicular protein Caly and calmodulin Calm1 (Figure 3.18B). Additionally, the most enriched GO terms in biological pathways were related to negative regulation of neurogenesis, neuron differentiation, negative regulation of cell development, and nervous system development (Figure 3.18C). The

highest enriched terms in cellular components were related to neuron part and synapse. To elucidate the mechanism of H19/miR-675-mediated regulation, I performed KEGG pathway analysis and found that cell adhesion molecules, genes related to the synaptic signaling as well as apoptosis pathway were preferentially expressed in tetH19 mOSNs. These observations are highly related to the previous data that induction of H19 disrupted the singular projection pattern of OSN axons and extended the lifespan of early generated OSNs.

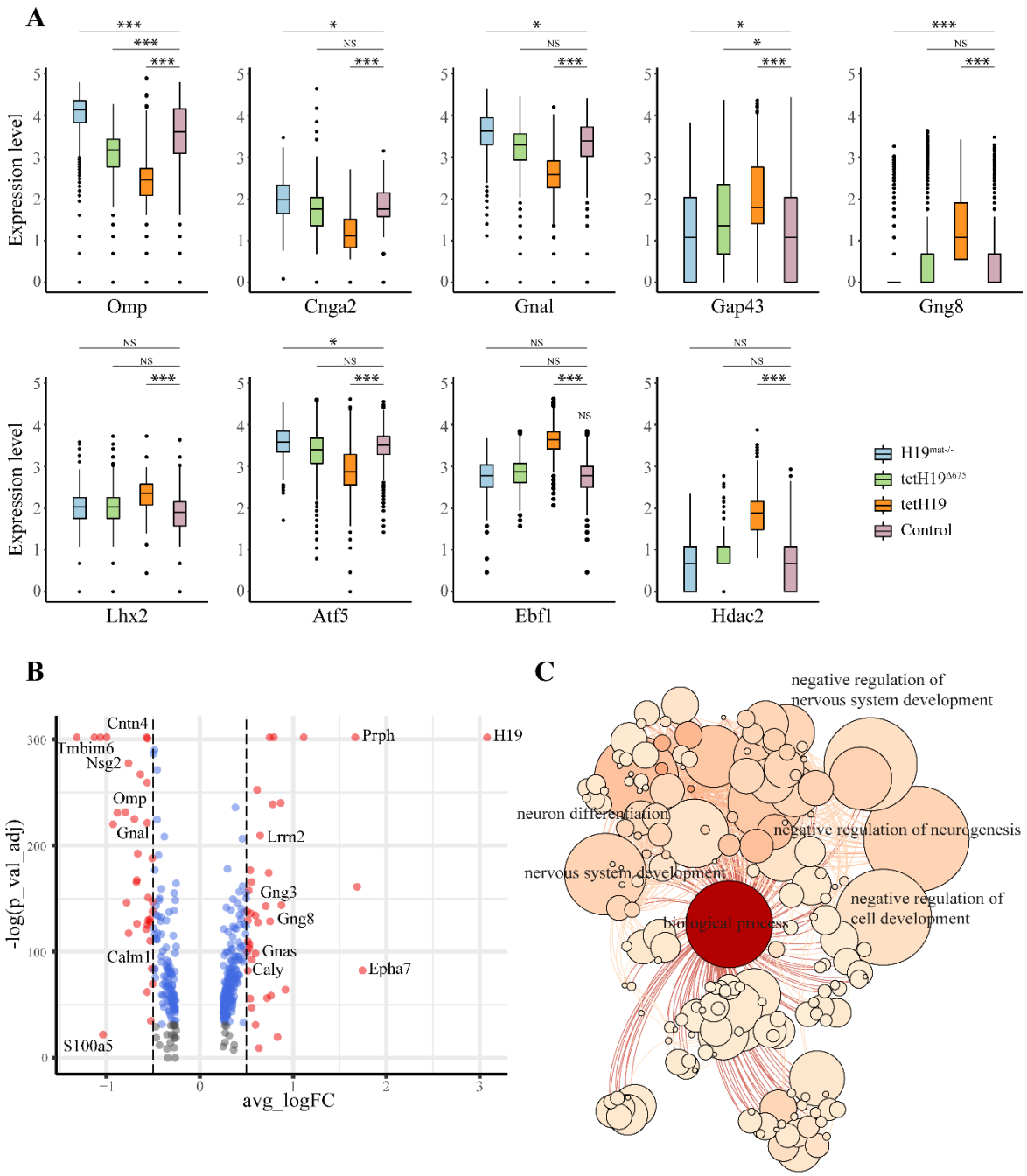

Figure 3. 18 Differentially expressed genes and GO term analyses of tetH19 mOSN populations

(A) Expression levels of marker genes and transcription factors in mOSN. Boxes represent interquartile range (IQR), and lines represent the 95% confidence interval of the median. The adjusted p-value is based on bonferroni correction using all genes in the dataset (∗p < 0.05; ∗∗p < 0.01; ∗∗∗p < 0.001).

(B) Volcano plot of significantly differentially expressed genes (p-value < 0.001) from tetH19 mOSNs compared to wild-type controls. The average fold change in x-axis is

comparing tetH19 to wild-type mOSNs. Shades of red indicate significantly differentially expressed genes with natural log (ln) value of fold change more than 0.5, whereas blue shades show differentially expressed genes with ln value of fold change less than 0.5.

(C) GO term enrichment is represented as a hierarchical map built from differentially expressed genes in tetH19 mOSNs. The size of the circle represents the significance of enrichment using -log2 of the adjusted p-value. Color code indicates the level of connectivity of a defined GO term. Only major GO terms are shown to simplify the graphs.

By analyzing the 379 differentially expressed genes from tetH19 mOSNs (Figure 3.18B) and 61 differentially expressed genes from $H19^{mat-/-}$ mOSNs (Figure 3.17C), I found these two datasets shared 21 transcripts that have reciprocal differential expression in tetH19 and $H19^{mat-/-}$ mOSNs. It is possible that these 21 candidates are the H19 downstream targets that contribute to the observed phenotypes in mutant lines. Notably, the $tetH19^{\Delta 675}$ transgenic mice expressing H19 transcript without an embedded miR-675 do not have an aberrant glomerular pattern, which suggests that the differentially expressed genes between the two datasets may be the targets of H19 that alter axon projection patterns. Therefore, I analyzed the differentially expressed gene set in $tetH19^{\Delta 675}$ mOSNs (Figure 3.19A) and found 6 candidates, including Prph, Cmip, Stmn1, Caly, Junb, and Wdfy1 (Figure 3.19B-C).

In terms of their expression changes in three mutant lines, these 6 candidates can be discussed as 3 groups. The first group contains Prph (peripherin), Stmn1, and Wdfy1 (WD repeat and FYVE domain-containing protein 1), which were upregulated in tetH19 mOSNs but significantly reduced in $H19^{mat-/-}$ mOSNs. They also had increased expression in $tetH19^{\Delta 675}$ mOSNs with less than a 2-fold difference. Because the $tetH19^{\Delta 675}$ mice ectopically express H19 molecules without miR-675, the positive correlation between Prph, Stmn1, Wdfy1, and H19 suggest that their expression is dependent on the H19 RNA sequences regardless of the embedded miR-675 precursor. Most neurons express neurofilaments which are the type IV family of intermediate filaments (Eng and Eng, 2009; Steinert and Roop, 1988). Several reports have shown that OSNs are atypical in that they do not demonstrate expression of the neurofilament triple proteins (Ophir and Lancet, 1988; Schwob et al., 1986). Rather, OSNs contain type III intermediate filament proteins including peripherin and vimentin (Escurat et al., 1990; Gorham et al., 1991; Schwob et al., 1986; Thompson and Ziff, 1989). Characterization of peripherin reveals that it is exclusively present in OSN axons (Akins and Greer, 2006; Gorham et al., 1991). In the

olfactory epithelia, Prph was mainly expressed in OSNs (Figure 3.19C). Peripherin has been shown to be required *in vitro* for neurite outgrowth (Helfand et al., 2003). Specifically, the inhibition of peripherin expression by siRNA approach suppresses the initiation, extension, and maintenance of neurites in PC12 cells (Helfand et al., 2003). An increase in peripherin expression coincides with the initiation and outgrowth of axons in PC12 cells (Aletta et al., 1989), accompanied by the rapid formation of motile peripherin particles (Prahlad et al., 1998). Given these results, the roles of the cytoskeleton in axon behavior, and the positive correlation between H19 and Prph, it is likely that Prph is regulated by H19 to promote the outgrowth of axons. This explains the less dynamic axons in $H19^{mat-/-}$ mice and the innervation of multiple glomeruli phenotype in tetH19 mice.

Stmn1 encodes a ubiquitous cytosolic phosphoprotein stathmin associated with the regulation of microtubule dynamics (Hanash et al., 1988). In particular, stathmin interacts with tubulin heterodimers and prevents them from forming microtubules (Curmi et al., 1997). After phosphorylation, stathmin releases tubulin, allowing microtubules formation. In addition, it has been proposed that stathmin induces the depolymerization of microtubules (Belmont and Mitchison, 1996), thus regulating both the formation of microtubules and their disassembly to function on axon growth. During the olfactory development, Stmn1 was detected as early as E12 (Camoletto et al., 2001). From E12 to adulthood, stathmin immunoreactivities were extensively colocalized with neuron-specific beta-III tubulin (Camoletto et al., 2001; Roskams et al., 1998). These data provide an idea that regulation of stathmin by H19 can control outgrowth of axons and dendrites, which is closely linked to the phenotypes in H19 mutant lines.

The protein encoded by Wdfy1 has been shown to abrogate early endosomal maturation and act as an adaptor protein for Toll-like receptor 3/4 for the generation of inflammatory cytokines (Dutta et al., 2016; Hu et al., 2015; Nandakumar and Paludan, 2015; Ridley et

al., 2001). WDFY1 reportedly acts downstream of Neuropilin-2 (Dutta et al., 2016), an axon guidance molecule known to mediate the targeting of OSNs (Takeuchi et al., 2010). However, the specific functional mechanisms of Wdfy1 in neurons remain to be understood.

The expression of both Caly and Junb were positively correlated with H19 (Figure 3.19B-C). Moreover, Caly remained unchanged and Junb showed reduced expression in tetH19$^{\Delta 675}$ mOSNs (Figure 3.19B), indicating their expression may be closely linked to miR-675. Caly has been shown to function on clathrin-mediated endocytosis by interacting with clathrin light chain A and stimulating clathrin self-assembly (Xiao et al., 2006). In the olfactory epithelia, Caly was exclusively expressed in OSNs (Figure 3.19C). It is suggested that the clathrin-coated endocytic pathway participates in the internalization and recycling of olfactory receptors in mouse OSNs (Jacquier et al., 2006; Rankin et al., 1999). After prolonged odorant exposure, olfactory receptors are not targeted to lysosomal degradation but accumulate in recycling endosomes (Mashukova et al., 2006). The olfactory sensory membranes are rapidly cycled and that endocytosed materials are trapped within the olfactory epithelium (Bannister and Dodson, 1992). These results provide a hint that Caly, as well as Wdfy1, may be involved in the olfactory endocytic activities to regulate olfactory transduction.

The transcription factor Junb has been implicated in regulating key steps in cell proliferation and differentiation processes (Schlingensiepen et al., 1994; Schlingensiepen et al., 1993; Shaulian and Karin, 2002). In cultured PC12 cells, neuronal differentiation induced by nerve growth factor was prevented by inhibition of JunB protein synthesis (Schlingensiepen et al., 1994). In the absence of JunB, PC12 cells not only failed to grow neurites but also remained in the proliferative state (Schlingensiepen et al., 1994). Furthermore, in cultured primary neurons from rat hippocampus, inhibition of JunB expression markedly reduced morphological differentiation (Schlingensiepen et al., 1994).

This result suggests that the downregulation of Junb in $H19^{mat-/-}$ mOSNs may be linked to the phenotype that axons of $H19^{mat-/-}$ go directly to their destination without circling around or branching out to other glomeruli (Figure 3.7C-D).

Cmip showed reduced expression in tetH19 mOSNs but remained upregulated in $H19^{mat-/-}$ mOSNs (Figure 3.19B-C). The Cmip gene encodes a c-Maf inducing protein which is suggested to plays a role in T-cell signaling pathway (Sahali et al., 2002). Overproduction of Cmip in mouse podocyte cell lines causes nephrin signaling changes at the podocyte slit diaphragm, resulting in cytoskeletal disorganization (Zhang et al., 2010). The overexpression of isoform 2 c-mip protein in Jurkat T cells induces a cellular redistribution of the actin bundling protein L-plastin, promoting the cytoskeleton rearrangement (Grimbert et al., 2003). Although Cmip is not well-studied in neurons, these results provide a clue that Cmip may function on cytoskeleton redistribution.

In conclusion, the single-cell transcriptome analyses reveal distinct differentially expressed genes among the mOSN groups of three mutant lines. Together with previous observations, I identified several potential transcripts that may contribute to the phenotypes in $H19^{mat-/-}$ and tetH19 mutant mice, which paves the way for a deeper understanding of H19's function mechanism in neurons.

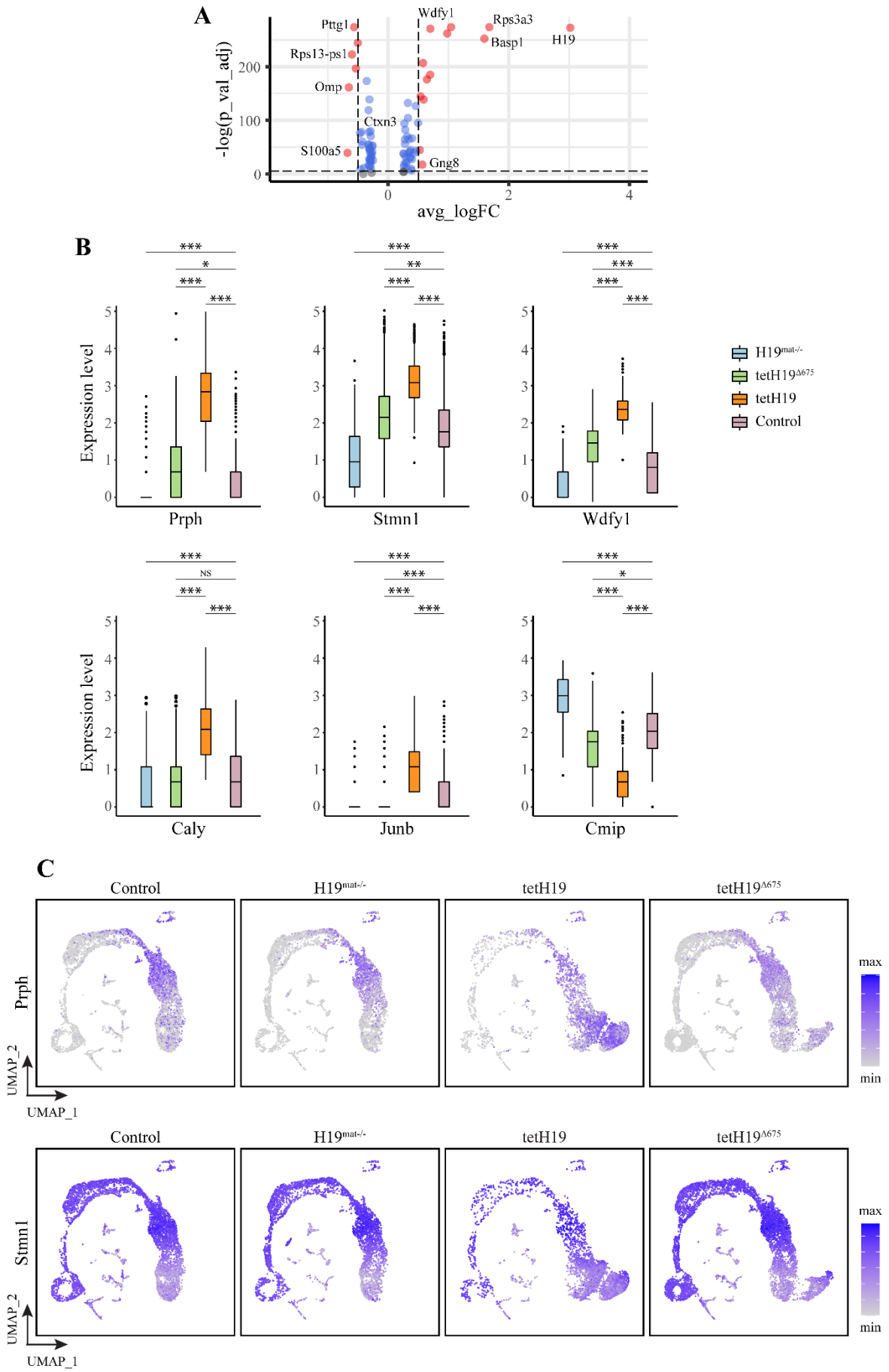
A
Pttg1
Wdfy1
Rps3a3
Basp1
H19
Rps13-ps1
Omp
Ctxn3
S100a5
Gng8
-log(p_val_adj)
avg_logFC
B
Expression level
Prph
Stmn1
Wdfy1
Caly
Junb
Cmip
H19mat-/-
tetH19Δ675
tetH19
Control
C
Control
H19mat-/-
tetH19
tetH19Δ675
Prph
Stmn1
UMAP_2
UMAP_1
max
min

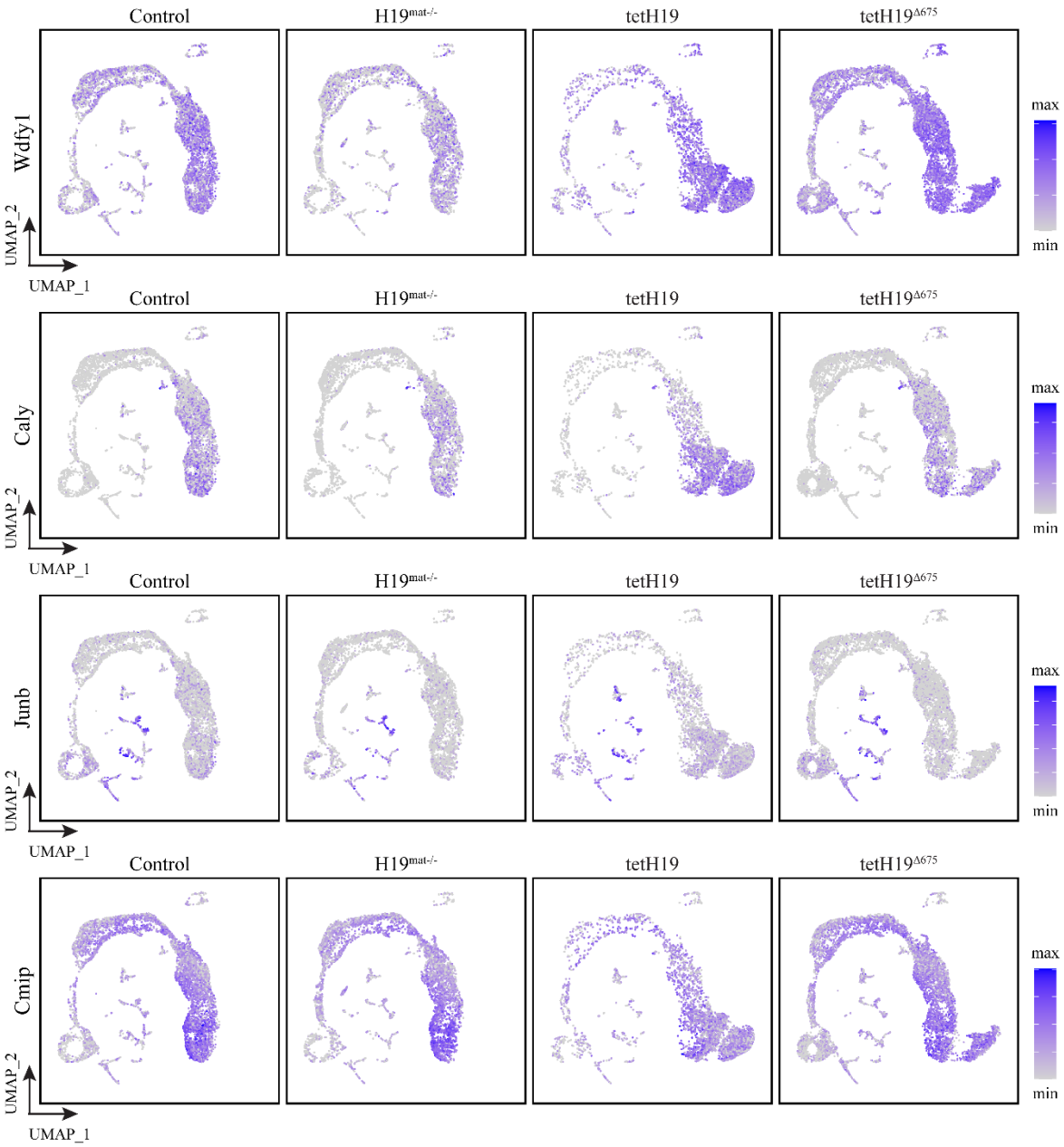

Figure 3. 19 Transcriptomic analysis of potential target mRNAs of H19

(A) Volcano plot of significantly differentially expressed genes (p-value < 0.001) from tetH19$^{\Delta675}$ mOSNs compared with wild-type controls. The x-axis shows the average fold change comparing tetH19$^{\Delta675}$ to wild-type mOSNs. Shades of red indicate significantly differentially expressed genes with natural log (ln) value of fold change more than 0.5, whereas blue shades show differentially expressed genes with ln value of fold change less than 0.5.

(B) Expression of H19 putative targets in mOSN of different mutant lines as well as controls. Boxes represent interquartile range (IQR), and lines represent the 95% confidence interval of the median. The adjusted p-value is based on bonferroni correction using all genes in the dataset (∗p < 0.05; ∗∗p < 0.01; ∗∗∗p < 0.001).

(C) All cells expressing Prph, Stmn1, Wdfy1, Caly, Junb and Cmip are mapped to UMAP plot.

3.7.2 Prediction of miR-675 targets

MiR-675 targets a myriad of transcripts primarily through binding to the partially-complementary motifs on their 3'-UTRs. The previous observation identified the significant upregulation of both miR-675-5p and miR-675-3p in the tetH19 olfactory epithelia (Figure 3.12B). Therefore, I sought to investigate putative binding partners of miR-675-5p or miR-675-3p in the identified differentially expressed gene set (Figure 3.17C and 3.18B).

I used TargetScan to highlight predicted miR-675-3p or miR-675-5p targets (Agarwal et al., 2015). I found 36 miR-675-3p predicted targets, and 13 miR-675-5p predicted targets (Figure 3.20A). And the transcript Rap1gap (Rap1 GTPase-activating protein) is the only predicted target shared by both miR-675-3p and miR-675-5p (Figure 3.20A).

Interestingly, I found Omp, encoding the highly expressed marker protein in mOSNs, was a putative target of miR-675-3p (Figure 3.20A). It is of note that both $OMP^{-/-}$;P2-lacZ and $OMP^{-/-}$;M72-GFP mice show duplicated glomeruli in close proximity of one another (Albeanu et al., 2018). In another two independent lines, OMP-tau:LacZ mice and OMP-GFP mice which the Omp coding region has been replaced by reporter molecules, the projections of primary olfactory axons both overshoot their target layer and grow into the external plexiform layer compared to that in wild-type animals (St. John et al., 2003). These studies suggest that OMP is necessary for local glomerular refinement and raise the possibility that Omp downregulation may contribute to the exuberant axon growth phenotype in tetH19 mice to some degree. However, although Omp showed reduced expression in tetH19Δ675 mOSNs, it is not as lower as that in tetH19 mOSNs (Figure 3.18A), which challenges the idea that H19/miR-675-3p plays a function in glomerular map formation through regulating OMP. The previously discussed Wdfy1 (Figure 3.19B-C) was predicted as a miR-675-5p target (Figure 3.20A). However, Wdfy1 was induced in

tetH19 mOSNs but downregulated in $H19^{mat-/-}$ mOSNs (Figure 3.19B-C), which is not accordant with the hypothesis of suppressive regulation by miR-675-5p.

Among the 48 predicted miR-675 targets, 23 (including Omp) transcripts were reduced in tetH19 mOSNs, but were not down-regulated in $H19^{mat-/-}$ or $tetH19^{\Delta 675}$ mOSNs (Figure 3.20B). They generally belong to three major signaling pathways: odorant signal transduction (Omp, Rap1gap, Slc8a1, Slc24a2/Nckx2, Dlg2, Clstn2, Calm1, Ric8b), cell adhesion molecules (Cntn4, Fstl5, Unc5b, Pcdh17, Ctxn3) and transcriptional regulators (Prune2, Trnp1, Cdkn1a/ p21Cip1, Nfix, Tshz2). Moreover, some of them or their superfamily have been shown to be essential for olfactory development, such as Rap1gap, Ric8b, and Cntn4.

Rap1gap (RAP1 GTPase Activating Protein) was specifically expressed in mOSNs and iOSNs compared to other cell types (Figure 3.21). The Ras-related small GTPase RAP1 is a significant signaling hub in neuronal development, as it promotes neurite outgrowth (Chen et al., 2005b; York et al., 1998), maturation of dendritic spines in hippocampus pyramidal neurons (McAvoy et al., 2009; Xie et al., 2005) and supports cortical neuron migration and orientation during development (Jossin and Cooper, 2011). RAP1 switches between inactive GDP-bound and active GTP-bound signaling states, which are delicately coordinated through interactions with RAP1 regulatory proteins like RAP1GAP. RAP1GAP is capable of deactivating RAP1 and accelerates Rap1-GTP hydrolysis toward an inactive GDP-bound state. Moreover, Rap1gap has been shown to restrict neuronal process outgrowth (He et al., 2006; Jordan et al., 2005). One of the mouse RAP1 regulator Rap1gap2 has been shown to significantly stunts OSN axon outgrowth *in vitro* when overexpressed, and results in dramatically elongated OSN axons when knocked down, providing insight for the involvement of Rap1 signaling in H19/miR-675-mediated regulation in OSN development.

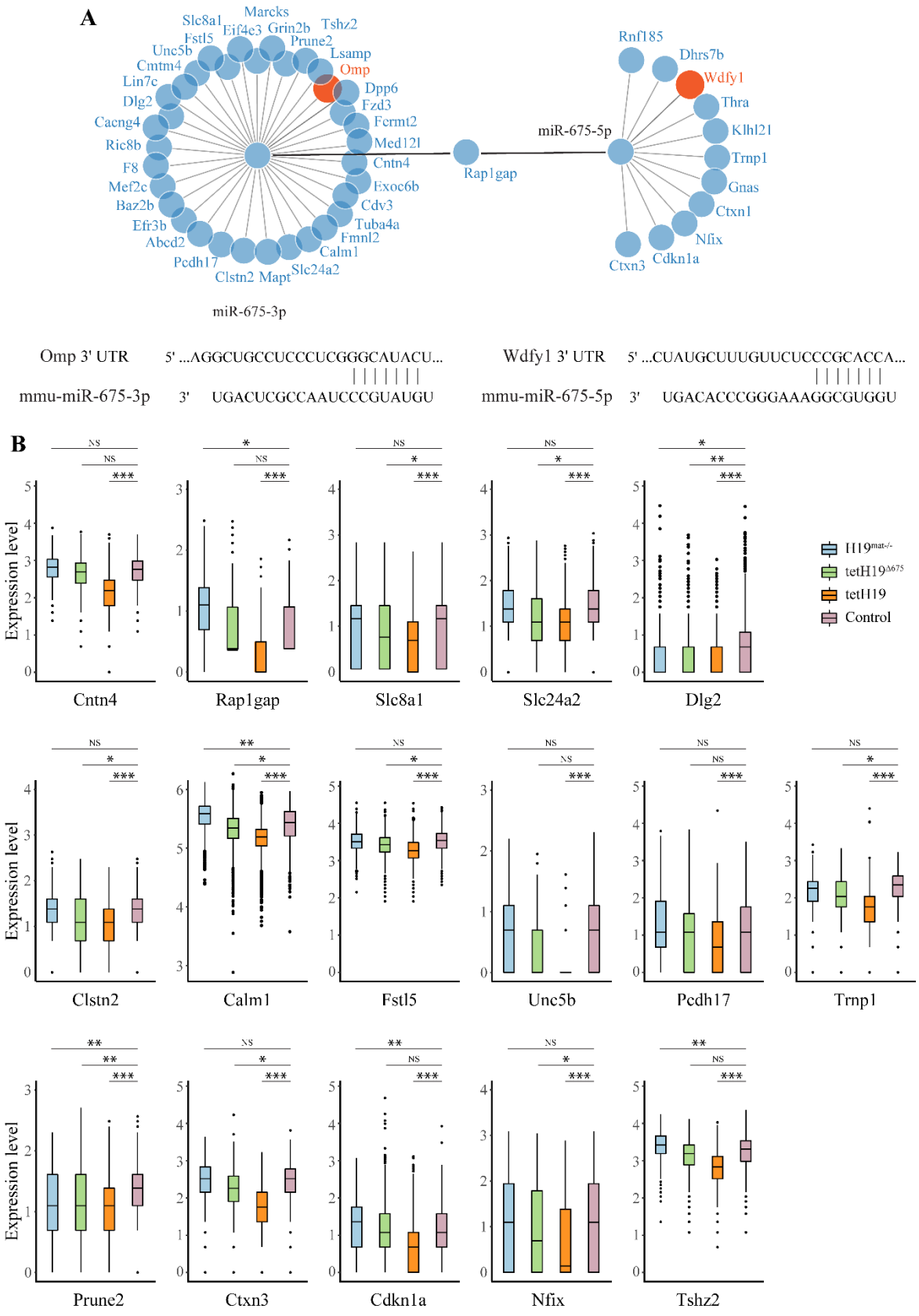

Figure 3. 20 Predicted direct targets of miR-675-3p and miR-675-5p

(A) Schematic of predicted miR-675-3p and miR-675-5p targets screened from the identified genes that are differentially expressed gene in either $H19^{mat-/-}$ or tetH19 mOSNs (Chapter 3.7.1). Each circle represents a target gene. Each line connects the miRNA with

its target. The orange color highlights the genes that are significantly differentially expressed in both in both H19 mutant lines. The sequences below show the predicted consequential pairing between miR-675-3p and Omp, miR-675-5p and Wdfy1 from TargetScan database.

(B) Expression of Cntn4, Rap1gap, Slc8a1, Slc24a2, Dlg2, Clstn2, Calm1, Fstl5, Unc5b, Pcdh17, Trnp1, Prune2, Ctxn3, Cdkn1a, Nfix and Tshz2 in mOSNs of different mutant lines as well as controls. Boxes represent interquartile range (IQR), and lines represent the 95% confidence interval of the median. The adjusted p-value is based on bonferroni correction using all genes in the dataset ($*p < 0.05$; $**p < 0.01$; $***p < 0.001$).

Another OSN abundant transcript Ric8b (Figure 3.21) has also been well-studied (Von Dannecker et al., 2005, 2006) in the OSNs. Different from Rap1gap, Ric8b encodes a guanine nucleotide exchange factor that interacts with G_{olf} and catalyzes the exchange of GDP for GTP. Therefore, Ric8b has been considered as a positive regulator for amplifying odorant signaling (Von Dannecker et al., 2006). The Ric8b-deficient OSNs were not activated by odorants and showed an increased rate of cell death, indicating Ric8b is essential for the odorant signal transduction (Machado et al., 2017).

The BIG-2/Cntn4 (contactin-4) also shows a unique expression pattern in the olfactory neurons (Figure 3.21). Cntn4 encodes an axonal glycoprotein and is required for the convergence of OSN axons. In Cntn4-deficient mice, olfactory axons frequently mistargeted to multiple ectopic glomeruli (Kaneko-Goto et al., 2008). Another cell adhesion molecule Fstl5, which encodes a secretory glycoprotein, has been shown to be specifically abundant in the olfactory system (Masuda et al., 2014; Saraiva et al., 2015).

Together, these analyses provide additional information about putative miR-675 targets that may contribute to the phenotypes in H19 mutant mice. Some of these predicted miR-675 targets directly influence odorant signal transduction, some are axon guidance molecules guiding the navigating axon toward its target area, and others are pivotal proliferation and differentiation regulators ensuring transcription stability.

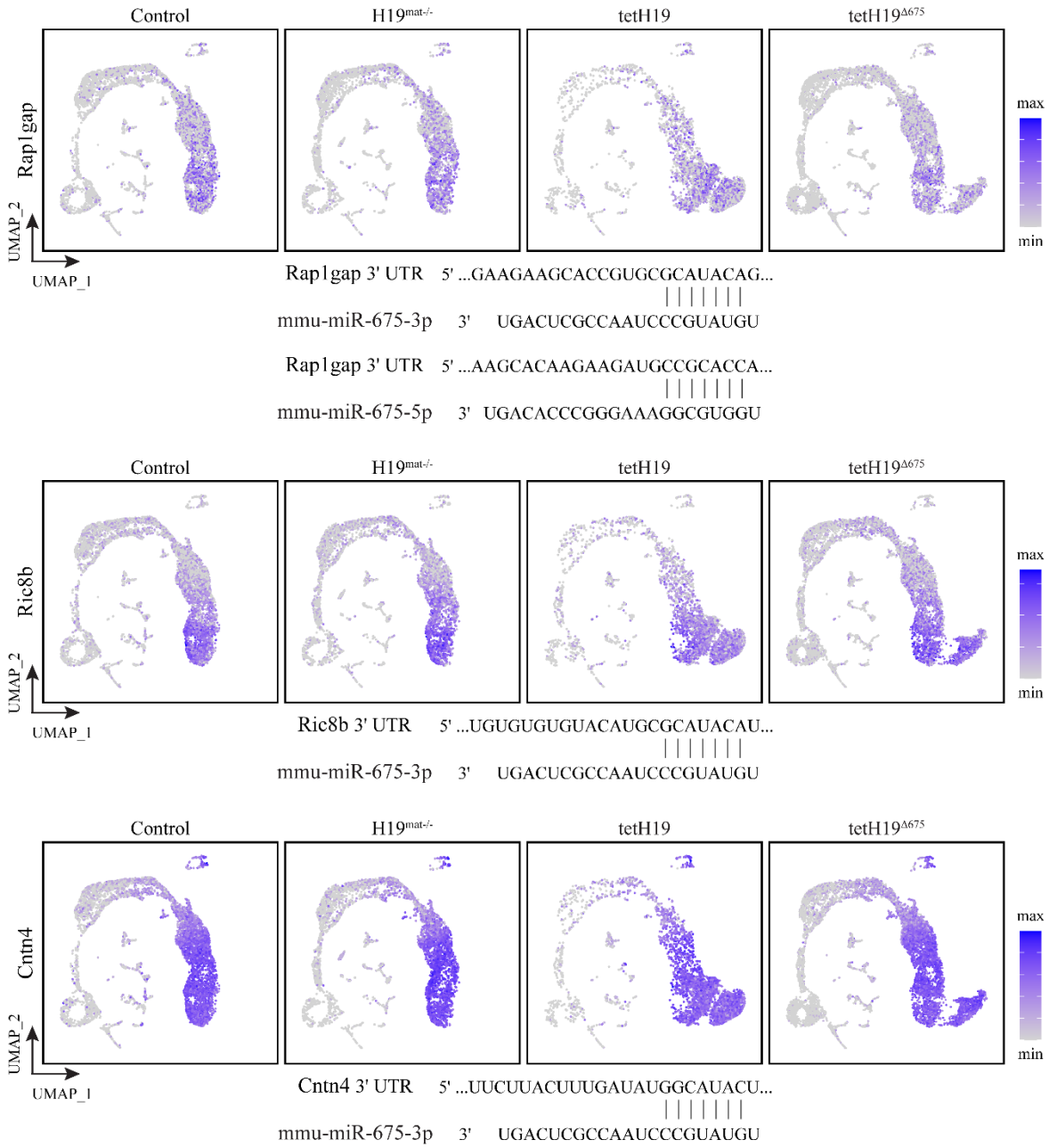

Figure 3. 21 The expression and consequential pairing of Rap1gap, Ric8b and Cntn4

Visualization of the expression pattern of Rap1gap, Ric8b and Cntn4 on UMAP. These plots represent the expression features of Rap1gap, Ric8b and Cntn4 in different mutant mice as well as wild-type control. Rap1gap is predicted direct target of miR-675-3p and miR-675-5p, whereas Ric8b and Cntn4 are predicted targets of miR-675-3p. These sequences adapted from TargetScan database show the predicted consequential pairing between miR-675-3p and 3'-UTR, miR-675-5p and 3'-UTR.

3.7.3 Identifying involvement of H19/miR-675-3p in IGF signaling pathway

The IGF signaling pathway is a highly conserved regulatory module that coordinates growth, development, and metabolism (Baker et al., 1993b; Brogiolo et al., 2001). However, H19 contains short open reading frames that are poorly conserved between mice and humans (Brannan et al., 1990). Therefore, the imprinted loci Igf2-H19 and the base-pair matching between H19-derived miR-675-3p and 3'-UTR of Igf1r mRNA are the critical links that build H19 to IGF family during evolution.

To evaluate the regulation of H19 in Igf2 and Igf1r, I first examined the expression of Igf2, Igf1r, Igf1, and Igf2r from P3 wild-type scRNA-seq data (Figure 3.22A). I found Igf1r is highly abundant in most cell types in the epithelia, whereas Igf2r has a relatively lower expression in both iOSNs and mOSNs compared to other cell types (Figure 3.22A). Due to the sequencing depth limitation, I detected very few Igf2 positive mOSNs from P3 wild-type scRNA-seq data (Figure 3.22A). Because of the relatively low level of Igf2 expression in the mOSNs, I was not able to evaluate their changes in the tetH19 line, in which H19 was ectopically expressed in mOSNs only. However, H19 and IGF family members were all highly expressed in a cluster of cells, which are likely derived from the lamina propria underlying the epithelium. Then I checked the expression level of H19, Igf2, and Igf1r in $H19^{mat-/-}$ and control lamina propria cells. I found Igf1r and Igf2r are both upregulated in $H19^{mat-/-}$ lamina propria cells where H19 was completely knocked out (Figure 3.22B). This negative correlation of H19 with Igf2 and Igf1r indicates the possibility of H19 acting antagonistically to Igf2 and Igf1r in the olfactory system. It is of note that Igf1r is highly expressed in the olfactory system, so future extensions of this work will build upon Igf1r to deepen our understanding of the regulation of H19 in Igf1r.

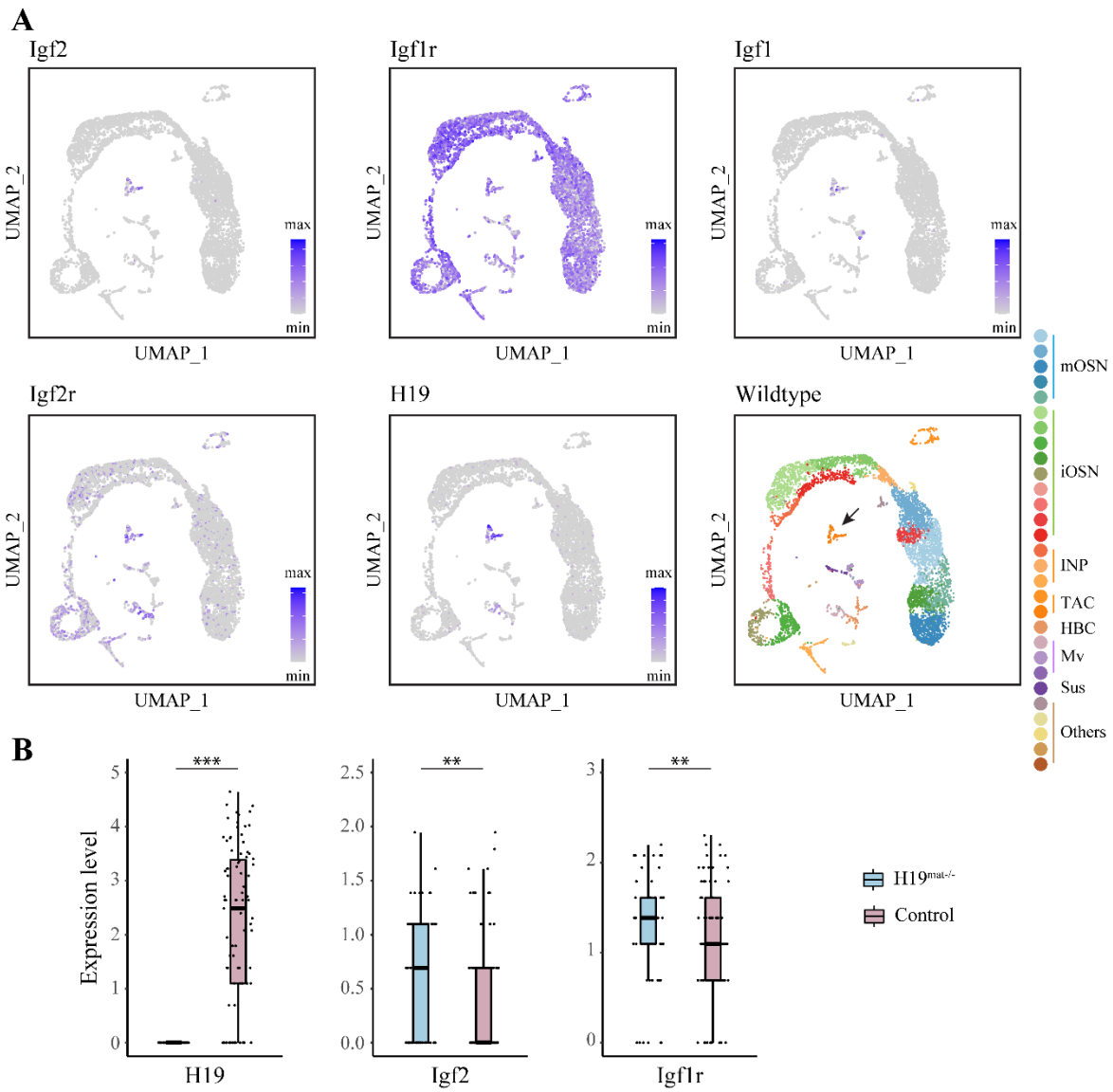

Figure 3. 22 The expression of IGF signaling molecules in developmental olfactory epithelium

(A) UMAP plots of H19, four IGF pathway family genes and all clusters. These plots represent the gene expression features in wild-type mice. The wild-type UMAP plot shows different clusters assigned by the expression of different marker genes. Arrow indicates the lamina propria cell cluster.

(B) Expression of H19, Igf2 and Igf1r in the lamina propria cells. Each dot represents the expression from one cell. Boxes represent interquartile range (IQR), and lines represent the 95% confidence interval of the median. The adjusted p-value is based on Bonferroni correction using all genes in the dataset (∗p < 0.05; ∗∗p < 0.01; ∗∗∗p < 0.001).

3.8 Conditional knockout of Ago2 suggests miRNAs may regulate neuronal differentiation

The miRNA-seq data has revealed the repertoire of miRNAs in the olfactory system (Figure 3-13), which includes several miRNA families that have been extensively investigated. However, the contribution of specific miRNAs to the development and function of olfactory tissues is yet poorly understood. Canonical miRNAs are first produced by conserved biogenesis machinery Drosha and Dicer (Kim et al., 2009). The primary miRNA (pri-miRNA) transcripts containing one or more hairpin structures are cleaved in the nucleus by the Drosha RNase III enzyme and its dsRNA binding partner DGCR8 to yield precursor miRNA (pre-miRNA) hairpins (Kim et al., 2009). These are cleaved again in the cytoplasm by the Dicer RNase III enzyme to yield a miRNA duplex, from which usually one strand matures in a complex with an Argonaute 2 (Ago2) protein (Hammond et al., 2001; Kim et al., 2009; Liu et al., 2004). The miRNA guides the Ago2 complex to target transcripts, often bearing 7-nt complements to the 5′ end of the miRNA, for destabilization or translational inhibition (Hammond et al., 2001; Liu et al., 2004).

In order to evaluate the potential roles played by miRNAs in mOSNs, I used a previously established conditional null allele of Ago2 to inactivate the Ago2 function within mOSNs (Figure 3.23A) (O'Carroll et al., 2007). Mice harboring the Ago2 LoxP allele were crossed with a mouse line in which Cre recombinase is expressed under the control of the endogenous OMP promoter (Figure 3.23A). To verify the efficiency of this genetic strategy, I monitored the expression of miR-675-3p, let-7a-5p, and let-7b-5p in olfactory epithelia of control and mutant animals at P7. Upon Cre-mediated deletion of Ago2, the expression of miR-675-3p, let-7a-5p, and let-7b-5p were significantly reduced from the neuroepithelium (Figure 3.23B). The qRT-PCR results in mutant mice showed the expression of miR-675-3p, let-7a-5p, and let-7b-5p throughout the neuroepithelium, indicating these three miRNAs were also expressed in other cell types like iOSNs.

Comparing to the littermate control, I found conditional knockout of Ago2 in mOSNs resulted in axons innervating multiple glomeruli in the olfactory bulb at P30 (Figure 3.23C-E). Quantification of partially innervated glomeruli showed an average 2-fold increase in the number of M72 glomeruli in the olfactory bulb of mutant mice compared to wild-type controls (Figure 3.23D), suggesting that mutant olfactory axons have projection defects. Moreover, I performed immunostaining for olfactory mature marker OMP and the marker NCAM expressed in both immature and mature neurons. I found that expression of OMP was barely detectable in $Ago2^{-/-}$ OB and OE by P30 (Figure 3.23F-G), suggesting that mutant OSNs lose their differentiation state.

Through analyzing adult tissues in which Ago2 function had been specifically ablated in mOSNs, I find that miRNAs are required during olfactory neuronal development. Our data gain insights into the putative contribution of miRNA-mediated regulation in axon projection and maintenance of neuron maturation state, providing interesting new functional aspects for the roles of miRNAs in neurons.

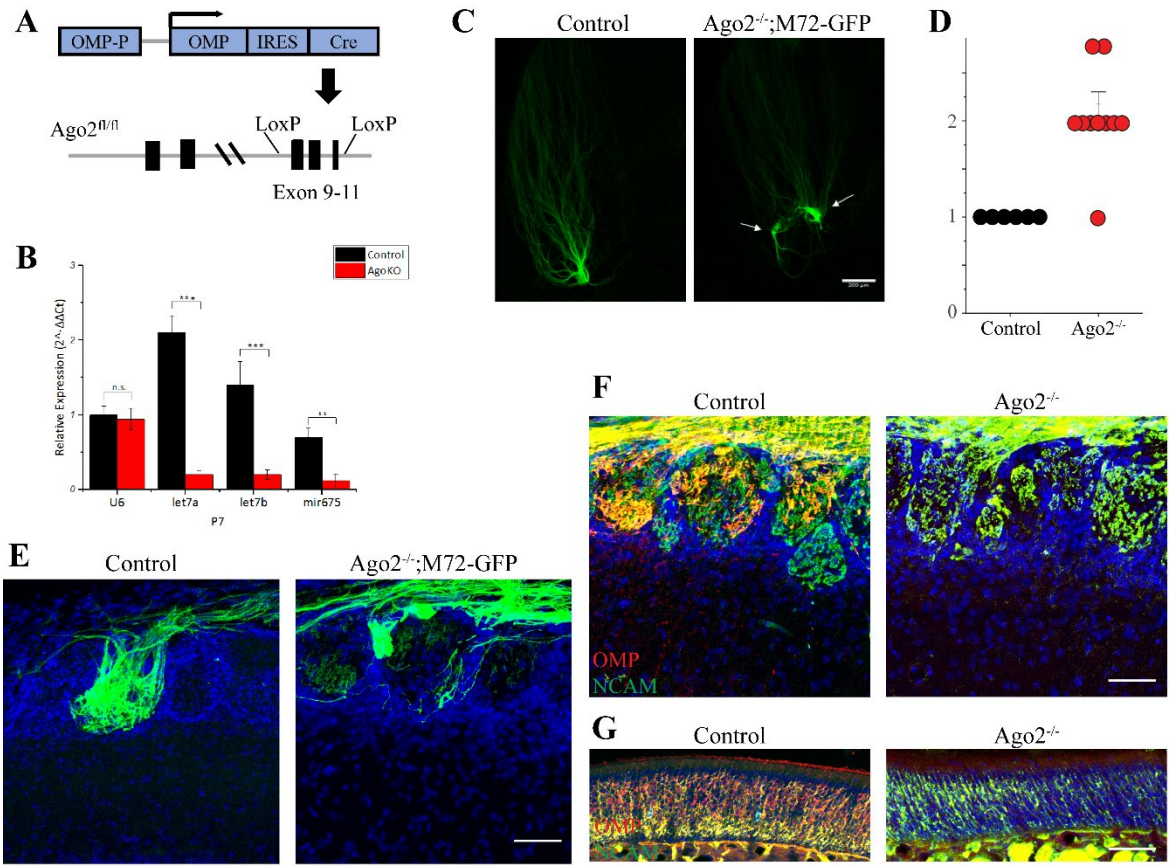

Figure 3. 23 Conditional knockout of Ago2 in mOSNs affects neuronal differentiation

(A) Schematic of conditional Ago2 knockout mice. The OMP+ OSNs express the protein Cre recombinase. Two LoxP sites face in the same direction are located in intron 8 and intron 11, respectively. The sequences between the LoxP sites are excised by Cre recombinase.

(B) qRT-PCR of miR-675-3p, let-7a and let-7b in control and mutant animals normalized by U6 snRNA. Olfactory epithelia were collected at P7 with 3 biological replicates (∗p < 0.05; ∗∗p < 0.01; ∗∗∗p < 0.001).

(C) Whole-mount images of M72 glomeruli in control and Ago2$^{-/-}$ mouse. Scale bar, 200 μm. Compared to littermate control, neurons expressing the M72 receptor target to another partially innervated glomeruli that are close to the predominant M71 glomerulus site in Ago2$^{-/-}$;M72-IRES-tauGFP animal. GFP, green. Scale bar, 200 μm.

(D) The number of M72 glomeruli per half bulb in control and Ago2$^{-/-}$ mice. Each dot represents a single data point, and the horizontal bars represent mean ± SEM with p value calculated from one-tailed Student's t test (∗p < 0.05; ∗∗p < 0.01; ∗∗∗p < 0.001).

(E) Representative image of M72 glomeruli in control and Ago2$^{-/-}$ mouse. Scale bar, 50 μm. GFP, green. DAPI, blue.

(F) Representative image of OB stained with antibodies against OMP (red) and NCAM (green). DAPI, blue. Scale bar, 25 μm.

(G) Representative image of OE stained with antibodies against OMP (red) and NCAM (green). DAPI, blue. Scale bar, 25 μm.

3.9 Discussion

In the mouse olfactory system, OSNs are continuously renewed to form and refine the olfactory map. Therefore, the timing of neuronal proliferation and maturation must be well controlled. How do the OSNs effectively govern all the cellular molecules for their development? There is no doubt that many signaling pathways are involved in regulation, but H19 could be a productive master for shaping this complex process. The precursor for miR-675 and the regulatory role as lncRNA enable H19 with multifaceted functions.

In this study, we find the prevalence of H19 in OSNs during the critical period does not affect olfactory axon projection pattern, it affects the refinement of OSNs. H19 knockout mice are deficient in the ability to recover convergent axon projection patterns following odorant exposure during the critical period. In the olfactory system, the perinatal OSNs exhibit unique characteristics in their path-finding dynamics during the critical period. And H19 may be one of the factors that endorse the exuberant axon growth of these perinatal OSNs. Transgenic expression of H19 in OSNs disrupts the convergent projection pattern of OSN axons. This effect is associated with the ability of H19 to affect the mature state of the OSNs, and its ability to extend the lifespan of navigator OSNs which exhibit exuberant axon growth during the critical period. In contrast, the transgenic expression of $H19^{\Delta 675}$ does not affect olfactory axon projection. In addition, axons with miR-675 knockdown do not project exuberantly, suggesting H19 regulates the OSN developmental plasticity through regulating miR-675 expression. It is also known that miR-675 binds to 3'UTRs of multiple target genes and coordinately downregulates their expression. My study identified a lot of new potential miR-675 targets including olfactory signal transduction molecules, cell adhesion molecules, and transcription regulators, thereby profiling a multilayer gene regulatory network that is crucial for the proper formation of the olfactory map.

3.9.1 Coupling H19/miR-675-3p and IGF pathway in different olfactory developing stages

My study has been focusing on postnatal olfactory development especially within and after the critical period. Because of the sequencing depth limit of scRNA-seq, both H19 and Igf2 have a relatively low expression in most cell types except in lamina propria cells after birth (Figure 3.21A). Although it is hard to dissect whether the IGF pathway is linked to the function of H19/miR-675-3p in mOSNs, there are other connections of H19 with the IGF signaling pathway in the developing olfactory system according to the published work.

The IGF signaling has been investigated as early as at embryonic (E) day 14.5. At E14.5, IGF2 protein is expressed in the leptomeninges surrounding the bulb as well as in the bone of the cribriform plate, whereas IGF1R protein localizes to the olfactory neuron axons within the olfactory nerve layer as well as in the glomerular layer of the bulb (Scolnick et al., 2008). And at E13.5, H19 is clearly detected in the nasal septum (Drewell et al., 2000). In addition, ablating both IGF1 and IGF2 or their common receptor IGF1R leads to the redistribution of olfactory sensory axons away from the lateral olfactory bulb toward the ventral-medial face (Scolnick et al., 2008), indicating IGF signaling is required for the correct positioning of glomeruli in the lateral olfactory bulb. These studies provide important functional links of H19, Igf2, and Igf1r. First, H19 and Igf2 are expressed in the same tissues during prenatal development (Drewell et al., 2000; Scolnick et al., 2008), as suggested by their close linkage and their reciprocal imprinting. Second, each of the IGF ligands IGF1 or IGF2 can compensate for the lack of the other for binding to and activating the common receptor IGF1R (Scolnick et al., 2008), suggesting IGF1R is the indispensable role for IGF signaling in axon guidance and providing support for H19/miR-675-3p in balancing Igf1r expression during embryonic development.

The adult olfactory mucosa is a site of continuing neurogenesis that expresses IGF1 and IGF1R (McCurdy et al., 2005). When IGF-I was applied to olfactory mucosa slice cultures, there was an increase in the number of olfactory neurons (McCurdy et al., 2005). These results provide more evidence of the contribution of IGF signaling in olfactory development. In the future, I may focus on protein level to study whether IGF signaling contributes to the phenotype in H19 mutant lines.

3.9.2 Role of H19 in olfactory sensory map formation

The stereotypic nature of the olfactory sensory map suggests that the precise convergence and targeting of sensory axons in the olfactory bulb is the result of specific spatiotemporal guidance cues in the target tissue and along the axonal trajectory. In this scenario, a hierarchy of regulators directs axons to their programmed glomerular targets in the olfactory bulb. Here we show H19 shapes the olfactory axon projection mainly through extending the lifespan of navigator cells. Navigator cells enable exuberant growth during the critical period that help establish single glomerular projection patterns. Mice deficit in H19 loss this navigator cells plasticity and are not able to prune the misrouted axons under chronic odorant exposure. We favor a model in which H19-derived miR-675 H19 inhibits a group of molecules including signal transduction molecules, cell adhesion molecules, and transcription regulators to regulate axon projection.

Apart from miR-675 predicted targets, there are some very significantly differentially expressed transcripts that worth further investigation. For instance, the cell adhesion molecule Epha7 is highly upregulated in tetH19 mOSNs. However, EphA7 was revealed to be expressed by both mOSNs and iOSNs cell bodies but absent from the axons and dendrites (John et al., 2002), which is unlikely to form ligand and receptor interaction with its ephrin partners in the glomerular layer. A previous study disclosed that the EphA7 receptor regulates apoptosis via PTEN/Akt signaling pathway *in vitro* (Xiang et al., 2015), suggesting an alternative function of EphA7 in the olfactory system. The ER-located

transmembrane protein Tmbim6, the most downregulated gene in tetH19 mOSNs (Figure 3.18B), is known to be involved in the suppression of intrinsic cell death mediated by ER calcium release (Xu et al., 2008). Tmbim6 has been shown to be highly expressed in OSN (Kanageswaran et al., 2015), indicating Tmbim6 could be the suppressor of OSN apoptosis.

Previous research demonstrated the role of H19 as a molecular scaffold (Keniry et al., 2012; Luo et al., 2013; Monnier et al., 2013). It is interesting to figure out RNA-binding proteins that are associated with H19 in the mouse olfactory system. In our preliminary experiment, we performed biotinylated RNA-affinity assays and mass spectrometry to identify proteins binding H19 in mouse olfactory epithelia. The protein sequencing data identified a number of proteins bound to H19, including miRNAs processing-related DICER1. However, this data is too preliminary to make any solid conclusion. My next step is to verify and quantitatively analyze the identified proteins, and seek to identify the links among H19/miR-675, H19 binding proteins, and identified differentially expressed targets in H19 mutant mice.

Although the data we presented focus on the functional role of H19 in mature neurons, it is notable that H19 is also expressed in the progenitor cells with a decreasing expression pattern during development. Early H19 lncRNA deficiency is shown to block endothelial-to-hematopoietic transition (Zhou et al., 2019). And it is demonstrated that conditional deletion of the maternal but not the paternal H19-DMR reduced adult HSC quiescence (Venkatraman et al., 2013). In addition, it is shown the olfactory cell proliferation increases fast from P3 to P14 and reaches the peak at P14 (Wu et al., 2018), and H19 is highly expressed before P3 in progenitor cells. It is possible that H19 is involved in cell proliferation in progenitor cells.

In summary, the data presented in my study clearly identify a role of H19/miR-675 in the development of the olfactory sensory map and add the H19/miR-675 to a growing list of

molecules involved in the olfactory neuron plasticity regulation in the developing nervous system.

Chapter 4 Regulation of mouse OSN development by Adar and circular RNAs

The second part of my thesis research is to study the function of Adar and circRNAs in the main olfactory system.

CircRNAs are an enigmatic class of RNAs characterized by back-splicing of pre-mRNA. It is found that circRNAs are substantially enriched in the mouse brain and are likely responsible for synapse formation and homeostatic plasticity (You et al., 2015). However, the functional roles for most neuron-specific circRNAs remain unclear. It is implied that circRNAs expression correlates negatively with the expression of the RNA-editing enzyme ADAR (Rybak-Wolf et al., 2015; Zhang et al., 2014). With the new RNA-seq platform, a large number of circRNAs have been identified. It is difficult to directly test the involvement of individual circRNA in regulating neurodevelopment. To broadly probe circRNAs function, we manipulated the expression of ADAR, an enzyme that is involved in circRNA biogenesis. We generated the transgenic mice expressing different Adar isoforms and the transgenic mice expressing editing-deficient ADAR as the control. By performing FACS-seq, we then identified the circRNA species that are downregulated in OSNs ectopically expressing Adar1p150 and Adar1La, respectively. Our analysis of circRNAs expression and the editing motifs from FACS-seq data in different transgenes provides clues on ADAR melting pre-loop structure of circRNA-forming exons. Additionally, the tetAdar mice have severely disrupted axon projection patterns like that of M72 OSNs, which diffusely target their axons to multiple glomeruli. We also examined the axon projection in Adar knockout mice and found that Adar-deficient OSNs display impaired axon targeting for certain OR types. These results indicate that Adar functions on olfactory axon projection in an OR-dependent way.

4.1 Identification and Characterization of circRNAs in olfactory epithelium

It is shown that circRNAs are upregulated during neuronal differentiation (Rybak-Wolf et al., 2015). To better characterize the expression of circRNAs, we sequenced ribosomal RNA (rRNA) depleted total RNA from adult mouse olfactory epithelium. We applied two well-maintained and high-performance algorithms (Hansen, 2018), CIRCexplorer2 (Zhang et al., 2016) and DCC (Cheng et al., 2016), to computationally identify *bona fide* circRNA species with annotated head-to-tail junctions (Figure 4.1A). To unbiasedly quantify circular expression, only the reads spanning the head-to-tail junction were counted for circular expression(Rybak-Wolf et al., 2015).

We detected a total of 3295 unique mouse circRNAs and the majority of their head-to-tail junctions were supported by a few reads. To validate the authenticity of identified circRNAs, I performed RT-PCR with divergent primers for some candidate circRNAs, and 11 out of 12 tested circRNAs generated circular products, including the rolling circles (Figure 4.1B). Analysis of annotated head-to-tail junctions showed that OSN-expressed circRNAs were generally derived from annotated exons (Figure 4.1C), with a clear preference for coding sequences (CDS). However, about 30% circRNAs were not classified (Figure 4.1C), which include circRNAs aligned to antisense of known transcripts and intronic sequences.

4.1.1 Identification of circRNAs specifically expressed in olfactory epithelium

Given the prevalence of circRNAs in the brain, we were interested in what the circRNAs were that specifically expressed in the olfactory epithelium. By comparing our sequencing data with published mouse whole brain RNA-seq data (Rybak-Wolf et al., 2015) and normalizing circRNA abundance to its host gene expression, we found that many circRNAs are exclusively present in the olfactory epithelium, like circErdr1, circStyx, circKansl2, circRecql, and circTxlng, which were the top candidates by abundance (Figure 4.1D). Some circRNAs are detected in both brain and olfactory epithelium tissue, among

which circTmem56, circPrr41l, circRtn4, circEri3, circPrkce, and circRims1 are more enriched in the olfactory epithelium (Figure 4.1D). GO analysis of the parent genes of these olfactory enriched circRNAs suggests that their functions are related to post-transcriptional modification and cell differentiation, potentially hinting at the function of circRNAs in the olfactory system.

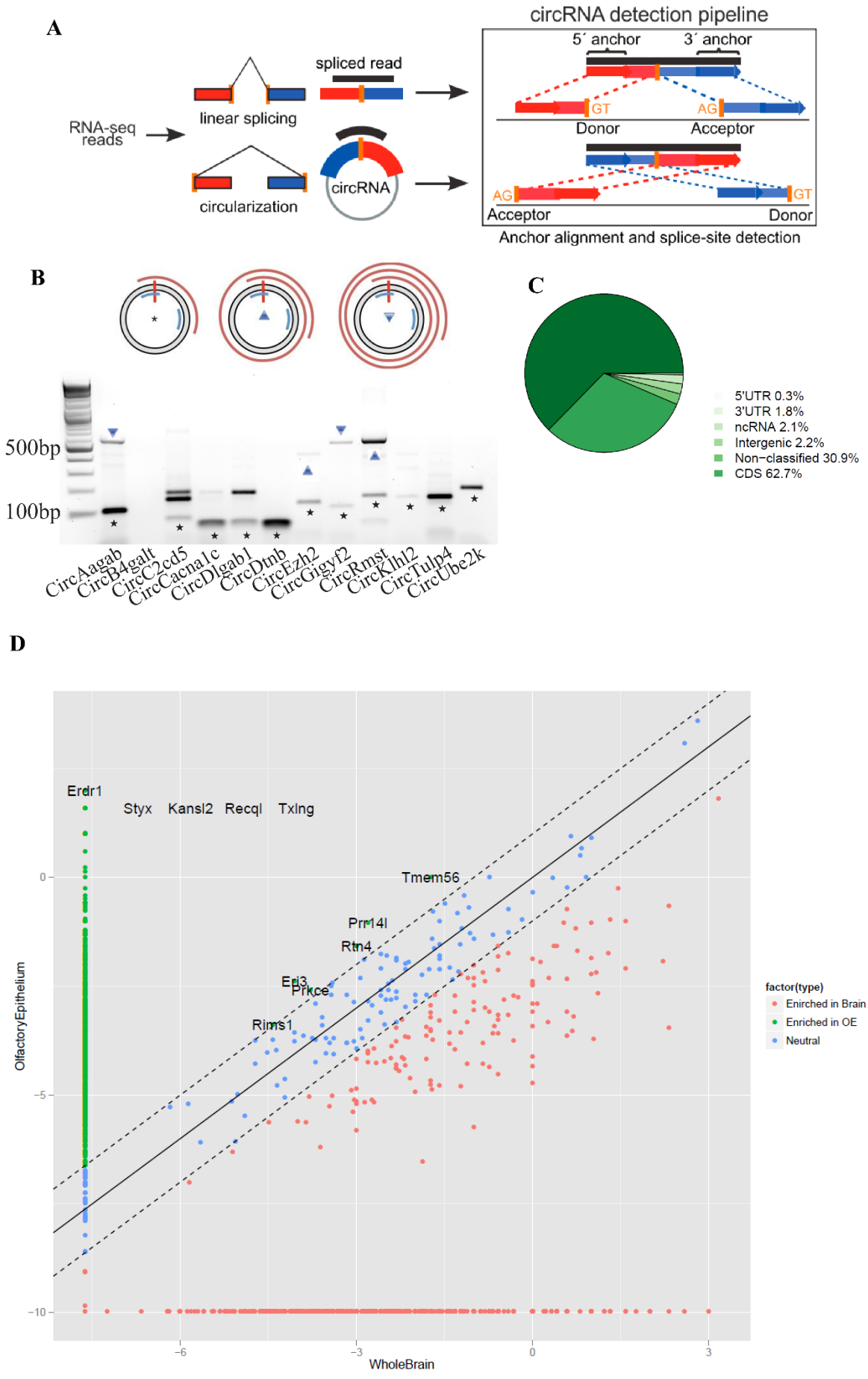
A
circRNA detection pipeline
5´ anchor
3´ anchor
spliced read
RNA-seq reads
linear splicing
GT
AG
Donor
Acceptor
circRNA
circularization
AG
GT
Acceptor
Donor
Anchor alignment and splice-site detection
B
500bp
100bp
CircAagab
CircB4galt
CircC2cd5
CircCacna1c
CircDlgab1
CircDtnb
CircEzh2
CircGigyf2
CircRmst
CircKlhl2
CircTulp4
CircUbe2k
C
5'UTR 0.3%
3'UTR 1.8%
ncRNA 2.1%
Intergenic 2.2%
Non−classified 30.9%
CDS 62.7%
D
Erdr1
Styx
Kansl2
Recql
Txlng
Tmem56
Prr14l
Rtn4
Epi3
Prkce
Rims1
OlfactoryEpithelium
WholeBrain
factor(type)
Enirched in Brain
Enriched in OE
Neutral

Figure 4. 1 Identification and characterization of circRNAs in olfactory epithelium

(A) Schematic of computational annotation of circRNAs. The junction-spanning reads align sequentially to the genome for linear (top) but in reversed orientation for head-to-tail spliced reads (bottom). Spliced reads must distribute completely to anchors, flanked by AG/GU. Modified from published work (Memczak et al., 2013).

(B) RT-PCR products from circRNAs. In the upper panel, the two blue arcs mark the location of divergent PCR primers, and the grey ring represents a circRNA with the red vertical bar marks the head-to-tail junction. The red spirals on the outside represent rolling circle PCR products. The asterisk, upward triangle, and downward triangle symbols on the gel image denote the 0-cycle, 1-cycle, and 2-cycle RT products identified by sequencing, respectively. The bottom panel is the gel image for PCR products of 12 circRNAs tested.

(C) This pie chart represents the classification of the annotation of identified head-to-tail junctions in the genome. These circRNAs detected in the olfactory epithelium span a broad expression range.

(D) The circRNAs enriched in the olfactory epithelium. The red dots show the circRNAs species that are enriched in the brain and the green dots denote the circRNAs enriched in the olfactory epithelium. The blue dots represent the circRNAs that are detected in both RNA-seq data.

4.2 Studying a possible regulatory role of ADAR in the biogenesis of neural circRNAs

Next, I sought to identify the molecules that regulate the specific expression of circRNAs in order to broadly probe circRNA function.

It is thought that circRNAs are derived from canonical splice sites and are predominantly produced by back-splicing reactions (Ashwal-Fluss et al., 2014). When pre-mRNA processing events are slowed down, nascent RNA can be directed to alternative pathways that facilitate backsplicing (Liang et al., 2017). The main hypothesis of backsplicing is that looping of the intron sequences flanking the splice sites brings these sites into proximity. This looping can be mediated by the dimerization of RNA-binding proteins such as QKI (Conn et al., 2015), which binds to specific motifs in the flanking introns, explaining at least some of the observed expression patterns of circRNAs. Additionally, the base pairing between inverted repeat elements (such as Alu elements), which are located in the upstream and downstream introns, favors the expression of circRNA. Interestingly, adenosine to inosine editing by ADAR reduces the pairing of intron sequences. It is reported Adar knockdown causes upregulation of circRNAs in cell line systems (Barrett and Salzman, 2016; Ivanov et al., 2015). Therefore, ADAR is suggested to be an antagonist of circRNA production through editing or hyper-editing of introns flanking circRNAs (Ivanov et al., 2015; Rybak-Wolf et al., 2015). Most human and mouse circRNAs have been linked to the relatively long introns and the complementary repeat sequences flanking the region of circularization (Ashwal-Fluss et al., 2014). As a result, we sought to study whether ectopically expressing Adar in mature OSNs would reduce the abundance of circRNAs.

4.2.1 The strategy of specifically overexpressing Adar in OSNs

To assess circRNAs function in olfactory neuronal development, we designed a transgenic approach to ectopically express Adar in mature OSNs. We expect to observe the

downregulation of most circRNAs which will allow us to probe the role of circRNAs in OSN development.

From the transcript annotation in *Ensembl*, there are five protein-coding isoforms of mouse Adar gene, including the full-length ADARp150, and a shorter N-terminally truncated ADARp110. The expression levels of ADARs vary wildly among cell types, and the effects of each of these isoforms on the global transcriptome are still fairly elusive (Nishikura, 2010). However, all ADARs share a common domain architecture consisting of a variable number of amino-terminal dsRNA binding domains (dsRBDs) and a carboxy-terminal catalytic deaminase domain. To probe the requirement for functional deaminase domain, we generated three different transgenic lines.

The full-length Adar cDNA was amplified by RT-PCR from mouse olfactory epithelium RNA and cloned to assembly tetO-Adar1p150-IRES-tdTomato vector. The transgenic animal, tetO-Adar1p150-IRES-tdTomato, was generated by pronuclear injection. This well-established tetracycline trans-activating system permits inducible ectopic expression of Adar1p150 in a promoter-specific manner. In mice carrying OMP-IRES-tTA:tetO-Adar-IRES-tdTomato (tetAdar mice), OMP promoter drives the expression of tTA which further induces the expression of Adar and tdTomato in mature OSNs (Figure 4.2A).

When I performed the DNA sequencing to confirm the sequences Adar1p150 cloned from mouse olfactory epithelium RNA, I found there was a second product from the sequencing results. It turned out to be Adar1La, the second longest Adar1 isoform, that shares 97.8% sequence identity with Adar1p150. The Adar1La CDS is 78 nucleotides shorter than Adar1p150. In other words, there are 26 amino acids between dsRBD and deaminase domain of ADAR1p150 that are missing in ADAR1La. Therefore, we generated another transgenic mouse OMP-IRES-tTA:tetO-Adar1La-IRES-tdTomato (tetAdarO mice), carrying the isoform Adar1La. A recent study by Walkley and colleagues described that a point mutation in the Adar gene that disrupts catalytic activity (E861A) in mice (Liddicoat

et al., 2015), which prompted us to generate the OMP-IRES-tTA:tetO-Adar1E861A-IRES-tdTomato (tetAdarE mice) line.

To specifically profile circRNAs in OSNs, I sorted tdTomato$^+$ OSNs from the transgenes for RNA-seq (Figure 4.2B). For each transgene, there were 4 adult biological replicates of FACS-seq samples to identify circRNAs expressed in the tdTomato$^+$ cells. The control mOSNs were collected from OMP-IRES-tTA;Tg(tetO-GCaMP2)12IRyu (tetG2) mice, which contains a circularly permutated EGFP/M13/Calmodulin fusion protein (GCaMP2) under the transcriptional control of OMP promoter (He et al., 2008). This will allow us to use EGFP signal from GCaMP2 to sort the mOSNs.

4.2.2 Ectopic expression of Adar1La effectively downregulates total circRNA levels in mOSNs

By combining CIRCexplorer2 (Zhang et al., 2016) and DCC (Cheng et al., 2016) algorithms for analysis, we identified 3826 low-confidence circRNA species. These candidates were filtered under the criteria that they have more than 1 read in any of the biological replicates, agreed upon by both algorithms, across all the RNA-seq samples. Meanwhile, the number of high-confidence circRNA species with more than 1 read in all 4 biological replicates in both algorithms is only 171. This is due to the fact that cDNA libraries for FACS-seq are generated from rRNA-depleted total RNAs in which the total circRNAs reads is around 0.2%.

Based on our hypothesis, RNA-seq samples from both tetAdar and tetAdarO would destabilize the flanking intron structure during circRNA biogenesis, which results in fewer circRNAs being generated. Therefore, we used normalized total circRNA reads as an indicator to evaluate the function of Adar1p150 and Adar1La in circRNA formation. By calculating the normalized total unique mapped circRNAs, we found that ectopic expression of editing-deficient ADAR (tetAdarE) resulted in an increase of circRNA expression (Figure 4.2C), suggesting A-to-I editing by ADAR is essential in circRNA

biogenesis. Contrary to the wild-type control tetG2, no significant difference was detected from the total circRNAs reads in tetAdar mice (Figure 4.2C). Overexpressing isoform ADAR1La in OSNs seems more effective in downregulating circRNA expression (Figure 4.2C).

Then we analyzed the editing information in circRNA flanking introns. We used edit-events (A to G mismatches viewed by the alignment program) to evaluate the editing activity in OSNs of different transgenic mice. By comparing the basic level of editing events detected in tetG2 OSNs, it is shown that the highest editing activity occurs in tetAdar OSNs (Figure 4.2D-F), which suggests Adar is actively functioning. In addition, we analyzed the editing sites (unique genomic editing locations) and found both tetAdarO and tetAdar OSNs presented more unique editing genomic sites, which further indicates there is active editing activity in tetAdarO and tetAdar OSNs.

In order to evaluate the editing specificity, we calculated the edit-rate (the normalized editing events on each unique genomic editing location) across different genotypes. The edit-rates of both tetAdar and tetAdarO OSNs are relatively lower than that of tetG2 (Figure 4.2E), indicating the widespread activity of either ADAR1p150 or ADAR1La results in less specificity in editing sites. Recently, transcriptome analysis of the $Adar^{-/-}$ mouse brain tissue has revealed A-to-I editing is not required for homeostatic gene expression or regulation of gene expression and its absence does not significantly alter the brain transcriptome (Chalk et al., 2019). It is possible that although the increased unique editing sites in tetAdar OSNs are located in the flanking introns of identified circRNAs, some are non-canonical hyper-editing sites and do not affect circRNAs biogenesis. In this scenario, the total number of circRNAs detected in tetAdar OSNs would not be significantly lower than that in tetG2 OSNs.

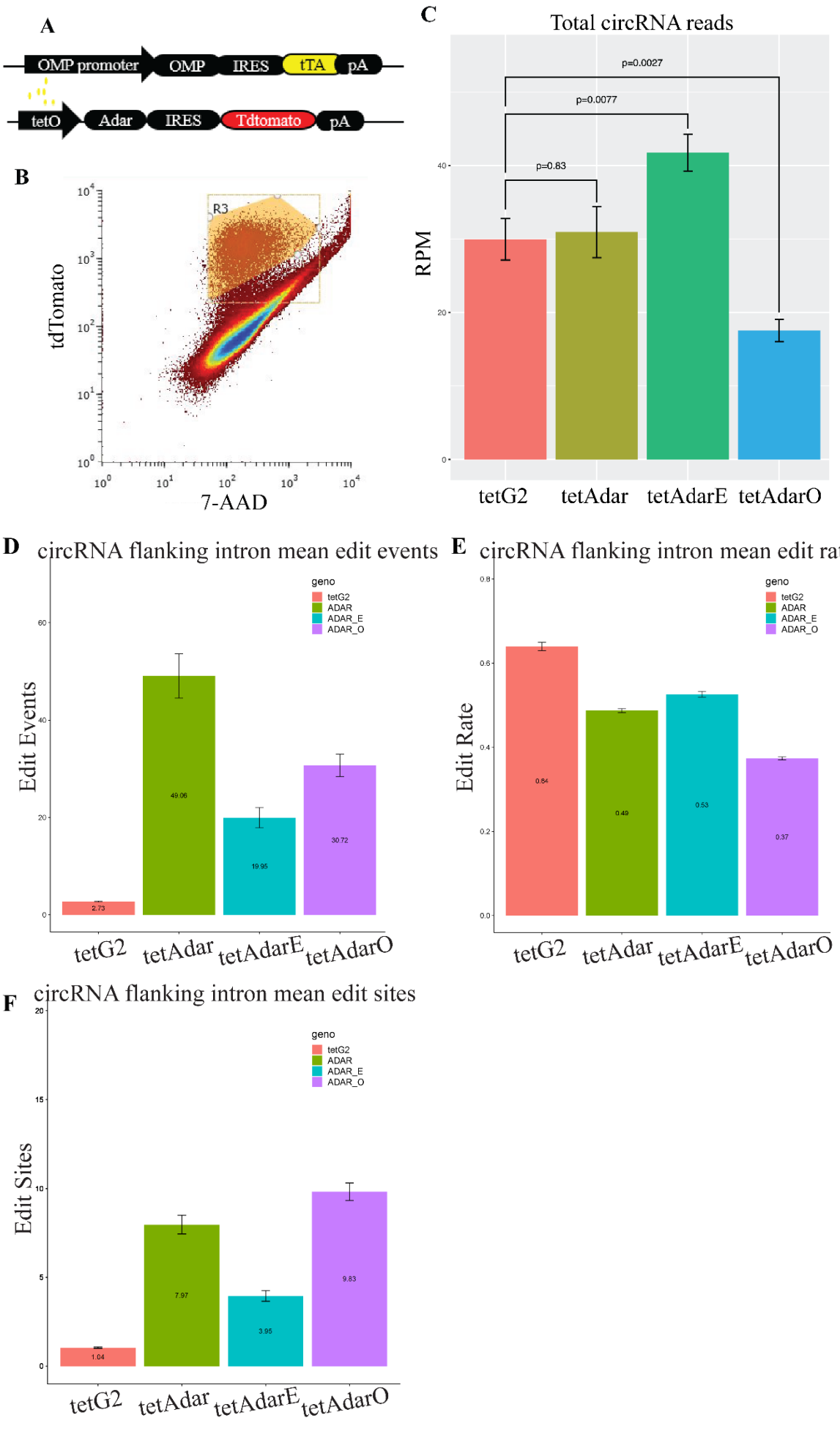
A
OMP promoter
OMP
IRES
tTA
pA
tetO
Adar
IRES
Tdtomato
pA
B
R3
tdTomato
7-AAD
C
Total circRNA reads
p=0.0027
p=0.0077
p=0.83
RPM
tetG2
tetAdar
tetAdarE
tetAdarO
D
circRNA flanking intron mean edit events
geno
tetG2
ADAR
ADAR_E
ADAR_O
Edit Events
2.73
49.06
19.95
30.72
tetG2
tetAdar
tetAdarE
tetAdarO
E
circRNA flanking intron mean edit rate
geno
tetG2
ADAR
ADAR_E
ADAR_O
Edit Rate
0.64
0.49
0.53
0.37
tetG2
tetAdar
tetAdarE
tetAdarO
F
circRNA flanking intron mean edit sites
geno
tetG2
ADAR
ADAR_E
ADAR_O
Edit Sites
1.04
7.97
3.95
9.83
tetG2
tetAdar
tetAdarE
tetAdarO

Figure 4. 2 Studying a possible regulatory role of ADAR in the biogenesis of neural circRNAs

(A) Schematic illustration of tetAdar mice. Ectopic expressing Adar along with the florescent marker tdTomato in Omp^+ OSNs. The similar transgenic strategy is applied to generate tetAdarO, tetAdarE, and tetG2 mice.

(B) Representative image of gating to sort $tdTomato^+$ OSNs. The cell debris are excluded through 7-AAD staining which is a high DNA binding constant for dead cell discrimination. The x-axis represents the 7-AAD signal and the y-axis denotes the tdTomato signal.

(C) Normalized mean total circRNA reads of FACS-seq sample in different genotypes. The error bars represent mean ± SEM. Welch's 2-sided t-test for unequal variances was used to determine significance.

RPM = (# $of\ mapped\ circRNAs$ ∗10^6) / ($total\ \#\ of\ mapped\ reads\ from\ library$)

(D) The average edit events detected in circRNA flanking introns across biological replicates. The error bars represent mean ± SEM.

(E) The average edit rate detected in circRNA flanking introns across biological replicates. The error bars represent mean ± SEM.

Edit-Rate = Edit-Events / Edit-Opportunities

Edit-Opportunities = Edit-Sites * Number of Reads per Site

(F) The mean edit sites detected in circRNA flanking introns, which includes canonical and non-canonical editing sites.

4.2.3 Overexpression of Adar leads to differentiation of circRNA species

We hypothesize that ectopic expression of both tetAdar and tetAdarO downregulates circRNA in OSNs. However, we found that only tetAdarO is effective for downregulating circRNA expression. To profile the circRNA species that are affected by tetAdarO, we sought to analyze the subset of differentially expressed high-confidence circRNAs in tetAdar and tetAdarO OSNs.

Among 171 identified high-confidence circRNA species, 16 circRNAs (circQrich1, circNol4, circDtnb, circZer1, circSlc24a2, circMalat1, circC230004F18Rik, circMapk1, circDcun1d4, circFstl5, circZzz3, circPik3c2a, circCrebrf, circStxbp5l, circTcf20, circRere) were significantly downregulated in tetAdar OSNs (Figure 4.3A) and 21 circRNAs (circMagi1, circAsxl2, circBckdhb, circCspp1, circCdh9, circRp2, circR3hcc1l, circDtnb, circCfap61, circGlis3, circZbbx, circZfp644, circTshz2, circUbn2, circC230004F18Rik, circStrbp, circPtbp3, circZmym4, circCdk13, circMed12l, circAkap6) were significantly downregulated in tetAdarO OSNs (Figure 4.3B). Some of these identified circRNAs are well-studied. For instance, circC230004F18Rik, which is well known as Cdr1as, regulates the stability and activity of miR-7 and is associated with neuropsychiatric disorders (Piwecka et al., 2017). CircMapk1 may contribute to brain aging (Xu et al., 2018). CircMagi1 is one of the most abundant and upregulated circRNAs during neuronal differentiation, from mouse embryonic stem cells to differentiated glutamatergic neurons (Hollensen et al., 2019). The lncRNA-derived circMalat1 interacts with PAX5 coding sequence and ribosomes to retard PAX5 mRNA translation (Chen et al., 2019). The dynamic expression of circCspp1 before birth may function on embryonic porcine brain development (Venø et al., 2015).

We have found that isoform Adar1La in OSNs is an effective regulator of circRNA biogenesis (Figure 4.2C). Moreover, we have identified various high-confidence

circRNAs that are downregulated by ectopic expression of Adar1p150 or ADAR1La. Next, we want to profile possible functions of these identified circRNAs.

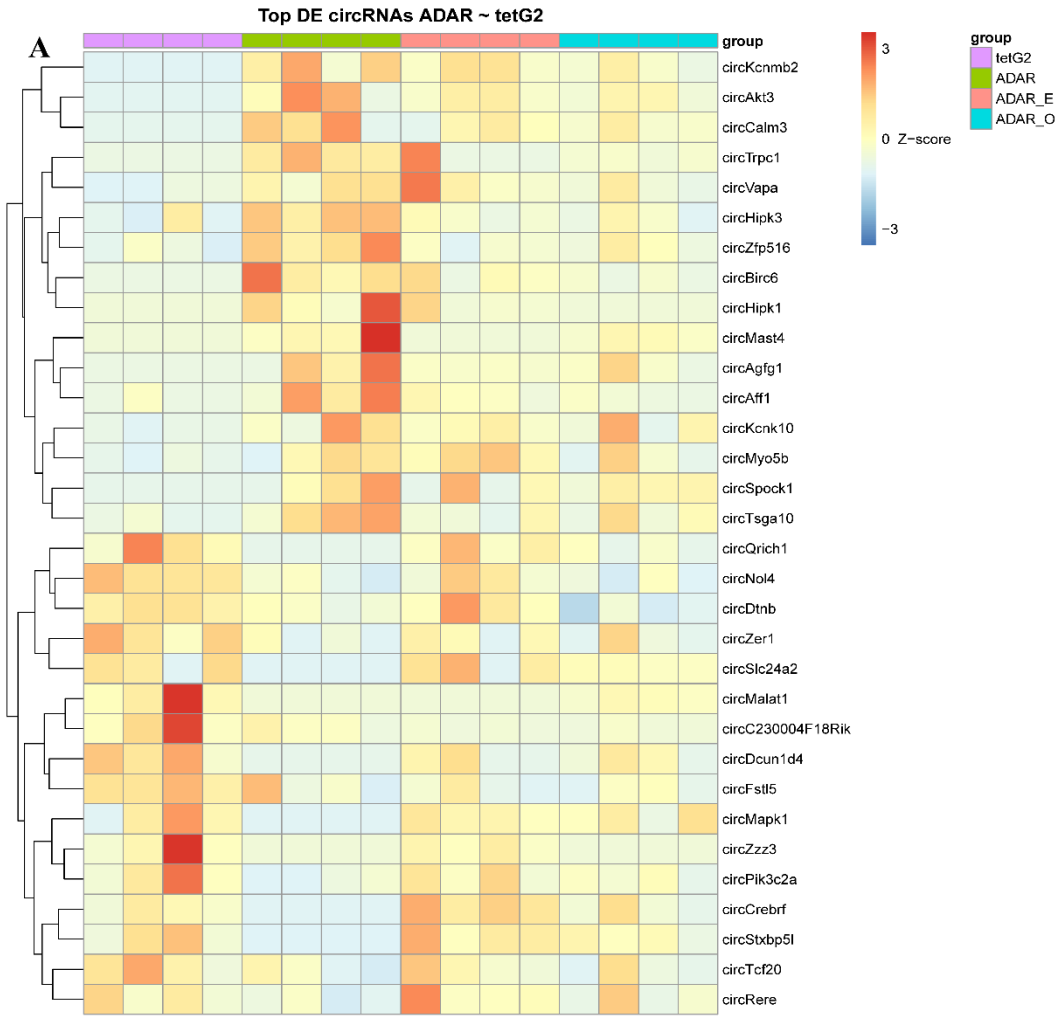
A
Top DE circRNAs ADAR ~ tetG2
group
circKcnmb2
circAkt3
circCalm3
circTrpc1
circVapa
circHipk3
circZfp516
circBirc6
circHipk1
circMast4
circAgfg1
circAff1
circKcnk10
circMyo5b
circSpock1
circTsga10
circQrich1
circNol4
circDtnb
circZer1
circSlc24a2
circMalat1
circC230004F18Rik
circDcun1d4
circFstl5
circMapk1
circZzz3
circPik3c2a
circCrebrf
circStxbp5l
circTcf20
circRere
3
0 Z−score
−3
group
tetG2
ADAR
ADAR_E
ADAR_O

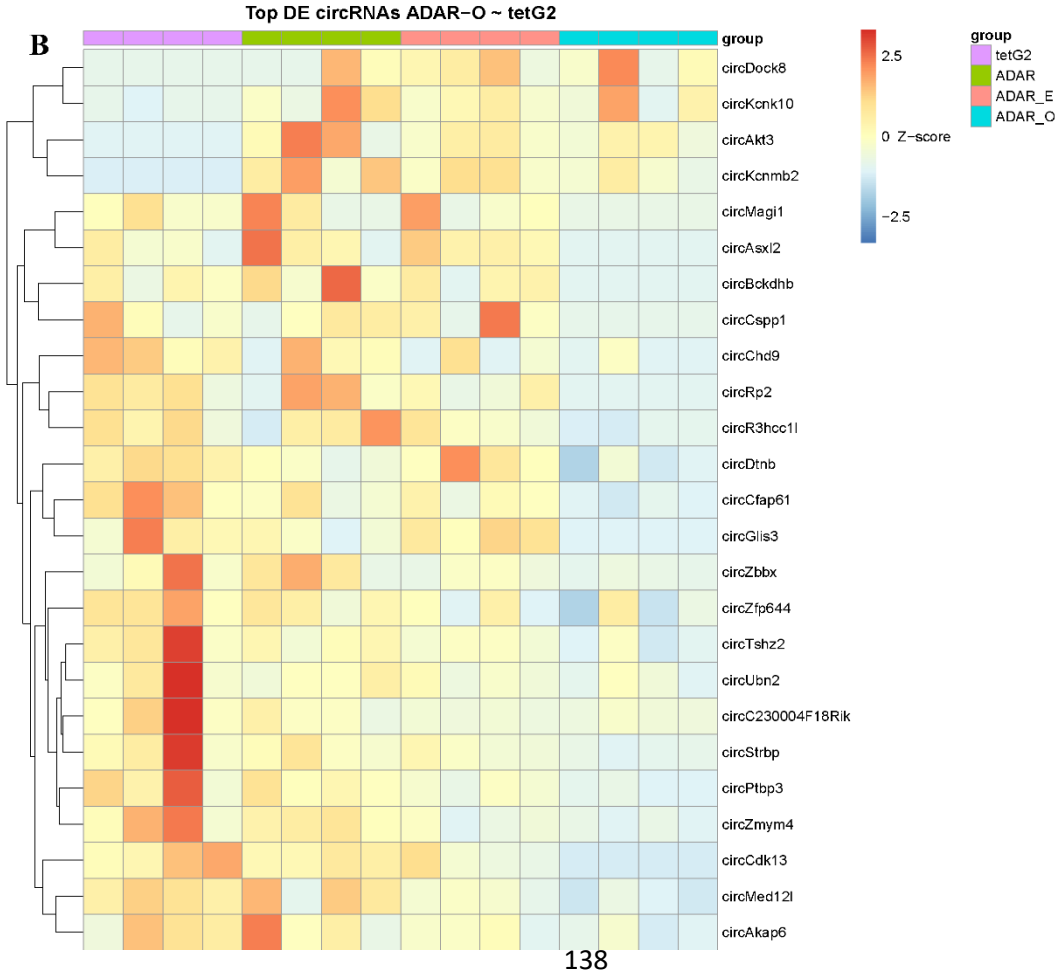
B
Top DE circRNAs ADAR−O ~ tetG2
group
circDock8
circKcnk10
circAkt3
circKcnmb2
circMagi1
circAsxl2
circBckdhb
circCspp1
circChd9
circRp2
circR3hcc1l
circDtnb
circCfap61
circGlis3
circZbbx
circZfp644
circTshz2
circUbn2
circC230004F18Rik
circStrbp
circPtbp3
circZmym4
circCdk13
circMed12l
circAkap6
2.5
0 Z−score
−2.5
group
tetG2
ADAR
ADAR_E
ADAR_O

Figure 4. 3 Overexpression of Adar leads to differentiation of circRNA species

(A) Heatmap of high-confidence differentially expressed circRNAs in tetAdar OSNs. The rightmost legend denotes the color for different genotypes. By comparing the tetAdar (green in the top of the heatmap) with tetG2 (purple in the top of the heatmap), 16 circRNAs are specifically downregulated in tetAdar OSNs.

Wald test of the negative binomial generalized linear model is applied for Adar ~ tetG2.

The heatmap colors represent the Z-score(log2(TPM + 1)).

(B) Heatmap of high-confidence differentially expressed circRNAs in tetAdarO OSNs.

Wald test of the negative binomial generalized linear model is applied for AdarO ~ tetG2.

The heatmap colors represent the Z-score(log2(TPM + 1)).

4.3 Transgenic expression of Adar1p150 in OSNs disrupts olfactory axon projection pattern

One of the major advantages of studying olfactory neurons is stereotypy in axon projection, which makes it possible to observe any alterations in the system. I first tested whether ectopic expression of Adar1La directly affects axon convergence.

Each transgenic line was crossed with M72-IRES-tauGFP mouse separately. Strikingly, the whole-mount image of tetAdar;M72-IRES-tauGFP olfactory bulb showed a severely disrupted axon projection pattern: the M72 axons project diffusely and form multiple glomeruli that nearly cover the entire posterior dorsal olfactory bulb (Figure 4.4A). On the contrary, the M72 axons in tetAdarO;M72-IRES-tauGFP and tetAdarE;M72-IRES-tauGFP mice project to a single glomerulus, similar to the wild-type M72-IRES-tauGFP control (Figure 4.4B-C).

To further explore the phenotype perceived in tetAdar;M72-IRES-tauGFP mice, I treated these mice with DOX from P0 to stop ectopic Adar expression (Figure 4.6A). I examined axon projections at P30 and found DOX administration from P0 could not restore the spreading projection of axon fibers, which suggests Adar may function on axon projection as early as the embryonic stage.

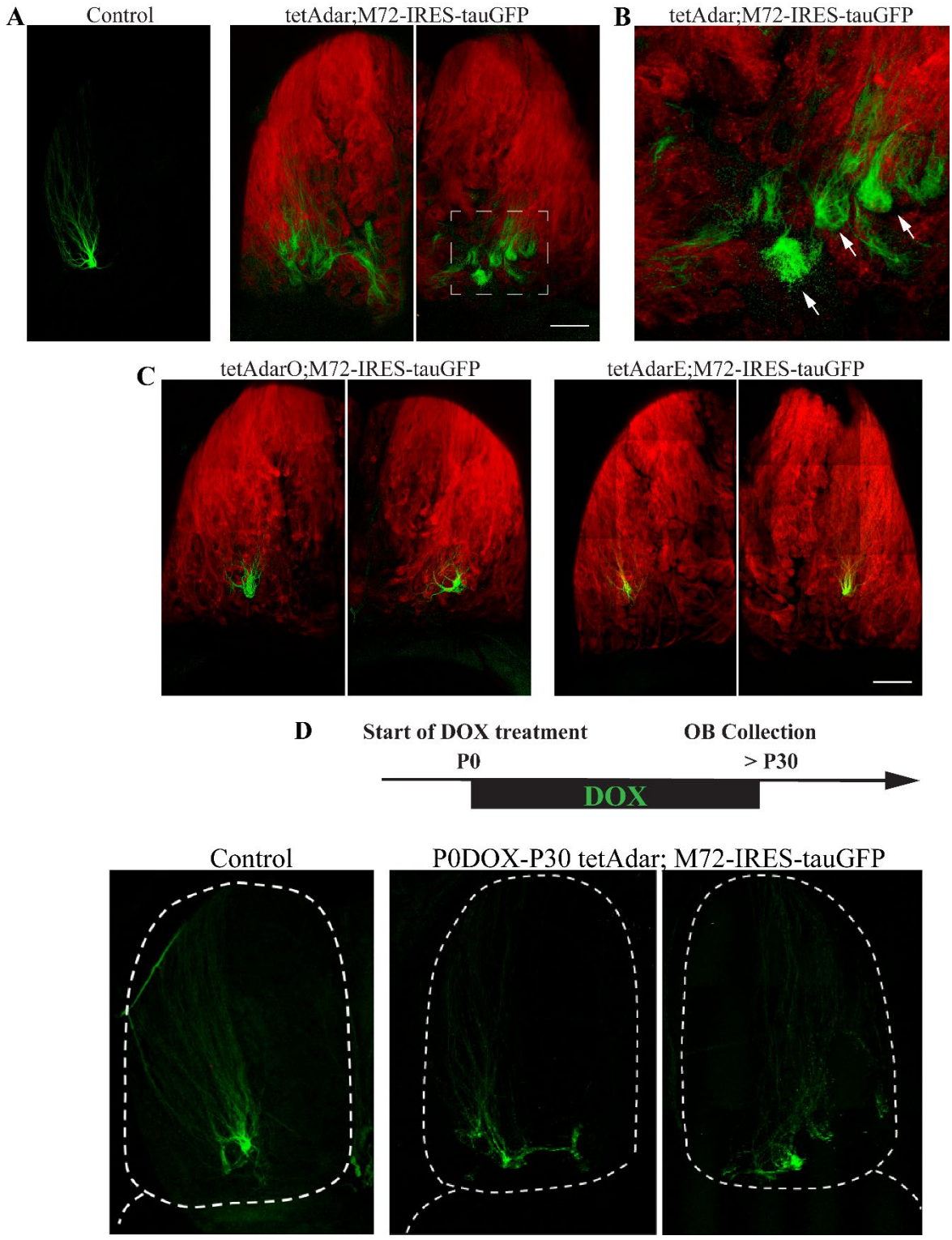

Figure 4. 4 Transgenic expression of Adar1p150 in OSNs disrupts olfactory axon projection pattern

(A) Whole-mount images of M72 glomeruli in littermate control and tetAdar;M72-IRES-tauGFP mice. Compared to control, neurons expressing the M72 receptor target to multiple partially innervated glomeruli that are close to the predominant M71 glomerulus site in tetAdar;M72-IRES-tauGFP animal. GFP, green; tdTomato, red. Scale bar, 500 µm.

(B) Zoomed-in image from the dash line square region in (A). The M72 axonal fibers in tetAdarO;M72-IRES-tauGFP animal form multiple glomeruli that nearly cover the entire posterior dorsal olfactory bulb. Arrowheads indicate the innervated glomeruli.

(C) Whole-mount images of M72 glomeruli in tetAdarO;M72-IRES-tauGFP and tetAdarE;M72-IRES-tauGFP mice, which is similar to control in (A). GFP, green; tdTomato, red. Scale bar, 500 μm.

(D) Whole-mount images of M72 glomeruli in M72-IRES-tauGFP (control) and P30 tetAdar;M72-IRES-tauGFP mice treated with DOX food from P0. The upper panel is the schematic illustration of DOX treatment to stop ectopic Adar and tdTomato expression in tetAdar; M72-IRES-tauGFP and control M72-IRES-tauGFP mice. In tetAdar;M72-IRES-tauGFP mice, the axon projection pattern is not recovered. DOX treatment prevents the ectopic expression of H19 and tdTomato. GFP, green.

4.3.1 Axon projection phenotype in tetAdar OSNs is related to altered neuronal activity

In tetAdar;M72-IRES-tauGFP animal, it appears that there are more M72 axons innervating into several glomeruli. Is this a result of an increase in M72 neurons? We examined the distribution of M72 OSNs in the epithelia section and found that M72 OSNs are sparsely located without significant growth in numbers. We then performed immunostaining against different populations of local neurons in the olfactory bulb, and we found the tyrosine hydroxylase (TH) activity in the dopaminergic periglomerular cells is particularly stronger in the tetAdar mice (Figure 4.5A). The periglomerular dopamine neurons receive excitatory glutamatergic input from olfactory axons and thus TH signal reflects the level of synaptic activity in the presynaptic olfactory neurons. It is reported that naris occlusion dramatically decreases the TH staining intensity (Baker et al., 1993a). The increased signal intensity of TH suggests that there is increased OSN activity in tetAdar animals.

In addition, we found expression of Vglut2 is also significantly upregulated in axon terminals of OSNs compared to control, tetAdarE, and tetAdarO (Figure 4.5B). OSNs convey sensory information directly to the OB via conventional glutamatergic synaptic contacts (Sassoè-Pognetto et al., 1993), and Vglut2 is the glutamate transporter responsible for the accumulation and storage of glutamate within synaptic vesicles. These results indicate increased activity of synaptic transmission in tetAdar OSNs.

The protein ADAR1La shares the same dsRBD and deaminase domain with ADAR1p150. However, the M72 axons in tetAdarO;M72-IRES-tauGFP mice display a singular projection pattern. These results suggest that the missing 26 amino acids within the linker region between dsRBD and deaminase domain in Adar1p150 can affect its function through potential structure change. In addition, the functional role of Adar1La remains

elusive. The analysis that identified circRNAs downregulated by Adar1La provides a clue for the potential function of Adar1p150 as a circRNA biogenesis regulator.

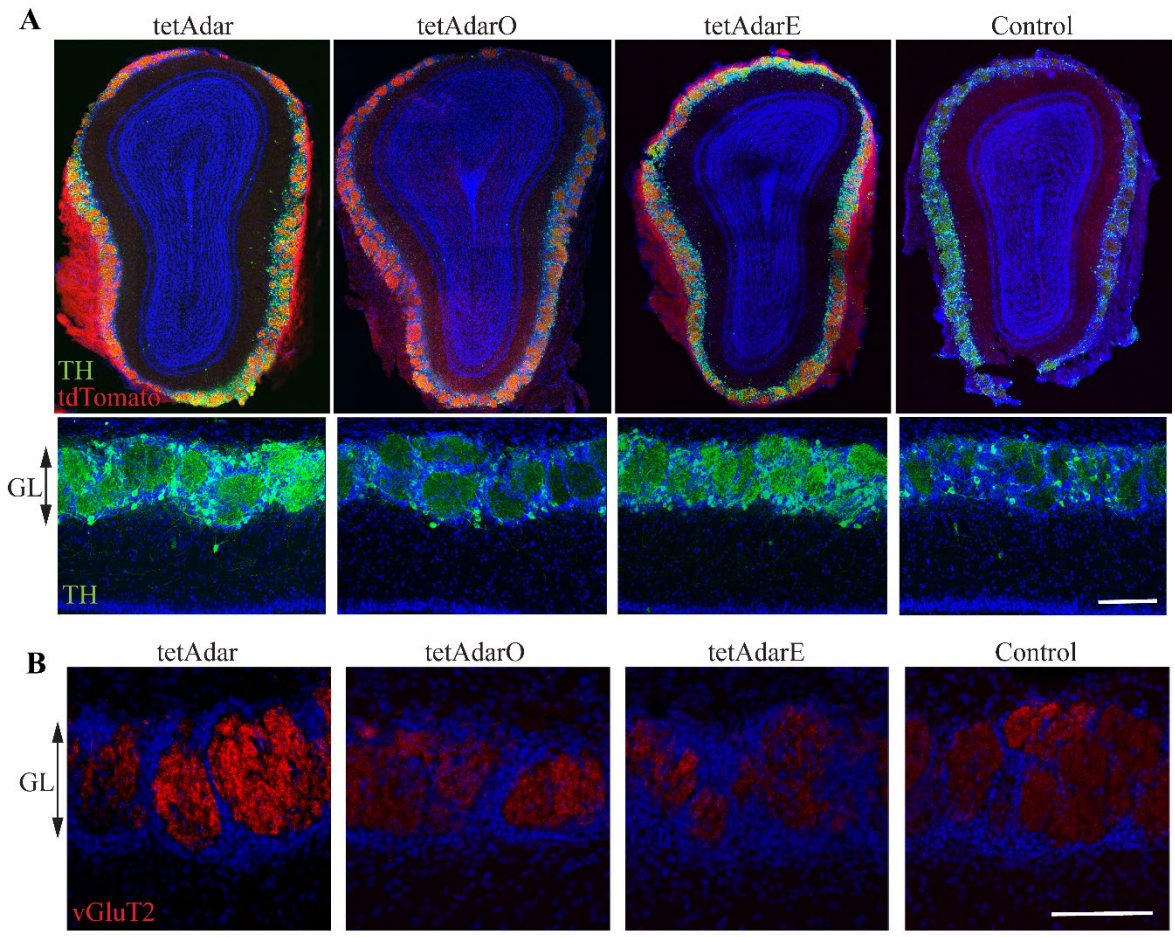

Figure 4. 5 Axon projection phenotype in tetAdar OSNs is related to altered neuronal activity

(A) Expression of tyrosine hydroxylase (green) and tdTomato (red) in the adult olfactory bulb. The upper panel shows the tyrosine hydroxylase and tdTomato in sections of the olfactory bulb from transgenes and control animals. The bottom panel represents the zoomed-in view of tyrosine hydroxylase staining in the glomerular layer, GL, consists of glomeruli, periglomerular cells, external tufted cells, and superficial short-axon cells. DAPI, blue. Scale bar, 100 µm.

(B) Expression of Vglut2 (red) in the glomerular layer of the adult olfactory bulb. Each panel represents a coronal section from each transgene or control. Vglut2 is exclusively expressed by fully differentiated OSNs. Here, the glomeruli are filled with axon terminals stained for Vglut2. DAPI, blue. Scale bar, 100 µm.

4.3.2 Ectopic expression of Adar1La broadly downregulates OR expression

To understand the differences between tetAdar and tetAdarO OSNs, we analyzed the transcriptome from the FACS-seq data of OSNs. We find the most discernible difference is most OR genes are significantly downregulated in tetAdar OSNs (Figure 4.6). The downregulation of many OR genes in tetAdar OSNs could be a phenotype associated with increased activity of synaptic transmission. The OSNs exhibit spontaneous activity which plays a role in establishing proper synaptic connections (Yu et al., 2004). The increased synaptic transmission in tetAdar OSNs in the absence of odor stimulation affects spontaneous firing of OSNs, which results in a change of the average OR expression.

However, overexpression of Adar1La does not affect axon projection and neuronal activity but there is also downregulation of many OR genes in tetAdarO OSNs (Figure 4.6). This result provides a link of ADAR1La function with OR expression. Further research is needed to explore how Adar1La affects OR expression and whether it is a result of downregulated circRNAs.

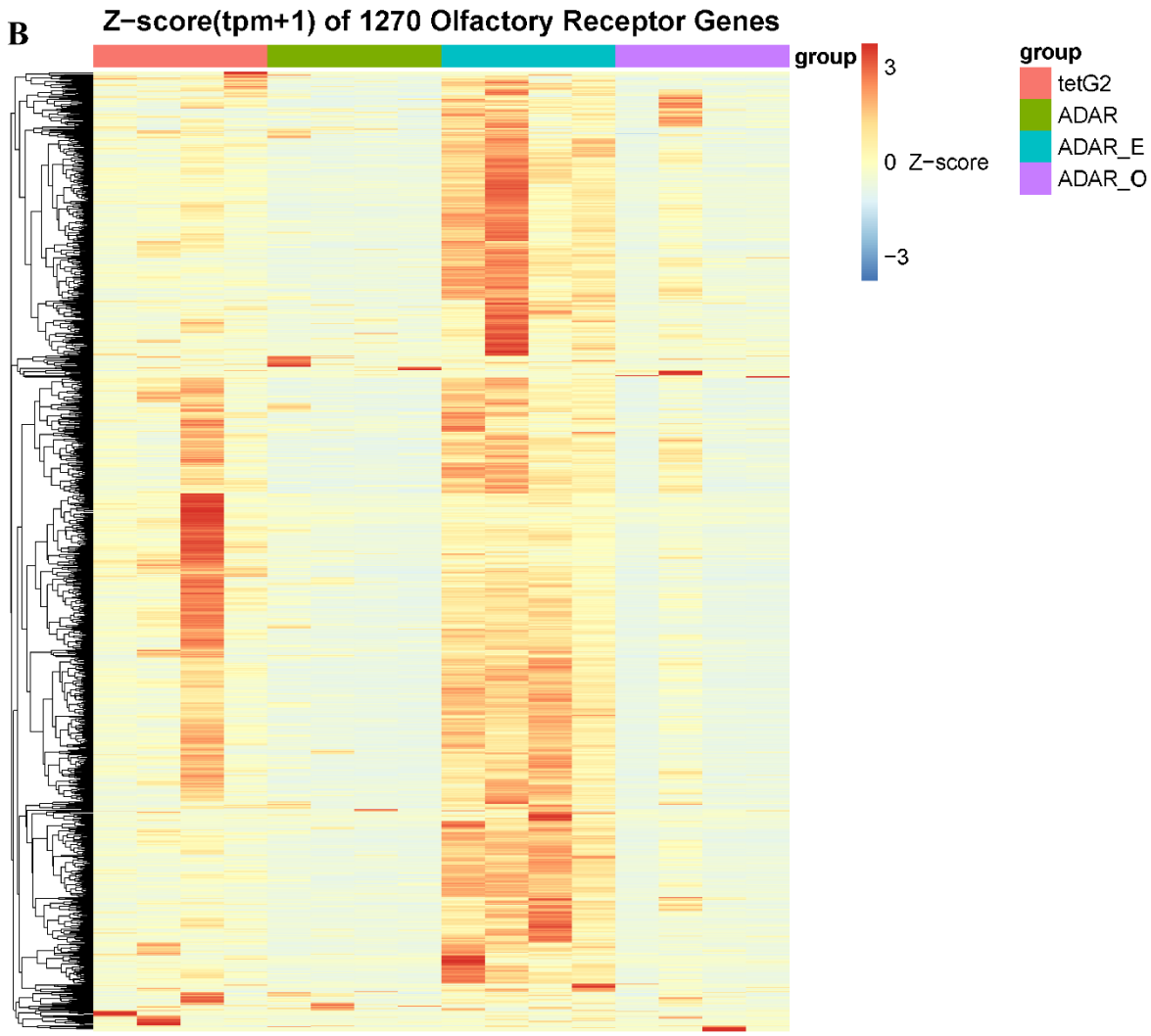

Figure 4. 6 Adar may function on axon projection as early as embryonic stage

Heatmap of differentially expressed OR genes from the OSNs FACS-seq of different transgenic lines. The average expression of most receptor genes from high to low is tetAdarE > tetG2 > tetAdarO > tetAdar. The heatmap colors represent the Z-score(log2(TPM + 1)).

4.4 Adar is required for olfactory axon projection, especially for some receptor types

In many cases, RNA editing of protein-coding genes results in generation of protein isoforms and diversification of protein functions. For instance, A-to-I editing on the Q/R site of GluR-B ion channel subunit plays a critical role in ion channel function (Higuchi et al., 1993). Ectopic expression of Adar1p150 could also affect the endogenous A-to-I editing process, and therefore complicate attempts at interpretation. To evaluate the necessity of Adar in OSN development, we generated the ADAR1$^{-/-}$;OMP-IRES-Cre mice (Adar$^{-/-}$ mice) by crossing ADAR1$^{flox/flox}$ (Wang et al., 2004) with OMP-IRES-Cre (Eggan et al., 2004).

To examine the projection pattern of individual OSN types, I crossed the Adar$^{-/-}$ mice with M72-IRES-tauGFP, M71-IRES-tauGFP (Olfr151) (Feinstein and Mombaerts, 2004), and MOR28-IRES-EGFP (Olfr1507) (Shykind et al., 2004) respectively. Remarkably, there were different phenotypes for different receptors at adulthood. In adult Adar$^{-/-}$;M71-IRES-tauGFP mice, severe ectopic axon projections were observed. M71 axons broadly projected to multiple innervated glomeruli instead of converging to the single glomerulus in dorsal lateral half OB (Figure 4.5A). In contrast, some exuberant axons project diffusely in the olfactory bulb and some axons target to the major glomeruli in Adar$^{-/-}$;M72-IRES-tauGFP mice (Figure 4.5A). Adar$^{-/-}$;MOR28-IRES-tauGFP mice exhibit a convergent projection pattern similar to that in wild-type animals, in which there are one lateral glomerulus and one medial glomerulus per half bulb (Figure 4.5A). These results suggest Adar is required for olfactory axon projection and the regulatory effect of Adar is uniquely correlated with the expressed OR species.

What leads to such discernible differences among different ORs? It is known that ADAR mainly binds double-stranded RNAs, editing the protein-coding sequence or non-coding sequences of target RNAs to affect splicing, translation, and mRNA stability. The

expression of a single OR per neuron is orchestrated by a network of interchromosomal enhancer interactions and large-scale changes in nuclear architecture (Monahan and Lomvardas, 2015). It is less likely that Adar is required to edit different OR mRNAs and thus act on OR translation. Both M71 and M72 axon targeting is along the anterior-posterior axis, but MOR28 project along the dorsal-ventral axis. Is it possible that Adar regulates axon targeting along the A-P axis? We subsequently stained the Omp^{+} and $Gap43^{+}$ axons in the OB sections of $Adar^{-/-}$ mice. In the control axons of mOSNs, Omp immunoreactivity filled their synaptic target glomeruli (Figure 4.5A). In $Adar^{-/-}$ mice, Omp^{+} axons did not fully innervate most glomeruli at dorsal, ventral, and medial level of the OB, which suggests Adar regulates axon projection of many OSNs expressing other ORs rather than just M71 or M72. When examining Omp^{+} axons within an individual glomerulus, we found that mature axons passed through the glomerular layer and terminated in the external plexiform layer at the adult stage (Figure 4.5B). Larger synapse structures can be found in axon terminal $Adar^{-/-}$ OSNs, which indicates Adar also affects synapse formation. Different ORs have different GPCR structures and different spontaneous activity patterns. It is possible that Adar may regulate the neuronal activity of OSNs and affect axon projection. However, more work needs to be done to test this hypothesis.

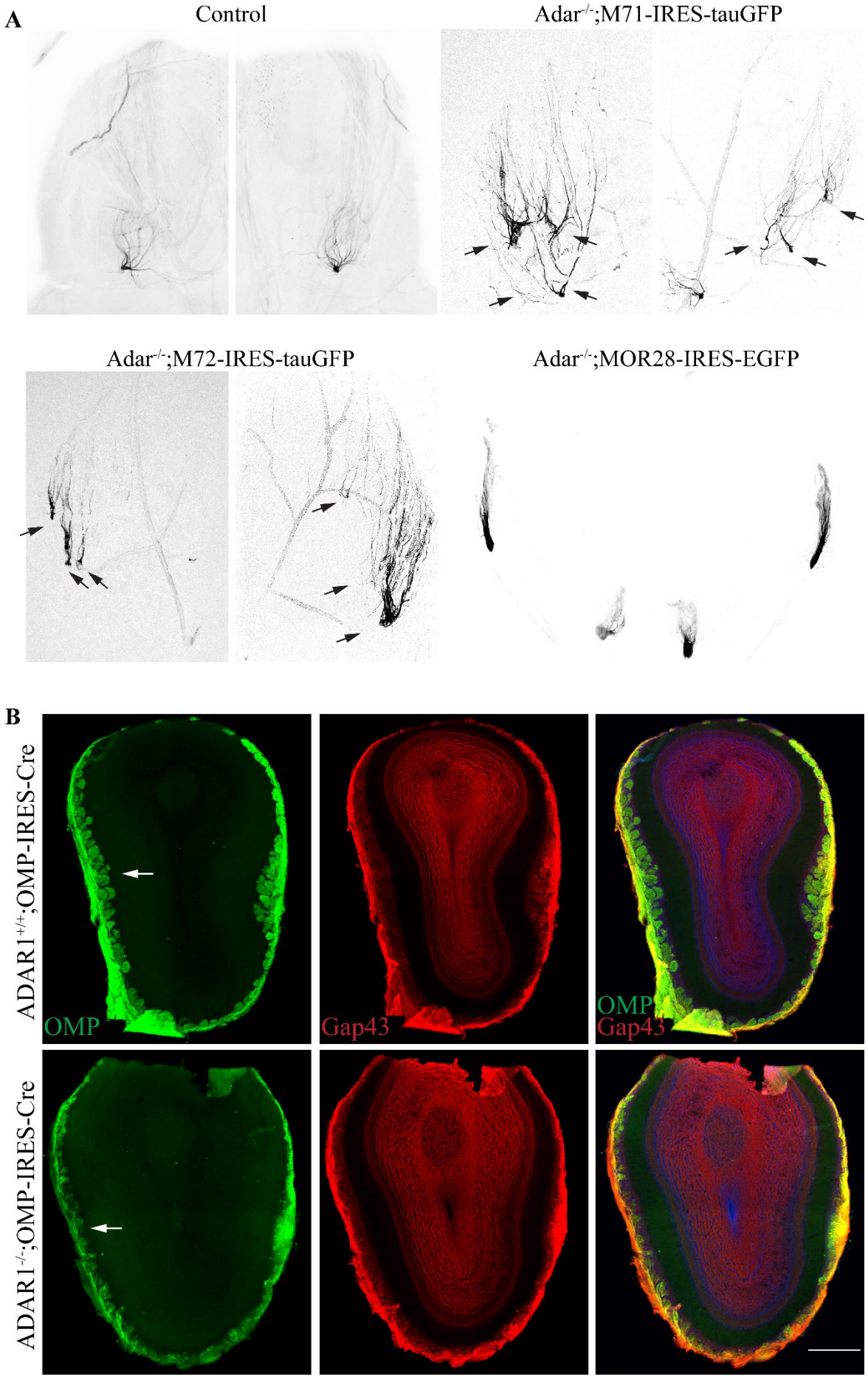
A
Control
Adar-/-;M71-IRES-tauGFP
Adar-/-;M72-IRES-tauGFP
Adar-/-;MOR28-IRES-EGFP
B
ADAR1+/+;OMP-IRES-Cre
ADAR1-/-;OMP-IRES-Cre
OMP
Gap43
OMP
Gap43

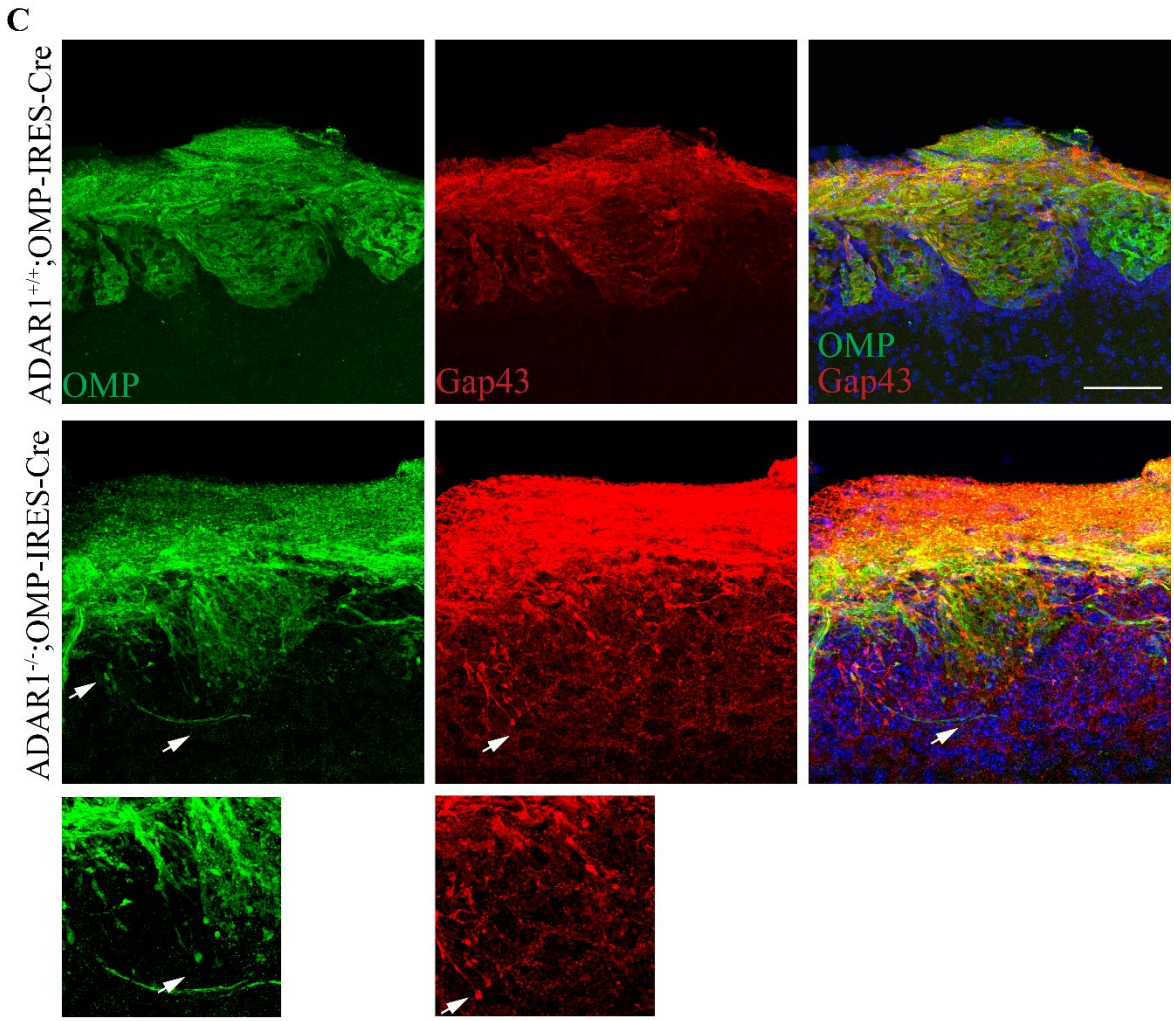

Figure 4. 7 Adar is required for olfactory axon projection, especially for some receptor types

(A) Whole-mount images of Adar$^{-/-}$;M71-IRES-tauGFP, Adar$^{-/-}$;M72-IRES-tauGFP, Adar$^{-/-}$;MOR28-IRES-tauGFP, and M71-IRES-tauGFP (control) OB at P30. Axons in grey color. Arrowheads indicate partially innervated glomeruli. OSN axons exhibit axon-targeting errors in the olfactory bulbs of both Adar$^{-/-}$;M71-IRES-tauGFP and Adar$^{-/-}$;M72-IRES-tauGFP mice.

(B) Immunostaining OMP and Gap43 of P30 Adar$^{-/-}$ and Adar$^{+/-}$ (control) OB coronal sections. Both Omp^{+} (green) and Gap43^{+} (red) axons detected in Adar$^{-/-}$ and control OB. Omp^{+} (green) axons in Adar$^{-/-}$ OB are deficit of filling an intact glomeruli. DAPI, blue. Scale bar, 500 μm.

(C) Representative images of glomeruli of P30 Adar$^{-/-}$ and Adar$^{+/-}$ mice. Sections are stained with Omp (green) and Gap43 (red). Arrowheads indicate exuberant axons invading the external plexiform layer and axon terminals. DAPI, blue. Scale bar, 100 μm.

4.5 Discussion

In this study, we found that RNA editing enzyme ADAR functions on olfactory axon projection in an OR-dependent way. We found that ectopic expression of Adar1p150 in OSNs disrupts olfactory axon projection pattern and affects neuronal activity. It also decreases the expression of a subset of circular RNAs. In addition, we identified that the Adar1 isoform Adar1La could widely downregulate circular RNAs and OR expression without affecting axon targeting, but the physiological function of Adar1La remains unknown.

The on-DOX experiment in tetAdar animal indicates that downregulation of Adar determines axon targeting during the embryonic stage when the olfactory system has not been exposed to any odors in the environment. The ectopic expression of Adar1p150 in OSNs affects neuronal activity, which indicates that Adar functions in the spontaneous firing of OSNs. It was reported that spontaneous firing rates are different among OSN classes (Connelly et al., 2013). We found ADAR-deficient OSNs display impaired axon targeting for certain OR types. This result further supports that Adar affects the spontaneous activity of OSNs.

Ectopic expression of Adar1p150 downregulates the expression of a subset of circRNAs, including Cdr1as. Deficiency of Cdr1as in the mouse brain leads to dysfunction of excitatory synaptic transmission (Piwecka et al., 2017). This result raises the possibility that ADAR functions in neuronal activity through regulating circRNAs. However, Cdr1as is also downregulated in OSNs ectopically expressing Adar1p150, which indicates there are other functional mechanisms of Adar in OSNs.

Reference

Abdelmohsen, K., Hutchison, E.R., Lee, E.K., Kuwano, Y., Kim, M.M., Masuda, K., Srikantan, S., Subaran, S.S., Marasa, B.S., and Mattson, M.P. (2010). miR-375 inhibits differentiation of neurites by lowering HuD levels. Molecular and cellular biology *30*, 4197-4210.

Ache, B.W., and Young, J.M. (2005). Olfaction: diverse species, conserved principles. Neuron *48*, 417-430.

Adams, D.R., and McFarland, L. (1971). Septal olfactory organ in Peromyscus. Comparative Biochemistry and Physiology Part A: Physiology *40*, 971-974.

Agarwal, V., Bell, G.W., Nam, J.-W., and Bartel, D.P. (2015). Predicting effective microRNA target sites in mammalian mRNAs. elife *4*, e05005.

Akhmanova, A., and Steinmetz, M.O. (2008). Tracking the ends: a dynamic protein network controls the fate of microtubule tips. Nature reviews Molecular cell biology *9*, 309-322.

Akins, M.R., and Greer, C.A. (2006). Cytoskeletal organization of the developing mouse olfactory nerve layer. Journal of Comparative Neurology *494*, 358-367.

Albeanu, D.F., Provost, A.C., Agarwal, P., Soucy, E.R., Zak, J.D., and Murthy, V.N. (2018). Olfactory marker protein (OMP) regulates formation and refinement of the olfactory glomerular map. Nature communications *9*, 1-12.

Aletta, J.M., Shelanski, M., and Greene, L. (1989). Phosphorylation of the peripherin 58-kDa neuronal intermediate filament protein. Regulation by nerve growth factor and other agents. Journal of Biological Chemistry *264*, 4619-4627.

Amandio, A.R., Necsulea, A., Joye, E., Mascrez, B., and Duboule, D. (2016). Hotair is dispensible for mouse development. PLoS genetics *12*, e1006232.

Aprea, J., Prenninger, S., Dori, M., Ghosh, T., Monasor, L.S., Wessendorf, E., Zocher, S., Massalini, S., Alexopoulou, D., and Lesche, M. (2013). Transcriptome sequencing during mouse brain development identifies long non‐coding RNAs functionally involved in neurogenic commitment. The EMBO journal *32*, 3145-3160.

Ashwal-Fluss, R., Meyer, M., Pamudurti, N.R., Ivanov, A., Bartok, O., Hanan, M., Evantal, N., Memczak, S., Rajewsky, N., and Kadener, S. (2014). circRNA biogenesis competes with pre-mRNA splicing. Molecular cell *56*, 55-66.

Bakalyar, H.A., and Reed, R.R. (1990). Identification of a specialized adenylyl cyclase that may mediate odorant detection. Science *250*, 1403-1406.

Baker, H., Morel, K., Stone, D.M., and Maruniak, J.A. (1993a). Adult naris closure profoundly reduces tyrosine hydroxylase expression in mouse olfactory bulb. Brain research *614*, 109-116.

Baker, J., Liu, J.-P., Robertson, E.J., and Efstratiadis, A. (1993b). Role of insulin-like growth factors in embryonic and postnatal growth. Cell *75*, 73-82.

Balmer, C.W., and LaMantia, A.S. (2004). Loss of Gli3 and Shh function disrupts olfactory axon trajectories. Journal of Comparative Neurology *472*, 292-307.

Balmer, C.W., and LaMantia, A.S. (2005). Noses and neurons: induction, morphogenesis, and neuronal differentiation in the peripheral olfactory pathway. Developmental Dynamics *234*, 464-481.

Bannister, L.H., and Dodson, H.C. (1992). Endocytic pathways in the olfactory and vomeronasal epithelia of the mouse: ultrastructure and uptake of tracers. Microscopy research and technique *23*, 128-141.

Barnea, G., O'Donnell, S., Mancia, F., Sun, X., Nemes, A., Mendelsohn, M., and Axel, R. (2004). Odorant receptors on axon termini in the brain. Science *304*, 1468-1468.

Barrett, S.P., and Salzman, J. (2016). Circular RNAs: analysis, expression and potential functions. Development *143*, 1838-1847.

Barry, G., Briggs, J.A., Nayler, S.P., Fortuna, P.R., Jonkhout, N., Dachet, F., Maag, J.L., Mestdagh, P., Singh, E.M., and Avesson, L. (2017). The long non-coding RNA NEAT1 is responsive to neuronal activity and is associated with hyperexcitability states. Scientific reports *7*, 1-11.

Bartolomei, M.S., Zemel, S., and Tilghman, S.M. (1991). Parental imprinting of the mouse H19 gene. Nature *351*, 153-155.

Beites, C.L., Kawauchi, S., Crocker, C.E., and Calof, A.L. (2005). Identification and molecular regulation of neural stem cells in the olfactory epithelium. Experimental cell research *306*, 309-316.

Belluscio, L., Gold, G.H., Nemes, A., and Axel, R. (1998). Mice deficient in Golf are anosmic. Neuron *20*, 69-81.

Belmont, L.D., and Mitchison, T.J. (1996). Identification of a protein that interacts with tubulin dimers and increases the catastrophe rate of microtubules. Cell *84*, 623-631.

Bernard, D., Prasanth, K.V., Tripathi, V., Colasse, S., Nakamura, T., Xuan, Z., Zhang, M.Q., Sedel, F., Jourdren, L., and Coulpier, F. (2010). A long nuclear-retained non-coding RNA regulates synaptogenesis by modulating gene expression. The EMBO journal *29*, 3082-3093.

Berteaux, N., Aptel, N., Cathala, G., Genton, C., Coll, J., Daccache, A., Spruyt, N., Hondermarck, H., Dugimont, T., and Curgy, J.-J. (2008). A novel H19 antisense RNA overexpressed in breast cancer contributes to paternal IGF2 expression. Molecular and cellular biology *28*, 6731-6745.

Bhattacharyya, S., and Bronner-Fraser, M. (2008). Competence, specification and commitment to an olfactory placode fate. Development *135*, 4165-4177.

Blackshaw, S., Harpavat, S., Trimarchi, J., Cai, L., Huang, H., Kuo, W.P., Weber, G., Lee, K., Fraioli, R.E., and Cho, S.-H. (2004). Genomic analysis of mouse retinal development. PLoS biology *2*, e247.

Bond, A.M., VanGompel, M.J., Sametsky, E.A., Clark, M.F., Savage, J.C., Disterhoft, J.F., and Kohtz, J.D. (2009). Balanced gene regulation by an embryonic brain ncRNA is critical for adult hippocampal GABA circuitry. Nature neuroscience *12*, 1020.

Bracko, O., Singer, T., Aigner, S., Knobloch, M., Winner, B., Ray, J., Clemenson, G.D., Suh, H., Couillard-Despres, S., and Aigner, L. (2012). Gene expression profiling of neural stem cells and their neuronal progeny reveals IGF2 as a regulator of adult hippocampal neurogenesis. Journal of Neuroscience *32*, 3376-3387.

Brann, J.H., Ellis, D.P., Ku, B.S., Spinazzi, E.F., and Firestein, S. (2015). Injury in aged animals robustly activates quiescent olfactory neural stem cells. Frontiers in neuroscience *9*, 367.

Brannan, C.I., Dees, E.C., Ingram, R.S., and Tilghman, S.M. (1990). The product of the H19 gene may function as an RNA. Molecular and cellular biology *10*, 28-36.

Brogiolo, W., Stocker, H., Ikeya, T., Rintelen, F., Fernandez, R., and Hafen, E. (2001). An evolutionarily conserved function of the Drosophila insulin receptor and insulin-like peptides in growth control. Current biology *11*, 213-221.

Brunet, L.J., Gold, G.H., and Ngai, J. (1996). General anosmia caused by a targeted disruption of the mouse olfactory cyclic nucleotide–gated cation channel. Neuron *17*, 681-693.

Buck, L., and Axel, R. (1991). A novel multigene family may encode odorant receptors: a molecular basis for odor recognition. Cell *65*, 175-187.

Bussemakers, M.J., Van Bokhoven, A., Verhaegh, G.W., Smit, F.P., Karthaus, H.F., Schalken, J.A., Debruyne, F.M., Ru, N., and Isaacs, W.B. (1999). Dd3:: A new prostate-specific gene, highly overexpressed in prostate cancer. Cancer research *59*, 5975-5979.

Cabili, M.N., Trapnell, C., Goff, L., Koziol, M., Tazon-Vega, B., Regev, A., and Rinn, J.L. (2011). Integrative annotation of human large intergenic noncoding RNAs reveals global properties and specific subclasses. Genes & development *25*, 1915-1927.

Cai, X., and Cullen, B.R. (2007). The imprinted H19 noncoding RNA is a primary microRNA precursor. Rna *13*, 313-316.

Camoletto, P., Colesanti, A., Ozon, S., Sobel, A., and Fasolo, A. (2001). Expression of stathmin and SCG10 proteins in the olfactory neurogenesis during development and after lesion in the adulthood. Brain research bulletin *54*, 19-28.

Capel, B., Swain, A., Nicolis, S., Hacker, A., Walter, M., Koopman, P., Goodfellow, P., and Lovell-Badge, R. (1993). Circular transcripts of the testis-determining gene Sry in adult mouse testis. Cell *73*, 1019-1030.

Cau, E., Casarosa, S., and Guillemot, F. (2002). Mash1 and Ngn1 control distinct steps of determination and differentiation in the olfactory sensory neuron lineage. Development *129*, 1871-1880.

Chalk, A.M., Taylor, S., Heraud-Farlow, J.E., and Walkley, C.R. (2019). The majority of A-to-I RNA editing is not required for mammalian homeostasis. Genome biology *20*, 1-14.

Chen, C., Ridzon, D.A., Broomer, A.J., Zhou, Z., Lee, D.H., Nguyen, J.T., Barbisin, M., Xu, N.L., Mahuvakar, V.R., and Andersen, M.R. (2005a). Real-time quantification of microRNAs by stem–loop RT–PCR. Nucleic acids research *33*, e179-e179.

Chen, D.Y., Stern, S.A., Garcia-Osta, A., Saunier-Rebori, B., Pollonini, G., Bambah-Mukku, D., Blitzer, R.D., and Alberini, C.M. (2011). A critical role for IGF-II in memory consolidation and enhancement. Nature *469*, 491-497.

Chen, L., Kong, R., Wu, C., Wang, S., Liu, Z., Liu, S., Li, S., Chen, T., Mao, C., and Liu, S. (2019). Circ-MALAT1 Functions as Both an mRNA Translation Brake and a microRNA Sponge to Promote Self-Renewal of Hepatocellular Cancer Stem Cells. Advanced Science, 1900949.

Chen, Y., Wang, P.Y., and Ghosh, A. (2005b). Regulation of cortical dendrite development by Rap1 signaling. Molecular and Cellular Neuroscience *28*, 215-228.

Cheng, J., Metge, F., and Dieterich, C. (2016). Specific identification and quantification of circular RNAs from sequencing data. Bioinformatics *32*, 1094-1096.

Chess, A., Simon, I., Cedar, H., and Axel, R. (1994). Allelic inactivation regulates olfactory receptor gene expression. Cell *78*, 823-834.

Cho, J.H., Lépine, M., Andrews, W., Parnavelas, J., and Cloutier, J.-F. (2007). Requirement for Slit-1 and Robo-2 in zonal segregation of olfactory sensory neuron axons in the main olfactory bulb. Journal of Neuroscience *27*, 9094-9104.

Choi, H.M., Schwarzkopf, M., Fornace, M.E., Acharya, A., Artavanis, G., Stegmaier, J., Cunha, A., and Pierce, N.A. (2018). Third-generation in situ hybridization chain reaction: multiplexed, quantitative, sensitive, versatile, robust. Development *145*, dev165753.

Chuang, J.-Z., Yeh, T.-Y., Bollati, F., Conde, C., Canavosio, F., Caceres, A., and Sung, C.-H. (2005). The dynein light chain Tctex-1 has a dynein-independent role in actin remodeling during neurite outgrowth. Developmental cell *9*, 75-86.

Clemson, C.M., Hutchinson, J.N., Sara, S.A., Ensminger, A.W., Fox, A.H., Chess, A., and Lawrence, J.B. (2009). An architectural role for a nuclear noncoding RNA: NEAT1 RNA is essential for the structure of paraspeckles. Molecular cell *33*, 717-726.

Clowney, E.J., LeGros, M.A., Mosley, C.P., Clowney, F.G., Markenskoff-Papadimitriou, E.C., Myllys, M., Barnea, G., Larabell, C.A., and Lomvardas, S. (2012). Nuclear aggregation of olfactory receptor genes governs their monogenic expression. Cell *151*, 724-737.

Clowney, E.J., Magklara, A., Colquitt, B.M., Pathak, N., Lane, R.P., and Lomvardas, S. (2011). High-throughput mapping of the promoters of the mouse olfactory receptor genes reveals a new type of mammalian promoter and provides insight into olfactory receptor gene regulation. Genome research *21*, 1249-1259.

Conn, S.J., Pillman, K.A., Toubia, J., Conn, V.M., Salmanidis, M., Phillips, C.A., Roslan, S., Schreiber, A.W., Gregory, P.A., and Goodall, G.J. (2015). The RNA binding protein quaking regulates formation of circRNAs. Cell *160*, 1125-1134.

Connelly, T., Savigner, A., and Ma, M. (2013). Spontaneous and sensory-evoked activity in mouse olfactory sensory neurons with defined odorant receptors. Journal of neurophysiology *110*, 55-62.

Connerty, P., Lock, R.B., and De Bock, C.E. (2020). Long Non-coding RNAs: Major Regulators of Cell Stress in Cancer. Frontiers in Oncology *10*.

Consortium, E.P. (2012). An integrated encyclopedia of DNA elements in the human genome. Nature *489*, 57-74.

Constância, M., Hemberger, M., Hughes, J., Dean, W., Ferguson-Smith, A., Fundele, R., Stewart, F., Kelsey, G., Fowden, A., and Sibley, C. (2002). Placental-specific IGF-II is a major modulator of placental and fetal growth. Nature *417*, 945-948.

Coolen, M., Katz, S., and Bally-Cuif, L. (2013). miR-9: a versatile regulator of neurogenesis. Frontiers in cellular neuroscience *7*, 220.

Costanzo, R.M. (2000). Rewiring the olfactory bulb: changes in odor maps following recovery from nerve transection. Chemical senses *25*, 199-205.

Cummings, D.M., and Belluscio, L. (2010). Continuous Neural Plasticity in the Olfactory Intrabulbar Circuitry. The Journal of Neuroscience *30*, 9172-9180.

Curmi, P.A., Andersen, S.S., Lachkar, S., Gavet, O., Karsenti, E., Knossow, M., and Sobel, A. (1997). The stathmin/tubulin interaction in vitro. Journal of Biological Chemistry *272*, 25029-25036.

Cuschieri, A., and Bannister, L.H. (1975). The development of the olfactory mucosa in the mouse: light microscopy. Journal of anatomy *119*, 277.

Dajas-Bailador, F., Bonev, B., Garcez, P., Stanley, P., Guillemot, F., and Papalopulu, N. (2012). microRNA-9 regulates axon extension and branching by targeting Map1b in mouse cortical neurons. Nature neuroscience *15*, 697.

Dalton, R.P., Lyons, D.B., and Lomvardas, S. (2013). Co-opting the unfolded protein response to elicit olfactory receptor feedback. Cell *155*, 321-332.

DeChiara, T.M., Efstratiadis, A., and Robertsen, E.J. (1990). A growth-deficiency phenotype in heterozygous mice carrying an insulin-like growth factor II gene disrupted by targeting. Nature *345*, 78-80.

Dent, E.W., Gupton, S.L., and Gertler, F.B. (2011). The growth cone cytoskeleton in axon outgrowth and guidance. Cold Spring Harbor perspectives in biology *3*, a001800.

Dey, B.K., Pfeifer, K., and Dutta, A. (2014). The H19 long noncoding RNA gives rise to microRNAs miR-675-3p and miR-675-5p to promote skeletal muscle differentiation and regeneration. Genes & development *28*, 491-501.

Diederichs, S. (2014). The four dimensions of noncoding RNA conservation. Trends in Genetics *30*, 121-123.

Dinger, M.E., Amaral, P.P., Mercer, T.R., Pang, K.C., Bruce, S.J., Gardiner, B.B., Askarian-Amiri, M.E., Ru, K., Soldà, G., and Simons, C. (2008). Long noncoding RNAs

in mouse embryonic stem cell pluripotency and differentiation. Genome research *18*, 1433-1445.

Dobin, A., Davis, C.A., Schlesinger, F., Drenkow, J., Zaleski, C., Jha, S., Batut, P., Chaisson, M., and Gingeras, T.R. (2013). STAR: ultrafast universal RNA-seq aligner. Bioinformatics *29*, 15-21.

Donner, A.L., Episkopou, V., and Maas, R.L. (2007). Sox2 and Pou2f1 interact to control lens and olfactory placode development. Developmental biology *303*, 784-799.

Drewell, R.A., Brenton, J.D., Ainscough, J., Barton, S.C., Hilton, K.J., Arney, K.L., Dandolo, L., and Surani, M.A. (2000). Deletion of a silencer element disrupts H19 imprinting independently of a DNA methylation epigenetic switch. Development *127*, 3419-3428.

Dulac, C., and Axel, R. (1995). A novel family of genes encoding putative pheromone receptors in mammals. Cell *83*, 195-206.

Dutta, S., Roy, S., Polavaram, N.S., Baretton, G.B., Muders, M.H., Batra, S., and Datta, K. (2016). NRP2 transcriptionally regulates its downstream effector WDFY1. Scientific reports *6*, 1-8.

Eggan, K., Baldwin, K., Tackett, M., Osborne, J., Gogos, J., Chess, A., Axel, R., and Jaenisch, R. (2004). Mice cloned from olfactory sensory neurons. Nature *428*, 44-49.

Eißmann, M., Gutschner, T., Hämmerle, M., Günther, S., Caudron-Herger, M., Groß, M., Schirmacher, P., Rippe, K., Braun, T., and Zörnig, M. (2012). Loss of the abundant

nuclear non-coding RNA MALAT1 is compatible with life and development. RNA biology *9*, 1076-1087.

Eng, D., and Eng, L. (2009). Intermediate Filaments.

Escurat, M., Djabali, K., Gumpel, M., Gros, F., and Portier, M. (1990). Differential expression of two neuronal intermediate-filament proteins, peripherin and the low-molecular-mass neurofilament protein (NF-L), during the development of the rat. Journal of Neuroscience *10*, 764-784.

Fan, X., Dong, J., Zhong, S., Wei, Y., Wu, Q., Yan, L., Yong, J., Sun, L., Wang, X., and Zhao, Y. (2018). Spatial transcriptomic survey of human embryonic cerebral cortex by single-cell RNA-seq analysis. Cell research *28*, 730-745.

Feinstein, P., Bozza, T., Rodriguez, I., Vassalli, A., and Mombaerts, P. (2004). Axon guidance of mouse olfactory sensory neurons by odorant receptors and the β2 adrenergic receptor. Cell *117*, 833-846.

Feinstein, P., and Mombaerts, P. (2004). A contextual model for axonal sorting into glomeruli in the mouse olfactory system. Cell *117*, 817-831.

Feng, J., Bi, C., Clark, B.S., Mady, R., Shah, P., and Kohtz, J.D. (2006). The Evf-2 noncoding RNA is transcribed from the Dlx-5/6 ultraconserved region and functions as a Dlx-2 transcriptional coactivator. Genes & development *20*, 1470-1484.

Fleischer, J., Schwarzenbacher, K., Besser, S., Hass, N., and Breer, H. (2006). Olfactory receptors and signalling elements in the Grueneberg ganglion. Journal of neurochemistry *98*, 543-554.

Fuss, S.H., Omura, M., and Mombaerts, P. (2005). The Grueneberg ganglion of the mouse projects axons to glomeruli in the olfactory bulb. European Journal of Neuroscience *22*, 2649-2654.

Gabory, A., Jammes, H., and Dandolo, L. (2010). The H19 locus: Role of an imprinted non-coding RNA in growth and development. Bioessays *32*, 473-480.

Gao, W.-l., Liu, M., Yang, Y., Yang, H., Liao, Q., Bai, Y., Li, Y.-x., Li, D., Peng, C., and Wang, Y.-l. (2012). The imprinted H19 gene regulates human placental trophoblast cell proliferation via encoding miR-675 that targets Nodal Modulator 1 (NOMO1). RNA biology *9*, 1002-1010.

Gogos, J.A., Osborne, J., Nemes, A., Mendelsohn, M., and Axel, R. (2000). Genetic ablation and restoration of the olfactory topographic map. Cell *103*, 609-620.

Gong, Q., and Shipley, M.T. (1995). Evidence that pioneer olfactory axons regulate telencephalon cell cycle kinetics to induce the formation of the olfactory bulb. Neuron *14*, 91-101.

Gorham, J.D., Ziff, E.B., and Baker, H. (1991). Differential spatial and temporal expression of two type III intermediate filament proteins in olfactory receptor neurons. Neuron *7*, 485-497.

Graziadei, G.M., and Graziadei, P.P.C. (1979). Neurogenesis and neuron regeneration in the olfactory system of mammals. II. Degeneration and reconstitution of the olfactory sensory neurons after axotomy. Journal of neurocytology *8*, 197-213.

Grimbert, P., Valanciute, A., Audard, V., Pawlak, A., Le gouvelo, S., Lang, P., Niaudet, P., Bensman, A., Guellaën, G., and Sahali, D. (2003). Truncation of C-mip (Tc-mip), a new proximal signaling protein, induces c-maf Th2 transcription factor and cytoskeleton reorganization. The Journal of experimental medicine *198*, 797-807.

Groskopf, J., Aubin, S.M., Deras, I.L., Blase, A., Bodrug, S., Clark, C., Brentano, S., Mathis, J., Pham, J., and Meyer, T. (2006). APTIMA PCA3 molecular urine test: development of a method to aid in the diagnosis of prostate cancer. Clinical chemistry *52*, 1089-1095.

Grüneberg, H. (1973). A ganglion probably belonging to the N. terminalis system in the nasal mucosa of the mouse. Zeitschrift für Anatomie und Entwicklungsgeschichte *140*, 39-52.

Guo, J.U., Agarwal, V., Guo, H., and Bartel, D.P. (2014). Expanded identification and characterization of mammalian circular RNAs. Genome biology *15*, 409.

Gupta, K.K., Li, C., Duan, A., Alberico, E.O., Kim, O.V., Alber, M.S., and Goodson, H.V. (2013). Mechanism for the catastrophe-promoting activity of the microtubule destabilizer Op18/stathmin. Proceedings of the National Academy of Sciences *110*, 20449-20454.

Guttman, M., Amit, I., Garber, M., French, C., Lin, M.F., Feldser, D., Huarte, M., Zuk, O., Carey, B.W., and Cassady, J.P. (2009). Chromatin signature reveals over a thousand highly conserved large non-coding RNAs in mammals. Nature *458*, 223-227.

Hall, S.E., Floriano, W.B., Vaidehi, N., and Goddard III, W.A. (2004). Predicted 3-D structures for mouse I7 and rat I7 olfactory receptors and comparison of predicted odor recognition profiles with experiment. Chemical senses *29*, 595-616.

Hammond, S.M., Boettcher, S., Caudy, A.A., Kobayashi, R., and Hannon, G.J. (2001). Argonaute2, a link between genetic and biochemical analyses of RNAi. Science *293*, 1146-1150.

Hanash, S.M., Strahler, J.R., Kuick, R., Chu, E., and Nichols, D. (1988). Identification of a polypeptide associated with the malignant phenotype in acute leukemia. Journal of Biological Chemistry *263*, 12813-12815.

Hansen, T.B. (2018). Improved circRNA identification by combining prediction algorithms. Frontiers in cell and developmental biology *6*, 20.

Hansen, T.B., Jensen, T.I., Clausen, B.H., Bramsen, J.B., Finsen, B., Damgaard, C.K., and Kjems, J. (2013). Natural RNA circles function as efficient microRNA sponges. Nature *495*, 384-388.

Hansen, T.V., Hammer, N.A., Nielsen, J., Madsen, M., Dalbaeck, C., Wewer, U.M., Christiansen, J., and Nielsen, F.C. (2004). Dwarfism and impaired gut development in insulin-like growth factor II mRNA-binding protein 1-deficient mice. Molecular and cellular biology *24*, 4448-4464.

Hark, A.T., Schoenherr, C.J., Katz, D.J., Ingram, R.S., Levorse, J.M., and Tilghman, S.M. (2000). CTCF mediates methylation-sensitive enhancer-blocking activity at the H19/Igf2 locus. Nature *405*, 486-489.

He, J., Ma, L., Kim, S., Nakai, J., and Yu, C.R. (2008). Encoding gender and individual information in the mouse vomeronasal organ. Science *320*, 535-538.

He, J.C., Neves, S.R., Jordan, J.D., and Iyengar, R. (2006). Role of the Go/i signaling network in the regulation of neurite outgrowth. Canadian journal of physiology and pharmacology *84*, 687-694.

Hébert, J.M., Lin, M., Partanen, J., Rossant, J., and McConnell, S.K. (2003). FGF signaling through FGFR1 is required for olfactory bulb morphogenesis. Development *130*, 1101-1111.

Helfand, B.T., Mendez, M.G., Pugh, J., Delsert, C., and Goldman, R.D. (2003). A role for intermediate filaments in determining and maintaining the shape of nerve cells. Molecular biology of the cell *14*, 5069-5081.

Herrada, G., and Dulac, C. (1997). A novel family of putative pheromone receptors in mammals with a topographically organized and sexually dimorphic distribution. Cell *90*, 763-773.

Hessels, D., Gunnewiek, J.M.K., van Oort, I., Karthaus, H.F., van Leenders, G.J., van Balken, B., Kiemeney, L.A., Witjes, J.A., and Schalken, J.A. (2003). DD3PCA3-based molecular urine analysis for the diagnosis of prostate cancer. European urology *44*, 8-16.

Higuchi, M., Single, F.N., Köhler, M., Sommer, B., Sprengel, R., and Seeburg, P.H. (1993). RNA editing of AMPA receptor subunit GluR-B: a base-paired intron-exon structure determines position and efficiency. Cell *75*, 1361-1370.

Hirota, J., and Mombaerts, P. (2004). The LIM-homeodomain protein Lhx2 is required for complete development of mouse olfactory sensory neurons. Proceedings of the National Academy of Sciences *101*, 8751-8755.

Hollensen, A.K., Linares, M.L., Thomsen, H.S., Kamstrup, A.B., Jensen, J.M., Luckmann, M., Birkmose, N., Jensen, T.H., Hansen, T.B., and Damgaard, C.K. (2019). Circular RNA ZNF827 tunes neuronal differentiation by facilitating transcriptional repression of Neuronal Growth Factor Receptor. bioRxiv, 791798.

Hoppe, R., Breer, H., and Strotmann, J. (2006). Promoter motifs of olfactory receptor genes expressed in distinct topographic patterns. Genomics *87*, 711-723.

Hu, Y.H., Zhang, Y., Jiang, L.Q., Wang, S., Lei, C.Q., Sun, M.S., Shu, H.B., and Liu, Y. (2015). WDFY 1 mediates TLR 3/4 signaling by recruiting TRIF. EMBO reports *16*, 447-455.

Hubel, D.H., and Wiesel, T.N. (1970). The period of susceptibility to the physiological effects of unilateral eye closure in kittens. The Journal of physiology *206*, 419-436.

Hutchinson, J.N., Ensminger, A.W., Clemson, C.M., Lynch, C.R., Lawrence, J.B., and Chess, A. (2007). A screen for nuclear transcripts identifies two linked noncoding RNAs associated with SC35 splicing domains. BMC genomics *8*, 39.

Imai, T., Suzuki, M., and Sakano, H. (2006). Odorant receptor–derived cAMP signals direct axonal targeting. Science *314*, 657-661.

Ip, J.Y., Sone, M., Nashiki, C., Pan, Q., Kitaichi, K., Yanaka, K., Abe, T., Takao, K., Miyakawa, T., and Blencowe, B.J. (2016). Gomafu lncRNA knockout mice exhibit mild hyperactivity with enhanced responsiveness to the psychostimulant methamphetamine. Scientific reports *6*, 1-13.

Ishii, T., Omura, M., and Mombaerts, P. (2004). Protocols for two-and three-color fluorescent RNA in situ hybridization of the main and accessory olfactory epithelia in mouse. Journal of neurocytology *33*, 657-669.

Ivanov, A., Memczak, S., Wyler, E., Torti, F., Porath, H.T., Orejuela, M.R., Piechotta, M., Levanon, E.Y., Landthaler, M., and Dieterich, C. (2015). Analysis of intron sequences reveals hallmarks of circular RNA biogenesis in animals. Cell reports *10*, 170-177.

Iwai, N., Zhou, Z., Roop, D.R., and Behringer, R.R. (2008). Horizontal basal cells are multipotent progenitors in normal and injured adult olfactory epithelium. Stem cells *26*, 1298-1306.

Jacquier, V., Prummer, M., Segura, J.-M., Pick, H., and Vogel, H. (2006). Visualizing odorant receptor trafficking in living cells down to the single-molecule level. Proceedings of the National Academy of Sciences *103*, 14325-14330.

Jeck, W.R., and Sharpless, N.E. (2014). Detecting and characterizing circular RNAs. Nature biotechnology *32*, 453.

Jeck, W.R., Sorrentino, J.A., Wang, K., Slevin, M.K., Burd, C.E., Liu, J., Marzluff, W.F., and Sharpless, N.E. (2013). Circular RNAs are abundant, conserved, and associated with ALU repeats. Rna *19*, 141-157.

John, J.A.S., and Key, B. (2003). Axon mis-targeting in the olfactory bulb during regeneration of olfactory neuroepithelium. Chemical Senses *28*, 773-779.

John, J.A.S., Pasquale, E.B., and Key, B. (2002). EphA receptors and ephrin-A ligands exhibit highly regulated spatial and temporal expression patterns in the developing olfactory system. Developmental brain research *138*, 1-14.

Jordan, J.D., He, J.C., Eungdamrong, N.J., Gomes, I., Ali, W., Nguyen, T., Bivona, T.G., Philips, M.R., Devi, L.A., and Iyengar, R. (2005). Cannabinoid receptor-induced neurite outgrowth is mediated by Rap1 activation through Gαo/i-triggered proteasomal degradation of Rap1GAPII. Journal of Biological Chemistry *280*, 11413-11421.

Jossin, Y., and Cooper, J.A. (2011). Reelin, Rap1 and N-cadherin orient the migration of multipolar neurons in the developing neocortex. Nature neuroscience *14*, 697.

Kallen, A.N., Zhou, X.-B., Xu, J., Qiao, C., Ma, J., Yan, L., Lu, L., Liu, C., Yi, J.-S., and Zhang, H. (2013). The imprinted H19 lncRNA antagonizes let-7 microRNAs. Molecular cell *52*, 101-112.

Kanageswaran, N., Demond, M., Nagel, M., Schreiner, B.S., Baumgart, S., Scholz, P., Altmüller, J., Becker, C., Doerner, J.F., and Conrad, H. (2015). Deep sequencing of the murine olfactory receptor neuron transcriptome. PloS one *10*, e0113170.

Kaneko-Goto, T., Yoshihara, S.-i., Miyazaki, H., and Yoshihara, Y. (2008). BIG-2 mediates olfactory axon convergence to target glomeruli. Neuron *57*, 834-846.

Keihani, S., Kluever, V., Mandad, S., Bansal, V., Rahman, R., Fritsch, E., Gomes, L.C., Gärtner, A., Kügler, S., and Urlaub, H. (2019). The long noncoding RNA neuroLNC regulates presynaptic activity by interacting with the neurodegeneration-associated protein TDP-43. Science advances *5*, eaay2670.

Keniry, A., Oxley, D., Monnier, P., Kyba, M., Dandolo, L., Smits, G., and Reik, W. (2012). The H19 lincRNA is a developmental reservoir of miR-675 that suppresses growth and Igf1r. Nature cell biology *14*, 659-665.

Kennard, M.A. (1938). Reorganization of motor function in the cerebral cortex of monkeys deprived of motor and premotor areas in infancy. Journal of Neurophysiology *1*, 477-496.

Khan, M., Vaes, E., and Mombaerts, P. (2011). Regulation of the probability of mouse odorant receptor gene choice. Cell *147*, 907-921.

Kim, V.N., Han, J., and Siomi, M.C. (2009). Biogenesis of small RNAs in animals. Nature reviews Molecular cell biology *10*, 126-139.

King, S.M., Dillman, J.F., Benashski, S.E., Lye, R.J., Patel-King, R.S., and Pfister, K.K. (1996). The mouse t-complex-encoded protein Tctex-1 is a light chain of brain cytoplasmic dynein. Journal of Biological Chemistry *271*, 32281-32287.

Kobilka, B.K., and Deupi, X. (2007). Conformational complexity of G-protein-coupled receptors. Trends in pharmacological sciences *28*, 397-406.

Kosik, K.S. (2006). The neuronal microRNA system. Nature Reviews Neuroscience *7*, 911-920.

Kraus, P., Sivakamasundari, V., Lim, S.L., Xing, X., Lipovich, L., and Lufkin, T. (2013). Making sense of Dlx1 antisense RNA. Developmental biology *376*, 224-235.

Kurahashi, T., and Yau, K.-W. (1993). Co-existence of cationic and chloride components in odorant-induced current of vertebrate olfactory receptor cells. Nature *363*, 71-74.

Lasda, E., and Parker, R. (2014). Circular RNAs: diversity of form and function. Rna *20*, 1829-1842.

Leighton, P.A., Ingram, R.S., Eggenschwiler, J., Efstratiadis, A., and Tilghman, S.M. (1995). Disruption of imprinting caused by deletion of the H19 gene region in mice. Nature *375*, 34-39.

Leung, C.T., Coulombe, P.A., and Reed, R.R. (2007). Contribution of olfactory neural stem cells to tissue maintenance and regeneration. Nature neuroscience *10*, 720-726.

Lèvai, O., and Strotmann, J. (2003). Projection pattern of nerve fibers from the septal organ: DiI-tracing studies with transgenic OMP mice. Histochemistry and cell biology *120*, 483-492.

Li, L., Liu, B., Wapinski, O.L., Tsai, M.-C., Qu, K., Zhang, J., Carlson, J.C., Lin, M., Fang, F., and Gupta, R.A. (2013). Targeted disruption of Hotair leads to homeotic transformation and gene derepression. Cell reports *5*, 3-12.

Li, L., Zhuang, Y., Zhao, X., and Li, X. (2019). Long Non-coding RNA in Neuronal Development and Neurological Disorders. Frontiers in Genetics *9*.

Liang, D., Tatomer, D.C., Luo, Z., Wu, H., Yang, L., Chen, L.-L., Cherry, S., and Wilusz, J.E. (2017). The output of protein-coding genes shifts to circular RNAs when the pre-mRNA processing machinery is limiting. Molecular cell *68*, 940-954. e943.

Liddicoat, B.J., Piskol, R., Chalk, A.M., Ramaswami, G., Higuchi, M., Hartner, J.C., Li, J.B., Seeburg, P.H., and Walkley, C.R. (2015). RNA editing by ADAR1 prevents MDA5 sensing of endogenous dsRNA as nonself. Science *349*, 1115-1120.

Liu, J., Carmell, M.A., Rivas, F.V., Marsden, C.G., Thomson, J.M., Song, J.-J., Hammond, S.M., Joshua-Tor, L., and Hannon, G.J. (2004). Argonaute2 is the catalytic engine of mammalian RNAi. Science *305*, 1437-1441.

Lorenzon, P., Redolfi, N., Podolsky, M.J., Zamparo, I., Franchi, S.A., Pietra, G., Boccaccio, A., Menini, A., Murthy, V.N., and Lodovichi, C. (2015). Circuit formation and function in the olfactory bulb of mice with reduced spontaneous afferent activity. Journal of Neuroscience *35*, 146-160.

Love, M.I., Huber, W., and Anders, S. (2014). Moderated estimation of fold change and dispersion for RNA-seq data with DESeq2. Genome biology *15*, 550.

Luo, M., Li, Z., Wang, W., Zeng, Y., Liu, Z., and Qiu, J. (2013). Long non-coding RNA H19 increases bladder cancer metastasis by associating with EZH2 and inhibiting E-cadherin expression. Cancer letters *333*, 213-221.

Lyons, D.B., Allen, W.E., Goh, T., Tsai, L., Barnea, G., and Lomvardas, S. (2013). An epigenetic trap stabilizes singular olfactory receptor expression. Cell *154*, 325-336.

Ma, C., Nong, K., Zhu, H., Wang, W., Huang, X., Yuan, Z., and Ai, K. (2014a). H19 promotes pancreatic cancer metastasis by derepressing let-7's suppression on its target HMGA2-mediated EMT. Tumor Biology *35*, 9163-9169.

Ma, L., Wu, Y., Qiu, Q., Scheerer, H., Moran, A., and Yu, C.R. (2014b). A Developmental Switch of Axon Targeting in the Continuously Regenerating Mouse Olfactory System. Science *344*, 194-197.

Maass, P.G., Glažar, P., Memczak, S., Dittmar, G., Hollfinger, I., Schreyer, L., Sauer, A.V., Toka, O., Aiuti, A., and Luft, F.C. (2017). A map of human circular RNAs in clinically relevant tissues. Journal of Molecular Medicine *95*, 1179-1189.

Machado, C.F., Nagai, M.H., Lyra, C.S., Reis-Silva, T.M., Xavier, A.M., Glezer, I., Felicio, L.F., and Malnic, B. (2017). Conditional deletion of Ric-8b in olfactory sensory neurons leads to olfactory impairment. Journal of Neuroscience *37*, 12202-12213.

Mackay‐Sim, A., and Kittel, P. (1991). On the life span of olfactory receptor neurons. European Journal of Neuroscience *3*, 209-215.

Maeda, N., Kasukawa, T., Oyama, R., Gough, J., Frith, M., Engström, P.G., Lenhard, B., Aturaliya, R.N., Batalov, S., and Beisel, K.W. (2006). Transcript annotation in FANTOM3: mouse gene catalog based on physical cDNAs. PLoS genetics *2*.

Magklara, A., Yen, A., Colquitt, B.M., Clowney, E.J., Allen, W., Markenscoff-Papadimitriou, E., Evans, Z.A., Kheradpour, P., Mountoufaris, G., and Carey, C. (2011). An epigenetic signature for monoallelic olfactory receptor expression. Cell *145*, 555-570.

Malnic, B., Hirono, J., Sato, T., and Buck, L.B. (1999). Combinatorial receptor codes for odors. Cell *96*, 713-723.

Mashukova, A., Spehr, M., Hatt, H., and Neuhaus, E.M. (2006). β-arrestin2-mediated internalization of mammalian odorant receptors. Journal of Neuroscience *26*, 9902-9912.

Masliah, E., Xie, F., Dayan, S., Rockenstein, E., Mante, M., Adame, A., Patrick, C.M., Chan, A.F., and Zheng, B. (2010). Genetic deletion of Nogo/Rtn4 ameliorates behavioral and neuropathological outcomes in amyloid precursor protein transgenic mice. Neuroscience *169*, 488-494.

Masuda, T., Sakuma, C., Nagaoka, A., Yamagishi, T., Ueda, S., Nagase, T., and Yaginuma, H. (2014). F ollistatin‐like 5 is expressed in restricted areas of the adult mouse brain: Implications for its function in the olfactory system. Congenital anomalies *54*, 63-66.

Matsunami, H., and Buck, L.B. (1997). A multigene family encoding a diverse array of putative pheromone receptors in mammals. Cell *90*, 775-784.

McAvoy, T., Zhou, M.-m., Greengard, P., and Nairn, A.C. (2009). Phosphorylation of Rap1GAP, a striatally enriched protein, by protein kinase A controls Rap1 activity and dendritic spine morphology. Proceedings of the National Academy of Sciences *106*, 3531-3536.

McCurdy, R.D., Féron, F., McGrath, J.J., and Mackay-Sim, A. (2005). Regulation of adult olfactory neurogenesis by insulin-like growth factor-I. European journal of Neuroscience *22*, 1581-1588.

McGinnis, C.S., Murrow, L.M., and Gartner, Z.J. (2019). DoubletFinder: doublet detection in single-cell RNA sequencing data using artificial nearest neighbors. Cell systems *8*, 329-337. e324.

McIntyre, J.C., Bose, S.C., Stromberg, A.J., and McClintock, T.S. (2008). Emx2 stimulates odorant receptor gene expression. Chemical senses *33*, 825-837.

Memczak, S., Jens, M., Elefsinioti, A., Torti, F., Krueger, J., Rybak, A., Maier, L., Mackowiak, S.D., Gregersen, L.H., and Munschauer, M. (2013). Circular RNAs are a large class of animal RNAs with regulatory potency. Nature *495*, 333-338.

Menon, S., and Gupton, S.L. (2016). Building blocks of functioning brain: cytoskeletal dynamics in neuronal development. In International review of cell and molecular biology (Elsevier), pp. 183-245.

Mercer, T.R., Dinger, M.E., and Mattick, J.S. (2009). Long non-coding RNAs: insights into functions. Nature reviews genetics *10*, 155-159.

Merlo, G.R., Mantero, S., Zaghetto, A.A., Peretto, P., Paina, S., and Gozzo, M. (2007). The role of Dlx homeogenes in early development of the olfactory pathway. Journal of molecular histology *38*, 347-358.

Meyers, E.N., Lewandoski, M., and Martin, G.R. (1998). An Fgf8 mutant allelic series generated by Cre-and Flp-mediated recombination. Nature genetics *18*, 136-141.

Miller, A.M., Maurer, L.R., Zou, D.-J., Firestein, S., and Greer, C.A. (2010). Axon fasciculation in the developing olfactory nerve. Neural development *5*, 20.

Miyamichi, K., Serizawa, S., Kimura, H.M., and Sakano, H. (2005). Continuous and overlapping expression domains of odorant receptor genes in the olfactory epithelium determine the dorsal/ventral positioning of glomeruli in the olfactory bulb. Journal of Neuroscience *25*, 3586-3592.

Mombaerts, P. (2004). Genes and ligands for odorant, vomeronasal and taste receptors. Nature Reviews Neuroscience *5*, 263-278.

Mombaerts, P., Wang, F., Dulac, C., Chao, S.K., Nemes, A., Mendelsohn, M., Edmondson, J., and Axel, R. (1996). Visualizing an olfactory sensory map. Cell *87*, 675-686.

Monahan, K., Horta, A., and Lomvardas, S. (2019). LHX2-and LDB1-mediated trans interactions regulate olfactory receptor choice. Nature *565*, 448-453.

Monahan, K., and Lomvardas, S. (2015). Monoallelic expression of olfactory receptors. Annual review of cell and developmental biology *31*, 721-740.

Monahan, K., Schieren, I., Cheung, J., Mumbey-Wafula, A., Monuki, E.S., and Lomvardas, S. (2017). Cooperative interactions enable singular olfactory receptor expression in mouse olfactory neurons. Elife *6*, e28620.

Monnier, P., Martinet, C., Pontis, J., Stancheva, I., Ait-Si-Ali, S., and Dandolo, L. (2013). H19 lncRNA controls gene expression of the Imprinted Gene Network by recruiting MBD1. Proceedings of the National Academy of Sciences *110*, 20693-20698.

Mori, K., Nagao, H., and Yoshihara, Y. (1999). The olfactory bulb: coding and processing of odor molecule information. Science *286*, 711-715.

Mori, K., Takahashi, Y.K., Igarashi, K.M., and Yamaguchi, M. (2006). Maps of odorant molecular features in the mammalian olfactory bulb. Physiological reviews *86*, 409-433.

Nakagawa, S. (2016). Lessons from reverse-genetic studies of lncRNAs. Biochimica et Biophysica Acta (BBA)-Gene Regulatory Mechanisms *1859*, 177-183.

Nakagawa, S., Ip, J.Y., Shioi, G., Tripathi, V., Zong, X., Hirose, T., and Prasanth, K.V. (2012). Malat1 is not an essential component of nuclear speckles in mice. Rna *18*, 1487-1499.

Nakagawa, S., Shimada, M., Yanaka, K., Mito, M., Arai, T., Takahashi, E., Fujita, Y., Fujimori, T., Standaert, L., and Marine, J.-C. (2014). The lncRNA Neat1 is required for

corpus luteum formation and the establishment of pregnancy in a subpopulation of mice. Development *141*, 4618-4627.

Nakashima, A., Ihara, N., Shigeta, M., Kiyonari, H., Ikegaya, Y., and Takeuchi, H. (2019). Structured spike series specify gene expression patterns for olfactory circuit formation. Science *365*, eaaw5030.

Nakashima, A., Takeuchi, H., Imai, T., Saito, H., Kiyonari, H., Abe, T., Chen, M., Weinstein, L.S., Yu, C.R., and Storm, D.R. (2013). Agonist-independent GPCR activity regulates anterior-posterior targeting of olfactory sensory neurons. Cell *154*, 1314-1325.

Nandakumar, R., and Paludan, S.R. (2015). Catching the adaptor—WDFY 1, a new player in the TLR–TRIF pathway. EMBO reports *16*, 397-398.

Nickell, M.D., Breheny, P., Stromberg, A.J., and McClintock, T.S. (2012). Genomics of mature and immature olfactory sensory neurons. Journal of Comparative Neurology *520*, 2608-2629.

Nigro, J.M., Cho, K.R., Fearon, E.R., Kern, S.E., Ruppert, J.M., Oliner, J.D., Kinzler, K.W., and Vogelstein, B. (1991). Scrambled exons. Cell *64*, 607-613.

Nishikura, K. (2010). Functions and regulation of RNA editing by ADAR deaminases. Annual review of biochemistry *79*, 321-349.

O'Carroll, D., Mecklenbrauker, I., Das, P.P., Santana, A., Koenig, U., Enright, A.J., Miska, E.A., and Tarakhovsky, A. (2007). A Slicer-independent role for Argonaute 2 in hematopoiesis and the microRNA pathway. Genes & development *21*, 1999-2004.

Ophir, D., and Lancet, D. (1988). Expression of intermediate filaments and desmoplakin in vertebrate olfactory mucosa. The Anatomical Record *221*, 754-760.

Otaegi, G., Pollock, A., Hong, J., and Sun, T. (2011). MicroRNA miR-9 modifies motor neuron columns by a tuning regulation of FoxP1 levels in developing spinal cords. Journal of Neuroscience *31*, 809-818.

Pachnis, V., Belayew, A., and Tilghman, S.M. (1984). Locus unlinked to alpha-fetoprotein under the control of the murine raf and Rif genes. Proceedings of the National Academy of Sciences *81*, 5523-5527.

Pachnis, V., Brannan, C., and Tilghman, S.M. (1988). The structure and expression of a novel gene activated in early mouse embryogenesis. The EMBO journal *7*, 673-681.

Packard, A., Schnittke, N., Romano, R.-A., Sinha, S., and Schwob, J.E. (2011). ΔNp63 regulates stem cell dynamics in the mammalian olfactory epithelium. Journal of Neuroscience *31*, 8748-8759.

Paralkar, V.R., Taborda, C.C., Huang, P., Yao, Y., Kossenkov, A.V., Prasad, R., Luan, J., Davies, J.O., Hughes, J.R., and Hardison, R.C. (2016). Unlinking an lncRNA from its associated cis element. Molecular cell *62*, 104-110.

Piwecka, M., Glažar, P., Hernandez-Miranda, L.R., Memczak, S., Wolf, S.A., Rybak-Wolf, A., Filipchyk, A., Klironomos, F., Jara, C.A.C., and Fenske, P. (2017). Loss of a mammalian circular RNA locus causes miRNA deregulation and affects brain function. Science *357*, eaam8526.

Poirier, F., Chan, C., Timmons, P., Robertson, E., Evans, M., and Rigby, P. (1991). The murine H19 gene is activated during embryonic stem cell differentiation in vitro and at the time of implantation in the developing embryo. Development *113*, 1105-1114.

Ponting, C.P., Oliver, P.L., and Reik, W. (2009). Evolution and functions of long noncoding RNAs. Cell *136*, 629-641.

Potter, S.M., Zheng, C., Koos, D.S., Feinstein, P., Fraser, S.E., and Mombaerts, P. (2001). Structure and emergence of specific olfactory glomeruli in the mouse. Journal of Neuroscience *21*, 9713-9723.

Prahlad, V., Yoon, M., Moir, R.D., Vale, R.D., and Goldman, R.D. (1998). Rapid movements of vimentin on microtubule tracks: kinesin-dependent assembly of intermediate filament networks. The Journal of cell biology *143*, 159-170.

Quan, Z., Zheng, D., and Qing, H. (2017). Regulatory Roles of Long Non-Coding RNAs in the Central Nervous System and Associated Neurodegenerative Diseases. Frontiers in cellular neuroscience *11*.

Rankin, M.L., Alvania, R.S., Gleason, E.L., and Bruch, R.C. (1999). Internalization of G protein-coupled receptors in single olfactory receptor neurons. Journal of neurochemistry *72*, 541-548.

Reed, R.R. (1992). Signaling pathways in odorant detection. Neuron *8*, 205-209.

Reijmers, L.G., Perkins, B.L., Matsuo, N., and Mayford, M. (2007). Localization of a stable neural correlate of associative memory. Science *317*, 1230-1233.

Reisert, J. (2010). Origin of basal activity in mammalian olfactory receptor neurons. Journal of General Physiology *136*, 529-540.

Renier, N., Wu, Z., Simon, D.J., Yang, J., Ariel, P., and Tessier-Lavigne, M. (2014). iDISCO: a simple, rapid method to immunolabel large tissue samples for volume imaging. Cell *159*, 896-910.

Ressler, K.J., Sullivan, S.L., and Buck, L.B. (1994). Information coding in the olfactory system: evidence for a stereotyped and highly organized epitope map in the olfactory bulb. Cell *79*, 1245-1255.

Ridley, S., Ktistakis, N., Davidson, K., Anderson, K., Manifava, M., Ellson, C., Lipp, P., Bootman, M., Coadwell, J., and Nazarian, A. (2001). FENS-1 and DFCP1 are FYVE domain-containing proteins with distinct functions in the endosomal and Golgi compartments. Journal of cell science *114*, 3991-4000.

Rinn, J.L., Kertesz, M., Wang, J.K., Squazzo, S.L., Xu, X., Brugmann, S.A., Goodnough, L.H., Helms, J.A., Farnham, P.J., and Segal, E. (2007). Functional demarcation of active and silent chromatin domains in human HOX loci by noncoding RNAs. cell *129*, 1311-1323.

Ripoche, M.-A., Kress, C., Poirier, F., and Dandolo, L. (1997). Deletion of the H19 transcription unit reveals the existence of a putative imprinting control element. Genes & development *11*, 1596-1604.

Roberts, T.C., Morris, K.V., and Wood, M.J. (2014). The role of long non-coding RNAs in neurodevelopment, brain function and neurological disease. Philosophical Transactions of the Royal Society B: Biological Sciences *369*, 20130507.

Romer-Seibert, J.S., Hartman, N.W., and Moss, E.G. (2019). The RNA-binding protein LIN28 controls progenitor and neuronal cell fate during postnatal neurogenesis. The FASEB Journal *33*, 3291-3303.

Roskams, A., Cai, X., and Ronnett, G. (1998). Expression of neuron-specific beta-III tubulin during olfactory neurogenesis in the embryonic and adult rat. Neuroscience *83*, 191-200.

Rothman, A., Feinstein, P., Hirota, J., and Mombaerts, P. (2005). The promoter of the mouse odorant receptor gene M71. Molecular and Cellular Neuroscience *28*, 535-546.

Runge, S., Nielsen, F.C., Nielsen, J., Lykke-Andersen, J., Wewer, U.M., and Christiansen, J. (2000). H19 RNA binds four molecules of insulin-like growth factor II mRNA-binding protein. Journal of Biological Chemistry *275*, 29562-29569.

Ryba, N.J., and Tirindelli, R. (1997). A new multigene family of putative pheromone receptors. Neuron *19*, 371-379.

Rybak-Wolf, A., Stottmeister, C., Glažar, P., Jens, M., Pino, N., Giusti, S., Hanan, M., Behm, M., Bartok, O., and Ashwal-Fluss, R. (2015). Circular RNAs in the mammalian brain are highly abundant, conserved, and dynamically expressed. Molecular cell *58*, 870-885.

Sahali, D., Pawlak, A., Valanciuté, A., Grimbert, P., Lang, P., Remy, P., Bensman, A., and Guellën, G. (2002). A novel approach to investigation of the pathogenesis of active minimal-change nephrotic syndrome using subtracted cDNA library screening. Journal of the American Society of Nephrology *13*, 1238-1247.

Sainath, R., and Gallo, G. (2015). Cytoskeletal and signaling mechanisms of neurite formation. Cell and tissue research *359*, 267-278.

Salzman, J., Chen, R.E., Olsen, M.N., Wang, P.L., and Brown, P.O. (2013). Cell-type specific features of circular RNA expression. PLoS genetics *9*.

Saraiva, L.R., Ibarra-Soria, X., Khan, M., Omura, M., Scialdone, A., Mombaerts, P., Marioni, J.C., and Logan, D.W. (2015). Hierarchical deconstruction of mouse olfactory sensory neurons: from whole mucosa to single-cell RNA-seq. Scientific reports *5*, 1-17.

Sassoè-Pognetto, M., Cantino, D., Panzanelli, P., di Cantogno Verdun, L., Giustetto, M., Margolis, F.L., De, S.B., and Fasolo, A. (1993). Presynaptic co-localization of carnosine and glutamate in olfactory neurones. Neuroreport *5*, 7-10.

Sauvageau, M., Goff, L.A., Lodato, S., Bonev, B., Groff, A.F., Gerhardinger, C., Sanchez-Gomez, D.B., Hacisuleyman, E., Li, E., and Spence, M. (2013). Multiple knockout mouse models reveal lincRNAs are required for life and brain development. elife *2*, e01749.

Schlackow, M., Nojima, T., Gomes, T., Dhir, A., Carmo-Fonseca, M., and Proudfoot, N.J. (2017). Distinctive patterns of transcription and RNA processing for human lincRNAs. Molecular cell *65*, 25-38.

Schlingensiepen, K.-H., Wollnik, F., Kunst, M., Schlingensiepen, R., Herdegen, T., and Brysch, W. (1994). The role of Jun transcription factor expression and phosphorylation in neuronal differentiation, neuronal cell death, and plastic adaptationsin vivo. Cellular and molecular neurobiology *14*, 487-505.

Schlingensiepen, K.H., Schlingensiepen, R., Kunst, M., Klinger, I., Gerdes, W., Seifert, W., and Brysch, W. (1993). Opposite functions of jun-B and c-jun in growth regulation and neuronal differentiation. Developmental genetics *14*, 305-312.

Schorderet, P., and Duboule, D. (2011). Structural and functional differences in the long non-coding RNA hotair in mouse and human. PLoS genetics *7*, e1002071.

Schwob, J., Farber, N.B., and Gottlieb, D.I. (1986). Neurons of the olfactory epithelium in adult rats contain vimentin. Journal of Neuroscience *6*, 208-217.

Scolnick, J.A., Cui, K., Duggan, C.D., Xuan, S., Yuan, X.-b., Efstratiadis, A., and Ngai, J. (2008). Role of IGF signaling in olfactory sensory map formation and axon guidance. Neuron *57*, 847-857.

Serizawa, S., Miyamichi, K., Nakatani, H., Suzuki, M., Saito, M., Yoshihara, Y., and Sakano, H. (2003). Negative feedback regulation ensures the one receptor-one olfactory neuron rule in mouse. Science *302*, 2088-2094.

Serizawa, S., Miyamichi, K., Takeuchi, H., Yamagishi, Y., Suzuki, M., and Sakano, H. (2006). A neuronal identity code for the odorant receptor-specific and activity-dependent axon sorting. Cell *127*, 1057-1069.

Shaulian, E., and Karin, M. (2002). AP-1 as a regulator of cell life and death. Nature cell biology *4*, E131-E136.

Shykind, B.M., Rohani, S.C., O'Donnell, S., Nemes, A., Mendelsohn, M., Sun, Y., Axel, R., and Barnea, G. (2004). Gene switching and the stability of odorant receptor gene choice. Cell *117*, 801-815.

Siomi, M.C., Sato, K., Pezic, D., and Aravin, A.A. (2011). PIWI-interacting small RNAs: the vanguard of genome defence. Nature reviews Molecular cell biology *12*, 246-258.

Slack, F.J., and Chinnaiyan, A.M. (2019). The role of non-coding RNAs in oncology. Cell *179*, 1033-1055.

St. John, J.A., Clarris, H.J., McKeown, S., Royal, S., and Key, B. (2003). Sorting and convergence of primary olfactory axons are independent of the olfactory bulb. Journal of Comparative Neurology *464*, 131-140.

Steinert, P.M., and Roop, D.R. (1988). Molecular and cellular biology of intermediate filaments. Annual review of biochemistry *57*, 593-625.

Stephan, A.B., Shum, E.Y., Hirsh, S., Cygnar, K.D., Reisert, J., and Zhao, H. (2009). ANO2 is the cilial calcium-activated chloride channel that may mediate olfactory amplification. Proceedings of the National Academy of Sciences *106*, 11776-11781.

Stewart, C.E., and Rotwein, P. (1996). Growth, differentiation, and survival: multiple physiological functions for insulin-like growth factors. Physiological reviews *76*, 1005-1026.

Stout, R., and Graziadei, P. (1980). Influence of the olfactory placode on the development of the brain in Xenopus laevis (Daudin): I. Axonal growth and connections of the transplanted olfactory placode. Neuroscience *5*, 2175-2186.

Stuart, T., Butler, A., Hoffman, P., Hafemeister, C., Papalexi, E., Mauck III, W.M., Hao, Y., Stoeckius, M., Smibert, P., and Satija, R. (2019). Comprehensive integration of single-cell data. Cell *177*, 1888-1902. e1821.

Stylianopoulou, F., Herbert, J., Soares, M.B., and Efstratiadis, A. (1988). Expression of the insulin-like growth factor II gene in the choroid plexus and the leptomeninges of the adult rat central nervous system. Proceedings of the National Academy of Sciences *85*, 141-145.

Suh, K.S., Kim, S.Y., Bae, Y.C., Ronnett, G.V., and Moon, C. (2006). Effects of unilateral naris occlusion on the olfactory epithelium of adult mice. Neuroreport *17*, 1139-1142.

Sun, H.-Q., Kwiatkowska, K., and Yin, H.L. (1996). -Thymosins Are Not Simple Actin Monomer Buffering Proteins INSIGHTS FROM OVEREXPRESSION STUDIES. Journal of Biological Chemistry *271*, 9223-9230.

Takeuchi, H., Inokuchi, K., Aoki, M., Suto, F., Tsuboi, A., Matsuda, I., Suzuki, M., Aiba, A., Serizawa, S., and Yoshihara, Y. (2010). Sequential arrival and graded secretion of

Sema3F by olfactory neuron axons specify map topography at the bulb. Cell *141*, 1056-1067.

Tepe, B., Hill, M.C., Pekarek, B.T., Hunt, P.J., Martin, T.J., Martin, J.F., and Arenkiel, B.R. (2018). Single-cell RNA-seq of mouse olfactory bulb reveals cellular heterogeneity and activity-dependent molecular census of adult-born neurons. Cell reports *25*, 2689-2703. e2683.

Thompson, M.A., and Ziff, E.B. (1989). Structure of the gene encoding peripherin, an NGF-regulated neuronal-specific type III intermediate filament protein. Neuron *2*, 1043-1053.

Thorvaldsen, J.L., Duran, K.L., and Bartolomei, M.S. (1998). Deletion of the H19 differentially methylated domain results in loss of imprinted expression of H19 and Igf2. Genes & development *12*, 3693-3702.

Toyoda, R., Assimacopoulos, S., Wilcoxon, J., Taylor, A., Feldman, P., Suzuki-Hirano, A., Shimogori, T., and Grove, E.A. (2010). FGF8 acts as a classic diffusible morphogen to pattern the neocortex. Development *137*, 3439-3448.

Toyoshima, H., and Hunter, T. (1994). p27, a novel inhibitor of G1 cyclin-Cdk protein kinase activity, is related to p21. Cell *78*, 67-74.

Tran, V.G., Duputié, A., Antoine, E., Aptel, N., Milligan, L., Carbonell, F., Lelay-Taha, M.-N., Piette, J., Weber, M., and Montarras, D. (2012). H19 antisense RNA can up-regulate Igf2 transcription by activation of a novel promoter in mouse myoblasts. PloS one *7*, e37923-e37923.

Treloar, H.B., Miller, A.M., Ray, A., and Greer, C.A. (2010). Development of the olfactory system. The neurobiology of olfaction *20092457*, 131-155.

Tsai, L., and Barnea, G. (2014). A critical period defined by axon-targeting mechanisms in the murine olfactory bulb. Science *344*, 197-200.

Tsang, W.P., Ng, E.K., Ng, S.S., Jin, H., Yu, J., Sung, J.J., and Kwok, T.T. (2010). Oncofetal H19-derived miR-675 regulates tumor suppressor RB in human colorectal cancer. Carcinogenesis *31*, 350-358.

Ulitsky, I., and Bartel, D.P. (2013). lincRNAs: genomics, evolution, and mechanisms. Cell *154*, 26-46.

Vassar, R., Chao, S.K., Sitcheran, R., Nun, J.M., Vosshall, L.B., and Axel, R. (1994). Topographic organization of sensory projections to the olfactory bulb. Cell *79*, 981-991.

Venkatraman, A., He, X.C., Thorvaldsen, J.L., Sugimura, R., Perry, J.M., Tao, F., Zhao, M., Christenson, M.K., Sanchez, R., and Jaclyn, Y.Y. (2013). Maternal imprinting at the H19–Igf2 locus maintains adult haematopoietic stem cell quiescence. Nature *500*, 345-349.

Venø, M.T., Hansen, T.B., Venø, S.T., Clausen, B.H., Grebing, M., Finsen, B., Holm, I.E., and Kjems, J. (2015). Spatio-temporal regulation of circular RNA expression during porcine embryonic brain development. Genome biology *16*, 245.

Von Dannecker, L.E.C., Mercadante, A.F., and Malnic, B. (2005). Ric-8B, an olfactory putative GTP exchange factor, amplifies signal transduction through the olfactory-specific G-protein Gαolf. Journal of Neuroscience *25*, 3793-3800.

Von Dannecker, L.E.C., Mercadante, A.F., and Malnic, B. (2006). Ric-8B promotes functional expression of odorant receptors. Proceedings of the National Academy of Sciences *103*, 9310-9314.

Wang, F., Nemes, A., Mendelsohn, M., and Axel, R. (1998). Odorant receptors govern the formation of a precise topographic map. Cell *93*, 47-60.

Wang, L., Song, G., Liu, M., Chen, B., Chen, Y., Shen, Y., Zhu, J., and Zhou, X. (2016). MicroRNA-375 overexpression influences P19 cell proliferation, apoptosis and differentiation through the Notch signaling pathway. International journal of molecular medicine *37*, 47-55.

Wang, Q., Miyakoda, M., Yang, W., Khillan, J., Stachura, D.L., Weiss, M.J., and Nishikura, K. (2004). Stress-induced apoptosis associated with null mutation of ADAR1 RNA editing deaminase gene. Journal of Biological Chemistry *279*, 4952-4961.

Wang, R., Zhou, S., Wu, P., Li, M., Ding, X., Sun, L., Xu, X., Zhou, X., Zhou, L., and Cao, C. (2018). Identifying involvement of H19-miR-675-3p-IGF1R and H19-miR-200a-PDCD4 in treating pulmonary hypertension with melatonin. Molecular Therapy-Nucleic Acids *13*, 44-54.

Wang, S.-Z., Ou, J., Zhu, L.J., and Green, M.R. (2012). Transcription factor ATF5 is required for terminal differentiation and survival of olfactory sensory neurons. Proceedings of the National Academy of Sciences *109*, 18589-18594.

Westholm, J.O., Miura, P., Olson, S., Shenker, S., Joseph, B., Sanfilippo, P., Celniker, S.E., Graveley, B.R., and Lai, E.C. (2014). Genome-wide analysis of drosophila circular RNAs reveals their structural and sequence properties and age-dependent neural accumulation. Cell reports *9*, 1966-1980.

Whitlock, K.E., and Westerfield, M. (2000). The olfactory placodes of the zebrafish form by convergence of cellular fields at the edge of the neural plate. Development *127*, 3645-3653.

Wiesel, T.N., and Hubel, D.H. (1963). Effects of visual deprivation on morphology and physiology of cells in the cat's lateral geniculate body. Journal of neurophysiology *26*, 978-993.

Worringer, K.A., Rand, T.A., Hayashi, Y., Sami, S., Takahashi, K., Tanabe, K., Narita, M., Srivastava, D., and Yamanaka, S. (2014). The let-7/LIN-41 pathway regulates reprogramming to human induced pluripotent stem cells by controlling expression of prodifferentiation genes. Cell stem cell *14*, 40-52.

Wu, Y., Ma, L., Duyck, K., Long, C.C., Moran, A., Scheerer, H., Blanck, J., Peak, A., Box, A., Perera, A.*, et al.* (2018). A Population of Navigator Neurons Is Essential for Olfactory Map Formation during the Critical Period. Neuron *100*, 1066-1082.e1066.

Xiang, C., Lv, Y., Wei, Y., Wei, J., Miao, S., Mao, X., Gu, X., Song, K., and Jia, S. (2015). Effect of EphA7 silencing on proliferation, invasion and apoptosis in human laryngeal cancer cell lines Hep-2 and AMC-HN-8. Cellular Physiology and Biochemistry *36*, 435-445.

Xiao, J., Dai, R., Negyessy, L., and Bergson, C. (2006). Calcyon, a novel partner of clathrin light chain, stimulates clathrin-mediated endocytosis. Journal of Biological Chemistry *281*, 15182-15193.

Xie, Z., Huganir, R.L., and Penzes, P. (2005). Activity-dependent dendritic spine structural plasticity is regulated by small GTPase Rap1 and its target AF-6. Neuron *48*, 605-618.

Xu, C., Xu, W., Palmer, A.E., and Reed, J.C. (2008). BI-1 regulates endoplasmic reticulum Ca2+ homeostasis downstream of Bcl-2 family proteins. Journal of Biological Chemistry *283*, 11477-11484.

Xu, K., Chen, D., Wang, Z., Ma, J., Zhou, J., Chen, N., Lv, L., Zheng, Y., Hu, X., and Zhang, Y. (2018). Annotation and functional clustering of circRNA expression in rhesus macaque brain during aging. Cell discovery *4*, 1-18.

Yamakawa, H., Cheng, J., Penney, J., Gao, F., Rueda, R., Wang, J., Yamakawa, S., Kritskiy, O., Gjoneska, E., and Tsai, L.-H. (2017). The transcription factor Sp3 cooperates with HDAC2 to regulate synaptic function and plasticity in neurons. Cell reports *20*, 1319-1334.

Ye, Q., Callebaut, I., Pezhman, A., Courvalin, J.-C., and Worman, H.J. (1997). Domain-specific interactions of human HP1-type chromodomain proteins and inner nuclear membrane protein LBR. Journal of Biological Chemistry *272*, 14983-14989.

York, R.D., Yao, H., Dillon, T., Ellig, C.L., Eckert, S.P., McCleskey, E.W., and Stork, P.J. (1998). Rap1 mediates sustained MAP kinase activation induced by nerve growth factor. Nature *392*, 622-626.

You, D., and You, H. (2019). Repression of long non-coding RNA MEG3 restores nerve growth and alleviates neurological impairment after cerebral ischemia-reperfusion injury in a rat model. Biomedicine & Pharmacotherapy *111*, 1447-1457.

You, X., Vlatkovic, I., Babic, A., Will, T., Epstein, I., Tushev, G., Akbalik, G., Wang, M., Glock, C., and Quedenau, C. (2015). Neural circular RNAs are derived from synaptic genes and regulated by development and plasticity. Nature neuroscience *18*, 603.

Yu, C.R., Power, J., Barnea, G., O'Donnell, S., Brown, H.E., Osborne, J., Axel, R., and Gogos, J.A. (2004). Spontaneous neural activity is required for the establishment and maintenance of the olfactory sensory map. Neuron *42*, 553-566.

Yu, C.R., and Wu, Y. (2017). Regeneration and rewiring of rodent olfactory sensory neurons. Experimental neurology *287*, 395-408.

Yu, F.X., Yin, H.L., Morrison-Bogorad, M., and Lin, S.C. (1994). Effects of thymosin β4 and thymosin β10 on actin structures in living cells. Cell motility and the cytoskeleton *27*, 13-25.

Zemel, S., Bartolomei, M.S., and Tilghman, S.M. (1992). Physical linkage of two mammalian imprinted genes, H19 and insulin–like growth factor 2. Nature genetics *2*, 61-65.

Zhang, B., Arun, G., Mao, Y.S., Lazar, Z., Hung, G., Bhattacharjee, G., Xiao, X., Booth, C.J., Wu, J., and Zhang, C. (2012). The lncRNA Malat1 is dispensable for mouse development but its transcription plays a cis-regulatory role in the adult. Cell reports *2*, 111-123.

Zhang, H., Li, D., Zhang, Y., Li, J., Ma, S., Zhang, J., Xiong, Y., Wang, W., Li, N., and Xia, L. (2018). Knockdown of lncRNA BDNF-AS suppresses neuronal cell apoptosis via downregulating miR-130b-5p target gene PRDM5 in acute spinal cord injury. RNA biology *15*, 1071-1080.

Zhang, S.-Y., Kamal, M., Dahan, K., Pawlak, A., Ory, V., Desvaux, D., Audard, V., Candelier, M., BenMohamed, F., and Matignon, M. (2010). C-mip impairs podocyte proximal signaling and induces heavy proteinuria. Science signaling *3*, ra39-ra39.

Zhang, X.-O., Dong, R., Zhang, Y., Zhang, J.-L., Luo, Z., Zhang, J., Chen, L.-L., and Yang, L. (2016). Diverse alternative back-splicing and alternative splicing landscape of circular RNAs. Genome research *26*, 1277-1287.

Zhang, X.-O., Wang, H.-B., Zhang, Y., Lu, X., Chen, L.-L., and Yang, L. (2014). Complementary sequence-mediated exon circularization. Cell *159*, 134-147.

Zhang, X., and Firestein, S. (2002). The olfactory receptor gene superfamily of the mouse. Nature neuroscience *5*, 124-133.

Zhang, Y., Zhang, X.-O., Chen, T., Xiang, J.-F., Yin, Q.-F., Xing, Y.-H., Zhu, S., Yang, L., and Chen, L.-L. (2013). Circular intronic long noncoding RNAs. Molecular cell *51*, 792-806.

Zhou, J., Xu, J., Zhang, L., Liu, S., Ma, Y., Wen, X., Hao, J., Li, Z., Ni, Y., and Li, X. (2019). Combined single-cell profiling of lncRNAs and functional screening reveals that H19 is pivotal for embryonic hematopoietic stem cell development. Cell Stem Cell *24*, 285-298. e285.

Zhuang, M., Gao, W., Xu, J., Wang, P., and Shu, Y. (2014). The long non-coding RNA H19-derived miR-675 modulates human gastric cancer cell proliferation by targeting tumor suppressor RUNX1. Biochemical and biophysical research communications *448*, 315-322.

Ziegler, A.N., Feng, Q., Chidambaram, S., Testai, J.M., Kumari, E., Rothbard, D.E., Constancia, M., Sandovici, I., Cominski, T., and Pang, K. (2019). Insulin-like growth factor II: an essential adult stem cell niche constituent in brain and intestine. Stem cell reports *12*, 816-830.

Zou, D.-J., Feinstein, P., Rivers, A.L., Mathews, G.A., Kim, A., Greer, C.A., Mombaerts, P., and Firestein, S. (2004). Postnatal Refinement of Peripheral Olfactory Projections. Science *304*, 1976-1979.

Zou, Y., Chiu, H., Zinovyeva, A., Ambros, V., Chuang, C.-F., and Chang, C. (2013). Developmental decline in neuronal regeneration by the progressive change of two intrinsic timers. Science *340*, 372-376.